ECCS

Equaljoints PLUS
Volume with information brochures for 4 seismically qualified joints

1st Edition, 2018

Raffaele Landolfo
Mario D'Aniello
Silvia Costanzo
Roberto Tartaglia
Jean-François Demonceau
Jean-Pierre Jaspart
Aurel Stratan
Dominiq Jakab
Dan Dubina,
Ahmed Elghazouli
Dan Bompa

ECCS
CECM
EKS

Equaljoints PLUS
Volume with information brochures for 4 seismically qualified joints

NºEQJ1-EN, 1st Edition, 2018

Published by:
ECCS – European Convention for Constructional Steelwork
publications@steelconstruct.com
www.steelconstruct.com

ISBN: 978-92-9147-143-0

Printed in Macasi Artes Gráficas, Coimbra, Portugal

Legal deposit

INTRODUCTION

The current document has been developed within the European RFCS project Equaljoints PLUS (754048 — EQUALJOINTS-PLUS — RFCS-2016/RFCS-2016).
Equaljoint-PLUS is a 24 month RFCS project devoted to disseminate the knowledge achieved within the previous RCFS 36 months-project EQUALJOINTS
Within the previous RFCS project EQUALJOINTS (RFSR-CT-2013-00021), European seismic prequalification criteria of a set of steel been-to-column joints have been developed.
Equaljoint-PLUS aims at the valorisation, the dissemination and the extension of the developed prequalification criteria for practical applications to a wide audience (i.e. academic institutions, Engineers and architects, construction companies, steel producers).
The main objectives of the Equaljoints PLUS can be summarized as follows:

- To collect and organize informative material concerning the prequalified joint typologies: informative documents have been prepared in 12 languages (English, Spanish, French, German, Italian, Dutch, Portuguese, Czech, Bulgarian, Romanian, Greek, and Slovenian).
- To develop pre-normative design recommendations of seismically qualified joints based on results from Equaljoints project in 12 languages.
- To develop design guidelines to design steel structures accounting for the type of joints and their relevant non-linear response.
- To develop a software and an app for mobile to predict the inelastic response of joints.
- To organize seminars and workshops for disseminating the gained knowledge over EU and internationally.
- To create a web site with free access to the users to promote the obtained results.
- To create a You-Tube channel to make available the videos of the experimental tests and simulations to show the evolution of damage pattern.

The Equaljoints PLUS project is coordinated by the University of Naples Federico II. The Consortium consists of 15 partners, 7 of which already involved in the former Equaljoints project. All the partners involved are listed in the following table:

Equaljoitns PLUS Consortium	
Coordinator	Università degli Studi di Napoli Federico II (UNINA)
Partners	Arcelormittal Belval & Differdange SA (AM)
	Universite de Liege (Ulg)
	Universitatea Politehnica Timisoara (UPT)
	Universidade de Coimbra (UC)
	Convention Europeenne de la Construction Métallique (ECCS)
	Universita degli Studi di Salerno (UNISA)
	Imperial College of Science Technology and Medicine (IC)
	Centre Technique Industriel de la Construction Métallique (CTICM)
	National Technical University of Athens (NTUA)
	Ceske Vysoke Uceni Technicke V Praze (CVUT)
	Technische Universiteit Delft (TUD)
	Univerza V Ljubljani (UL)
	Universitet Po Architektura Stroitelstvo I Geodezija (UASG)
	Universitat Politecnica de Catalunya (UPC)
	Rheinisch-Westfaelische Technische Hochschule Aachen (RWTHA)

CONTENTS

INTRODUCTION		iii
1. REVIEW OF THE STATE OF ART		1
1.1	Haunched joints	2
1.2	Extended stiffened end-plate joints	4
1.3	Unstiffened extended end-plate joints	6
1.4	Dog-bone joints	7
2.	**DESCRIPTION OF THE MAIN FEATURES OF THE TESTED JOINTS**	11
2.1	Haunched joints	12
	2.1.1 Description of the joint configuration	14
	2.1.2 List of systems for which connection is prequalified	15
	2.1.3 List of limit values for prequalified data	15
2.2	Extended stiffened end-plate beam-to-column joints	18
	2.2.1 Description of the joint configuration	19
	2.2.2 List of systems for which connection is prequalified	20
	2.2.3 List of limit values for prequalified data	21
2.3	Extended unstiffened end-plate beam-to-column joints	22
	2.3.1 Description of the joint configuration	23
	2.3.2 List of limit values for prequalified data	24
2.4	Dogbone connections	26
3.	**EXPERIMENTAL SETUP AND MEASUREMENT INSTRUMENTATION**	27
3.1	Experimental setup	27
3.2	Loading procedure	28
	3.2.1 Loading rate	30
	3.2.2 Preloading	30
	3.2.3 Monotonic loading	30

		3.2.4 Cyclic loading protocol	31
4.	**DESIGN PROCEDURE FOR QUALIFIED JOINT TYPES**		**33**
	4.1	General performance objectives	33
	4.2	Design assumptions for connection zone	38
		4.2.1 Active bol rows in tension	38
		4.2.2 Centre of compression and lever arm	38
		4.2.3 Presence of rib stiffeners in ES joints	39
		4.2.4 Design assumption for column web panel zone	41
	4.3	Technological requirements	43
5.	**NON-LINEAR MOMENT-ROTATION RESPONSE ACCORDING TO EN 1993-1-8**		45
	5.1	Generality	45
	5.2	Moment-rotation curves of haunched joints according to EN 1993-1-8	47
	5.3	Moment-rotation curves of extended stiffened joints according to EN 1993-1-8	51
	5.4	Moment-rotation curves of extended unstiffened joints according to EN 1993-1-8	57
	5.5	Moment-rotation curves of dog-bone joints	63
6.	**PERFORMANCE PARAMETERS OF THE TESTED JOINTS**		**67**
	6.1	Haunched joints	68
		6.1.1 Performance parameters of tested joints	70
		6.1.2 Influence of beam depth	73
		6.1.3 Influence of haunch depth	74
		6.1.4 Influence of loading protocol	76
		6.1.5 Influence of steel beam over-strength	79
		6.1.6 Contribution of joint components to total rotation	79
		6.1.7 Overall remarks on haunched joints	82
	6.2	Extended stiffened end-plate joints	82
		6.2.1 Performance parameters of tested joints	84
		6.2.2 Failure mechanisms	86

	6.2.3 Influence of beam depth	87
	6.2.4 Influence of shot peening	87
	6.2.5 Influence of loading protocol	88
	6.2.6 Contribution of joint components to plastic rotation	89
	6.2.7 Overall remarks on extended stiffened end-plate joints	90
6.3	Extended unstiffened end-plate joints	90
	6.3.1 Performance parameters of tested joints	93
	6.3.2 Failure mechanisms	94
	6.3.3 Influence of shot peening	95
	6.3.4 Influence of loading protocol	96
	6.3.5 Contribution of joint components to plastic rotation	97
	6.3.6 Overall remarks on extended stiffened end-plate joints	97
6.4	Dog-bone joints	98
	6.4.1 Fabrication	98
	6.4.2 Experimental results on specimen SP2	99
	6.4.3 Experimental results on specimen SP4	101
	6.4.4 Contribution of joint components	102
	6.4.5 Influence of member sizes	104
	6.4.6 Influence of panel zone design	106
	6.4.7 Influence of RBS design	108
	6.4.8 Simplified modelling procedures	109
	6.4.9 Overall remarks on dog-bone joints	111
REFERENCES		113

1 REVIEW OF THE STATE OF ART

Nowadays, codified design procedures for steel bolted beam-to-column joints in seismic resistant steel frames are missing in Europe. At current stage, EN 1998 allows using dissipative joints, provided that the design is supported by testing, which results in impractical solutions within the time and budget constraints of real-life projects. Even though the lack analytical models to predict the joints behavior to meet code requirements is more evident for dissipative beam-to-column connections, reliable design tools for non-dissipative connections are also necessary: indeed, owing to the variability of steel strength, these connections could not have enough overstrength (e.g. min 1.1x1.25 $M_{b.rd}$, being $M_{b.rd}$ the bending strength of the beam), and full strength behaviour cannot be guaranteed. In such cases the plastic rotation capacity of the joint need to be prequalified by relevant test and numerically based procedures.
In contrast to current European design methodology, the approach used in other countries with high seismic hazard is based on codified and easy-to-use design tools and procedures. In particular, following the widespread damages observed after Northridge and Kobe earthquakes, North American practice was directed at prequalifying standard joints for seismic applications. In 1995, the US FEMA and the SAC joint venture initiated a comprehensive 6-year program of investigation, called FEMA/SAC program, to develop and evaluate guidelines for the inspection, evaluation, repair, rehabilitation, and construction of steel moment frame resisting structures. The US research effort was directed to feed into a specific standard (ANSI/AISC 358-05, 2005) containing design, detailing, fabrication and quality criteria for a set of selected types of connections including the most common used in US practice, which should be prequalified for use with special moment frames (SMF) and intermediate moment frames (IMF). Similarly to US design approach, also in Japan a prequalification activity was carried out. Unfortunately, joint typologies commonly used in both US and Japanese practices, are quite different from European ones, also employing different ranges of cross sections, material properties, bolt assemblies, etc. Therefore, the prequalification procedures obtained in non-European framework are not properly suitable for European joints. Another important issue limiting the direct application of American and Japanese prequalification is related to the loading protocol for experimental tests. Indeed, the type of seismic input, which affect the ductility demand on joints and connected members, differs between the different counties. In order to fill these gaps, the recently finished European research project “Equaljoints” was aimed to provide prequalification criteria of steel joints for the next version of EN 1998-1. In detail, the research activity covered the standardization of design and manufacturing

procedures with reference to a set of bolted joint types and a welded dog-bone with heavy profiles designed to meet different performance levels. Among the objectives of the project, there was also the development of a new loading protocol for European prequalification, representative of European seismic demand. Moreover, an experimental campaign devoted to the cyclic characterization of both European mild carbon steel and high strength bolts were successfully achieved.

1.1 Haunched joints

Extended end-plate connections with haunches are usually used in steel moment-resisting frames when it is desired that plastic hinges occur exclusively in the connected beams. Adding a haunch at the lower part of the beam increases the lever arms of bolts, which allows easier fulfilment of the overstrength requirements for non-dissipative connections in EN 1998. At the same time, it leads to larger stiffness of the connection. It is worth mentioning that the haunch increases the cost of the connection, therefore it is adopted in practice when rigid and full-strength joints are needed, which is a common requirement in seismic applications. Moreover, rigid and full-strength joints are preferred by designers as it simplifies modelling for global structural analysis.
Zoetemeijer, 1981 (in Bijlaard et al., 1989) investigated haunches with and without flanges as a mean of increasing connections stiffness, and proposed a design method. Jaspart (1997) and Maquoi and Chabrolin (1998) analysed in detail the beam-to-column joints with haunches, proposing design rules compatible with the component method in EN 1993-1-8. The following components were identified for characterisation of properties of bolted end-plate joints with haunches: haunch flange in compression, haunch web in shear, column web in compression, beam web in transverse compression.
After the 1994 Northridge earthquake, which caused widespread damage to welded connections in steel moment-resisting frames, haunches received a lot of attention as a means of repairing damaged connections, or strengthening existing and new steel constructions. (Lee and Uang 1997, NIST 1998, Gross et al. 1999, Yu et al. 2000). Cyclic tests were performed to prove the effectiveness the solution (Uang et al., 1998). Finite element analyses showed that with presence of the haunch on the bottom of the beam, the straight-line stress profile as predicted by a basic beam theory no longer holds (Lee and Uang, 1997). Moreover, the haunch creates a dual panel zone, which requires a more elaborate analysis and design. Yu et al. (2000) have shown that the haunch alters the moment distribution of the beam and that majority of the beam shear is transferred to the column through the haunch flange

rather than through beam and haunch web. A simplified model that considers both force interaction and deformation compatibility between the beam and the haunch was developed.

In the case of end-plate bolted composite connections, haunches located at the bottom side of the beam flanges are very convenient for constructional point of view. Gross et al. (1999) proposed to adopt a haunch depth equal to 0.33 times the beam depth, with an angle of the haunch equal to 30° to limit the haunch web slenderness. This assumption was based on the Whitmore theory of the propagation of internal stress in elastic system of about 30° slope. However, increasing the slope can be convenient because it allows reducing the size of the haunch as well as the design forces on the connection.

Experimental tests carried out by Lachal et al. (2006) showed that haunched bolted joints can improve significantly the cyclic performances as respect to unstiffened end-plate joints. They observed that the rotation capacity can exceed 35mrad without low cycle fatigue rupture in the welds connecting beam flanges on the end-plates. In addition, this type of joint guarantees a significant increase of rotational stiffness, moment resistance and rotation capacity were observed in comparison with similar beam-to-column composite joints without haunches.

EN 1993-1-8 (2005) gives rules for design of joints reinforced with haunches by providing additional criteria for the "beam flange and web in compression" component (Figure 1.1). The design compression resistance of the combined beam/haunch flange and web is given by the expression (6.21) in EN 1993-1-8, by dividing the design moment resistance of the beam cross-section at the location of the connection, $M_{c,Rd}$, to the distance between flange centrelines. For a haunched beam $M_{c,Rd}$ may be calculated neglecting the intermediate flange. Also, the design resistance of beam web in compression should be determined, similar to the rules given for the component "column web in transverse compression". Moreover, the following detailing rules apply:

- the steel grade of the haunch should match that of the member;
- the flange size and the web thickness of the haunch should not be less than that of the member;
- the angle of the haunch flange to the flange of the member should not be greater than 45°.

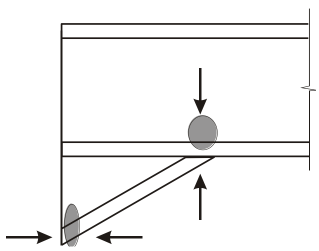

Figure 1.1: "Haunched beam" component in EN 1993-1-8

The SCI/BCSA publication P398 (2013) explains more in detail the design approach in EN 1993-1-8 for connections with haunches, giving also more guidance on the design of welds.
Bolted extended end plate beam to column connections with haunches for seismic applications were investigated experimentally within the EQUALJOINJTS project (Stratan et al., 2017). All tested specimens showed a stable hysteretic response, with plastic deformations concentrated in the beam next to the haunch, qualifying for seismic applications according to ANSI/AISC 358-10 criteria. Previous numerical simulations (Maris et al., 2015 and Stratan et al., 2016) have shown that presence of haunches affect some of the design assumptions in EN 1993-1-8. For example, under hogging moment, the centre of compression shifts above the haunch flange. On the other hand, only the bolts close to the tension flange of the beam are active in tension.

1.2 Extended stiffened end-plate joints

Extended stiffened (ES) end-plate bolted connections are popular among European steel fabricating industries and widely used in European practice as moment-resistant joints in low and medium rise steel frames, especially due to the simplicity and the economy of fabrication and erection. Indeed, this type of connection is characterized by a limited use of welds, being solely the end-plate and some stiffeners shop-welded to the beam, which allows keeping down the cost and guaranteeing good quality control. Then, the end-plate and beam assembly is field-bolted to the column flange, thus shortening the construction time.
ES joints can be theoretically designed to be either full or partial strength and full or semi-rigid. The experimental and theoretical evidence showed that this type of joint can behave as full strength. Conversely, a nominally rigid behaviour could not be obtained in several cases (Guo et al, 2006; Shi et al, 2007). Therefore, ES bolted joints can be easily conceived as semi-rigid joints, which results in an additional savings in the gravity load system (Bjorhodve and Colson, 1991). Moreover, in moment resisting frames subjected to seismic loads the use of semi-rigid joints can lead to lighter structures thanks to lower design forces due to increase of fundamental periods related to the increase of lateral flexibility (Elnashai A., Elghazouli, 1994). Within current EN 1993: 1-8, theoretical strength and stiffness of extended end-plate connections is predicted on the basis of yield line t-stub theory. However, no specific provision is provided for accounting the influence of the rib stiffeners on the ES joints moment-rotation capacity.

The numerical and experimental results on welded joints with rib stiffeners (Lee, 2002; Abidelah et al., 2012; Lee et al., 2015) highlights that bending is mainly transferred from beam-to-column by a truss mechanism rather than the classical beam theory, where the rib behaves as an inclined strut as shown in Figure 1.2.

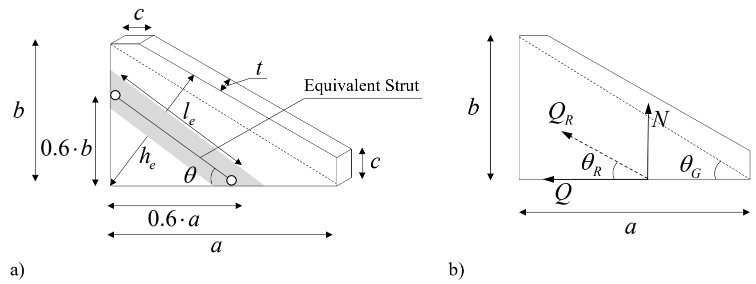

Figure 1.2: Geometry of rib stiffener (a) and forces developing at beam/column-to-rib interface according to Lee, 2002

However, in current code, the equivalent T-Stub and corresponding effective lengths are not clearly recommended for the bolt-rows of the rib-stiffened end-plate above beam flange in ES joints. This implies that a designer has two alternative choices, namely: (i) assuming the effective lengths of the bolt-rows of column flange adjacent to a stiffener; (ii) assuming the effective lengths of bolt-row below tension flange of beam. Of course, the second option allows taking advantage of the stiffener in terms of both strength and stiffness, but unaware engineers (as noticed by the Authors in their experience) can follow the first option that is considered more conservative. For the sake of clarity, appropriate yield line patterns for these bolt-rows are specified in the Green Book P398 (2013), which gives comprehensive rules to properly accounting for the presence of rib stiffeners.

Another key aspect is related to the position of the compression centre: for end-plate joints covered by EN 1993-1-8 provisions, the compression centre is located in the middle of thickness of beam flange. However, experimental and numerical results on bolted ES joints carried out by Abidelah et al. (2012) showed that the compression centre is generally shifted below the position assumed by EC3, and approximately located at the centroid of the “T” section made of the rib stiffener and the beam flange. It is clear that the position of centre of compression varies with the joint rotation demand due to the formation of plastic modes with different engagement of each joint component. However, tests on welded joints carried out by Lee et al. (2005) showed that up to interstorey drift ratios equal to 5% the strut model for rib is effective with centre of compression shifted at 0.6 times the rib height (see Figure 1.2a; Figure 1.3).

D’Aniello et al. (2017) deeply investigate and critically discuss the design criteria and related requirements for bolted extended stiffened end-plate beam-to-column joints currently codified in EN 1993, on the basis of a parametric study based on finite element analyses. In addition, D’Aniello et al. (2017) develop a capacity design procedure in the framework of components method, specifically accounting for the presence of ribs and able to control the joint response for different performance levels.

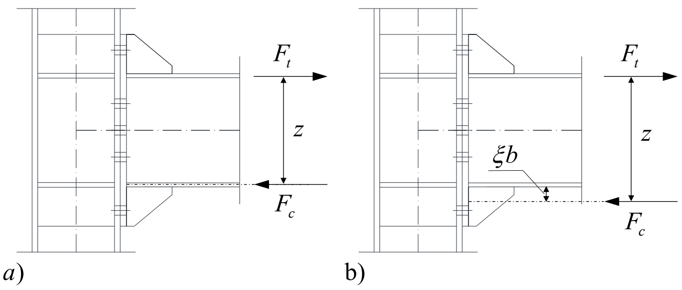

Figure 1.3: Centre of compression and lever arm: a) EC3:1-8 for end-plate connections; b) shifted position due to strut mechanism into the rib stiffener

1.3 Unstiffened extended end-plate joints

Unstiffened extended end-plate joints (“E”) are commonly used in steel construction to connect a steel I or H beam to a steel I or H column, especially in the case where significant bending moments have to be transferred. This configuration allows an easy erection by bolting while welding of the end-plate to the beam is realized in shop.
Depending on the joint detailing and the beam length, these joints may be considered as rigid or semi-rigid. In order to increase their rigidity in the case when the joint should be seen as “rigid”, it is usual to add transverse stiffeners on the column web. These elements reduce the overall joint flexibility through an efficient stiffening of the “column web in compression” and “column web in tension” joint components. This measure does not fully ensure that the joints will be rigid; so a specific check has to be achieved when such a requirement is imposed or decided through the use of so-called “classification stiffness criteria”.
As far as resistance is concerned, “E” joints may be usually considered as “partial strength”, as their bending resistance is often lower than the bending resistance of the connected members (this may be the result of the partial resistance character of the constitutive connections or of the column web panel in shear). To reach an “equal strength” situation in which the plastic resistance of the joint is roughly equal to the plastic resistance of the beam section may also be contemplated, but through an appropriate design.
Finally, their ductility in bending highly depends on the detailing of the joints, which influences the failure mode. If the joint component governing the failure is a ductile

one and if the resistance of the brittle active components is significantly higher, a ductile joint response may be contemplated; in the opposite case, no reliance should be made on the capacity of the joint to redistribute plasticity or, in a seismic area, to absorb energy.

Many numerical, experimental and analytical investigations on this type of joint configuration have been performed in the last decades and to report on all of them would constitute a long work in itself. From these studies design recommendations have been derived which, after discussions at the European level, were progressively introduced in the Structural Eurocodes, and more especially for steel joints into the so-called Part 1-8 of Eurocode 3 (CEN, 2005). The interested reader will find in a recent publication of the European Convention for Constructional Steelwork (Jaspart and Weynand, 2016) detailed information about these recommendations and the way to integrate them in daily practice.

This could let the user believe that all design aspects for these joints are completely mastered and no pending questions need further investigations. This does not reflect the reality, especially in terms of ductility aspects. Amongst the components meet in "E" joints:

- some exhibit a very ductile response (column web panels in shear for instance),
- some are known to be particularly brittle (bolts in tension and/or shear and welds),
- some have a ductility which may, according to the design situations, vary form pretty ductile to rather brittle (end-plate in bending and bolts in tension, column flange in bending and bolts in tension, …)

For the last category, the knowledge remains rather limited as evidenced by the very low number of recommendations provided by Eurocode 3 Part 1-8.

For the design of joints in non-seismic areas, this lack of knowledge is not as problematic as it is for buildings located in seismic ones in which the absorption of energy has to be achieved in "E" joints as long as these ones are classified as "partial strength". In Section 4 of the present document, the proposed design procedure will have to be carefully fitted so as to overcome this difficulty and to ensure to the prequalified "E" joints an adequate sufficient ductility. This will be achieved on the basis of the knowledge gained by the EQUALJOINTS+ partners all along their past and ongoing research activities and experiences.

1.4 Dog-bone joints

The need to prevent excessive strain demands developing on the welds of beam-to-column connections and leading to brittle fractures was highlighted following the

1994 Northridge and 1995 Kobe earthquake. The two main strategies that were adopted included either strengthening the connection or weakening the beam. The latter consists of using Dog-bone, also referred to as Reduced Beam Section (RBS), moment resisting connections.

The concept of purposely weakening the beam section at a certain distance from the interface by trimming the flanges was initially proposed by Plumier (1990), who introduced the trapezoidal (or straight) cut steel beam-to-column connection. However, experimental data before 1994 were quite limited. A number of early experimental studies on RBS moment frame connections (Chen, 1996; Engelhardt et al., 1996; Popov et al., 1996; Iwankiw and Carter, 1996; Tremblay et al, 1997; Zekioglu et al., 1997) followed. Additional research focusing on the radius cut RBS (Engelhardt et al., 2000; Gilton, Chi and Uang, 2000; Yu et al 2000) were conducted as part of the SAC study sponsored by FEMA (Kunnath and Malley, 2002; FEMA-350, 2000b). Among the different options for the profile of section reduction, the radius cut RBS tends to exhibit a relatively more ductile behaviour, delaying the ultimate fracture (Engelhardt et al., 1996-2000).

It should be noted however that early tests that led to the prequalification of the radius cut RBS connection mostly considered shallow wide flange sections and columns up to W14. Further studies addressed limits in terms of column depth (Zhang and Ricles, 2006b; Zhang and Ricles, 2006), given the benefits of deep columns in controlling seismic drifts. Tests were also conducted on up to W27 column sections, which have an average depth of 700mm (Uang et al, 2000; Chi and Uang, 2002). These studies raised attention to the susceptibility of the deep columns to twisting, which could deteriorate the inelastic performance of the RBS. This showed that RBS members are more prone to Lateral-Torsional Buckling (LTB), due to the decreased area of their flanges. Also, deep column sections tend to have a reduced torsional resistance, particularly that torsion can be introduced to the column by the eccentric lateral force developed by LTB of the beam. On the other hand, only one publication (Chen and Tu, 2004) has appears to have address the application of RBS to jumbo beam sections, by applying a tapered cut profile.

Further experimental and analytical research focusing on the application of RBS to deep columns (Zhang and Ricles, 2006) indicated that the presence of a composite floor slab can greatly reduce the amount of twisting developing in the column, as it offers bracing to the beam and reduces the lateral displacement of the bottom flange. The presence of composite floor slabs has been investigated not only in relation to deep column twisting. Early research (Tremblay et al, 1997) indicated that shear studs should not be placed within the RBS region, in order to diminish any interference with the yielding mechanism, which can reduce the plastic rotation capacity; stud welds can also become the source of fractures. Besides improving the stability of the beam against LTB, the presence of the slabs was also found to increase the strength of the connection and the rotational capacity in positive bending (Jones et al 2002; Uang and Fan, 2001).

Based on early experimental and analytical studies, the first design recommendations for RBS connections were provided by FEMA-350 (2000b), concerning radius cut RBS for application in both Special (SMF) and Ordinary Moment Resisting (OMF) frames. Prequalification data included several limitations regarding the size of sections, weight and flange thickness, rendering the W36x150 as the largest allowed beam section. Additionally, the largest allowed column section size for SMFs was W14. A design procedure was also included, which has been also adopted by the later versions of AISC codes with some refinement. The concept was to size the RBS geometry in order to achieve a reduction in the developed moment at the column face, compared to the full plastic moment capacity of the beam.

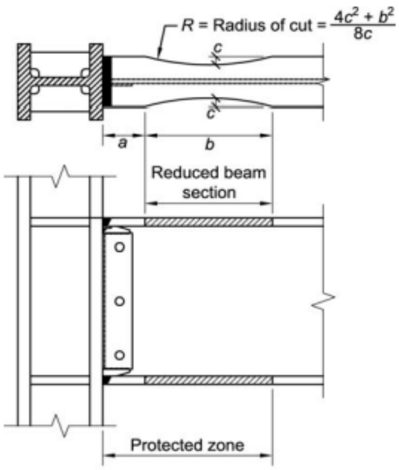

Figure 1.4: Configuration and dimensions of Reduced Beam Section Connections (ANSI/AISC 358, 2010a)

Prequalification of the radius cut RBS connection has been adopted in more recent ANSI/AISC 358 (2010a) with beam limitations similar to the ones included in FEMA-350 (2000b). The key design dimensions of a typical radius cut RBS connection are depicted in Figure 1.1. The current largest beam section allowed is the W36x300. Moreover, the permissible column section has been increased to W36, with no limitations regarding the column flange thickness or section weight. Further limitations concerning width-to-thickness ratios and lateral bracing of beams and columns imply conformance to the AISC Seismic Provisions (ANSI/AISC 341, 2010b). It is worth noting that the contribution of composite slabs in bracing is considered recent codes, while RBS connections in SMFs are limited to welded web connections.

At present RBS (or dog-bone) connections are not explicitly covered in Part 1 of Eurocode 8 (EN1998-1:2005). However, it is referred to in Part 3 is included in EN 1998-3:2005 as a retrofitting scheme to improve the ductility of beams. It is noted that RBS connections should have a rotational capacity of 40 mrad at the near collapse limit state. The proposed design procedure is essentially identical to those available in US guidelines, with some slight differences. Pachoumis et al. (2010) noted that limited research exists concerning the application of RBS to European profiles and conducted experimental tests and analytical work to evaluate the applicability of these recommendations in practice. It was concluded from that the RBS dimensions given in EN-1998-3:2005 may require alterations in order to be applied effectively to European sections. Therefore, information provided in EN 1998-3:2005 require further development and adaptation in order to be consistent with the design procedures provided in EN1998-1:2005.

Further information and recommendations on the behaviour and design of reduced beam section (RBS) connections is provided in subsequent sections of this report.

2 DESCRIPTION OF THE MAIN FEATURES OF THE TESTED JOINTS

Four bolted beam-to-column joint typologies are investigated within the project (namely (a) unstiffened extended end-plate bolted joints, (b) stiffened extended end-plate bolted joints, (c) haunched bolted joints, and (d) dog-bone welded joints (see Figure 2.1) designed to meet different performance levels. The bolted joints are designed according to a design procedure specifically developed within the project in the framework of EN 1993-1-8; The design of the dog-bone welded connections was compliant to US building code ASCE 7-10 (Minimum Design Loads for Buildings and Other Structures) and to the steel buildings specific standards AISC 341-16 (Seismic Provisions for Structural Steel Buildings), AISC 358-16 (Prequalified Connections for Seismic Applications) and AISC 360-16 .

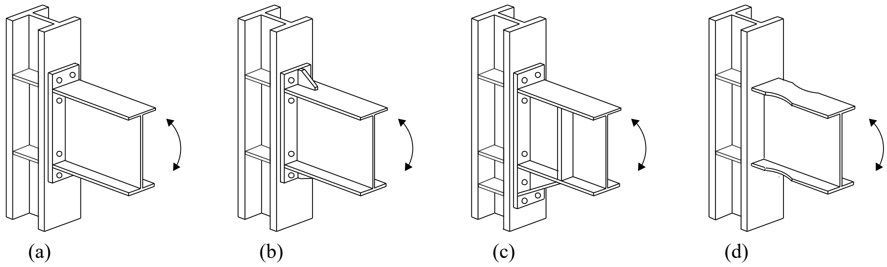

Figure 2.1: Beam-to-column joints prequalified in the framework of EQUALJOINTS project: a) Bolted haunched joint b) Bolted extended stiffened end-plate joint c) Bolted extended unstiffened end-plate joint d) Welded dog-bone joint

The investigated joints are proposed to be used for the following performance objectives:

- Full strength joint: all the plastic demand is concentrated in the connected beam, leaving the connection and the web panel free from the damage;
- Equal strength joint: the plastic demand is balanced between the joint and the connected beam;
- Partial strength joint: all the plastic demand is concentrated in the joint.

Moreover, in function of the resistance of the connection and column web panel for both equal and partial strength joint an addition classification can be introduced:

- Strong web panel: all the plastic demand is concentrated in the connection (partial strength joint) or in the connection and in the beam (equal strength joint);
- Balance web panel: the plastic demand is balance between the connection and the column web panel (partial strength joint), in the connection, in the web panel and in the beam (equal strength joint);

- Weak web panel: all the plastic demand is concentrated in the column web panel (partial strength joint) or in the web panel and in the beam (equal strength joint);

The experimental program (summarized in Table 2.1) includes 76 beam-to-column specimens by varying the joint typologies, the performance objectives, the joint configuration (internal/external joints), and the loading protocol (monotonic and two different cyclic loading protocols are used). In addition, the influence of shot peening will be investigated in order to verify its potential beneficial influence to enhance the local ductility in the welding between beam and extended end-plate of partial strength connections, which are expected to experience larger plastic deformation demands.

Table 2.1: **Experimental program: parameters of variation**

Parameter	Variation
Beam-to-column assembly	Small beam (1), medium beam (2), large beam (3) (see Table 2.2) *Dog-bone designed for W-type US profiles
Joint type	Haunched – Extended stiffened end-plate – Extended unstiffened end-plate – Dog-bone
Joint configuration	Internal/External
Performance objective	Full strength – Equal strength – Partial strength
Loading protocol	Monotonic – Cyclic AISC – Cyclic Proposed EU protocol
Shot Peening	Yes/No

Table 2.2: **Beam-to-column assemblies for bolted joints**

	Beam/column depth		
	1	2	3
Beam	IPE360	IPE450	IPE600
Column for exterior (T) joints	HEB280	HEB340	HEB500
Column for interior (X) joints	HEB340	HEB500	HEB650
Span in frame	6 m	6 m	8 m

Hereinafter, the experimental program and the relevant parameter of variation are described in detail with reference to each joint typology.

2.1 Haunched joints

The experimental program covers three groups of specimens:

- Group A: single-sided joint, full strength connection, shallow haunch (35° angle), strong web panel; two of the specimens (TSO) are fabricated with a strong beam;
- Group B: single-sided joint, full strength connection, steep haunch (45° angle), strong web panel;

- Group C: double-sided joint, full strength connection, shallow haunch (35° angle), balanced web panel.

Group 1 and Group 2 serve for qualifying two alternative haunch geometries (lower and upper limit of reasonable haunch angle) for considered range of beam size. Group 3 investigates joints with balanced panel zone strength, which also leads to a semi–rigid classification of the joint (connection and panel zone). Two supplementary web plates are used for the joints of Group 1 and Group 2, while for Group 3 only one supplementary web plate is used. Additionally, larger column depth increases the range of prequalified column sizes. The complete parameters considered within the experimental program are: loading protocol (monotonic and cyclic), member size, single-sided and double-sided connections, strong panel zone / balanced panel zone, strong beam and haunch geometry. Table 2.3 makes an overview of the parameters considered within the experimental program and describes the labelling of the specimens. As can be observed, the experimental program covers 24 tests on joint specimens, out of which three tests are performed under monotonic loading: EH2-TS-35-M, EH2-TS-45-M, and EH2-XB-35-M, in order to aid in calibration of finite-element models. All other tests are performed using cyclic loading. The ANSI/AISC 341-16 loading protocol is adopted for most of tests. Three of the cyclic tests (one for each beam size – CA series) are performed using a cyclic loading protocol developed within the EQUALJOINTS project.

Table 2.3: **Experimental program on haunched joints**

Group	Joint configuration	Haunch geometry	Loading protocol	Beam/column depth		
				1	2	3
1	TS	35°	M	-	EH2-TS-35-M	-
			C1	EH1-TS-35-C1	EH2-TS-35-C1	EH3-TS-35-C1
			C2	EH1-TS-35-C2	EH2-TS-35-C2	EH3-TS-35-C2
			CA	EH1-TS-35-CA	EH2-TS-35-CA	EH3-TS-35-CA
	TSO	35°	C	EH1-TSO-35-C	-	EH3-TSO-35-C
2	TS	45°	M	-	EH2-TS-45-M	-
			C1	EH1-TS-45-C1	EH2-TS-45-C1	EH3-TS-45-C1
			C2	EH1-TS-45-C2	EH2-TS-45-C2	EH3-TS-45-C2
3	XB	35°	M	-	EH2-XB-35-M	-
			C1	EH1-XB-35-C1	EH2-TS-35-C1	-
			C2	EH1-XB-35-C2	EH2-TS-35-C2	-

Notes:

- Joint configuration and panel zone: exterior joint with strong column web panel (TS), exterior joint with strong column web panel/strong beam (TSO), interior joint with balanced column web panel (XB);
- Haunch geometry: angle of haunch 35° (35), angle of haunch 45° (45);

- Loading protocol: monotonic (M), cyclic (C1, C2), alternative cyclic protocol (CA);
- For beam /column depths see Table 2.2.

2.1.1 Description of the joint configuration

Haunched extended end-plate beam-to-column connections are intended to provide a full-strength and rigid connection, with strong or balanced column web panel. The configuration of haunched extended end-plate beam-to-column joints is described in Figure 2.2. The connection uses an extended end-plate with high-strength bolts and it is reinforced using a haunch below the bottom flange of the beam.

Transverse column and beam stiffeners are mandatory. Supplementary web plates are optional, and it can be used to enhance the stiffness and strength of the column web panel.

Haunch angle is measured between the bottom flange of the beam and the flange of the haunch, and it can range from 30° to 45°.

Type of welds for which the haunched beam-to-column joints were prequalified are shown in Figure 2.3. All welds are designed to allow transfer of forces corresponding to the resistance of the welded parts. This is accomplished by using two fillet welds (both sides of the plate) with a minimum throat of 0.55 times the thickness of the plate. Critical welds (top beam flange, haunch flange, supplementary web plate to column flange) are full-penetration groove welds. Top beam flange and haunch flange groove welds are further reinforced with additional fillet welds.

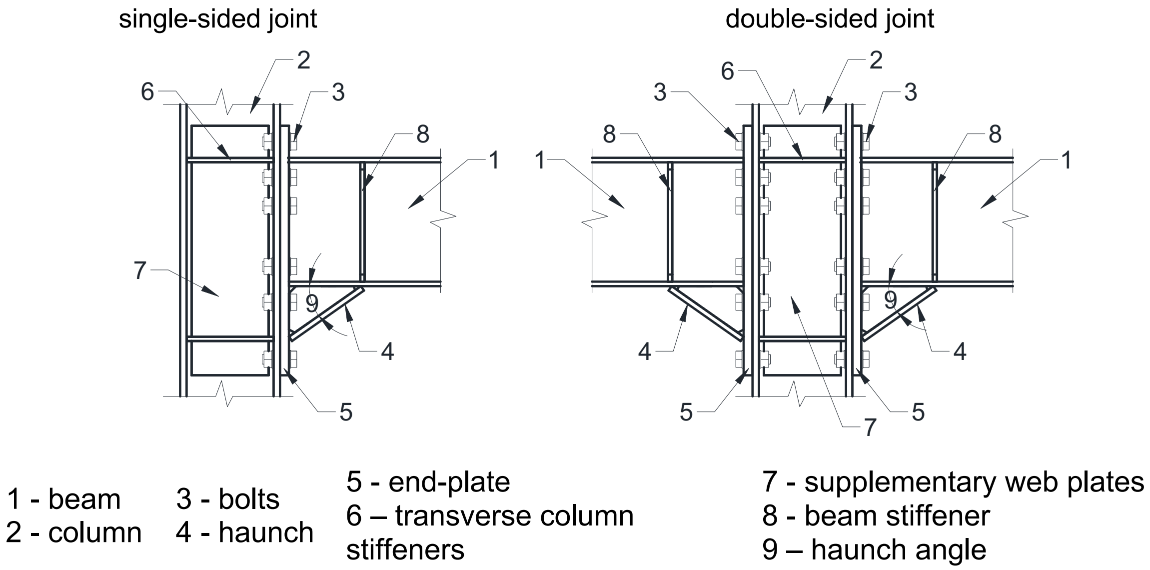

Figure 2.2: Description of haunched extended end-plate joints

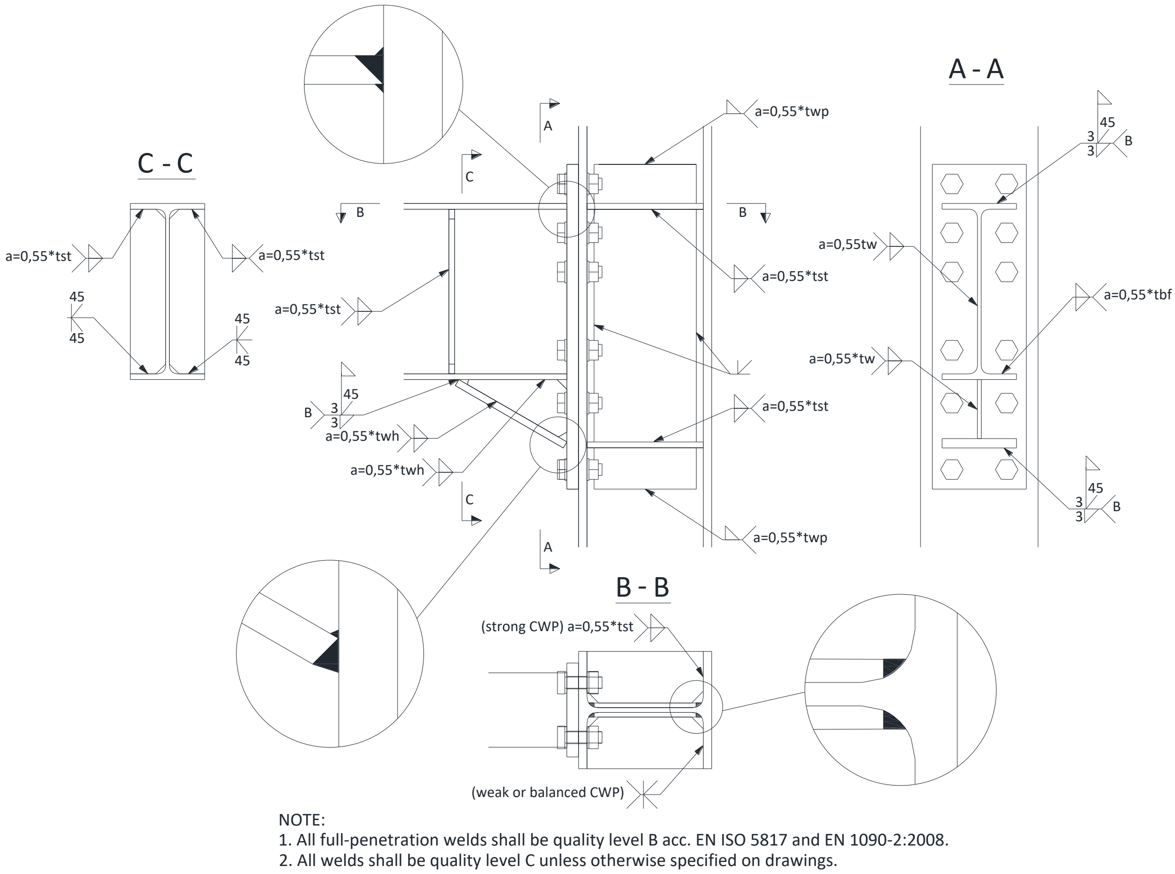

Figure 2.3: Weld details for haunched extended end-plate joints

2.1.2 List of systems for which connection is prequalified

Haunched extended end-plate beam-to-column connections described in this document are prequalified for the following structural systems:

- Moment Resisting Frames (MRFs);
- Dual Concentrically Braced Frames (i.e. MRF+ CBFs);
- Dual Eccentrically Braced Frames (i.e. MRF+ EBFs).

In addition, these joints should be used only in frames with perpendicular beam-column axis and regular span layout of the seismic resisting system, namely no sloped beams.

2.1.3 List of limit values for prequalified data

The limit values for prequalified data are listed in Table 2.4. In addition, the recommendations given in Table 2.5 can be used for initiating the connection geometries and materials.

Table 2.4: **Limit values for prequalified data for haunched joints**

Elements	Application range
Beam	Hot-rolled wide-flange beams ranging from IPE330 up to IPE600. Cross-section shall be class 1 according to EN 1993-1-1. Built-up beams with similar cross-section shape may be used, provided welds between the web and flanges are full-penetration groove welds reinforced with fillet welds.
Depth	330 to 600 mm
Clear span-to-depth ratio (between the assumed location of plastic hinges)	Minimum 7
Flange thickness	Minimum: 11 mm Maximum: 21 mm* (10% extrapolation with respect to the maximum tested)
Material	S235 to S355
Column	Hot-rolled wide-flange columns ranging from HEB260/HEM260 up to HEB550/HEM550. Cross-section shall be class 1 according to EN 1993-1-1. Built-up columns with similar cross-section shape may be used, provided welds between the web and flanges are full-penetration groove welds reinforced with fillet welds.
Depth	260 to 550 mm
Flange thickness	Minimum: 17.5 mm Maximum: 40 mm
Material	From S235 to S355
Beam/column depth	0.60-2.00
End-plate	20-40
Thickness	Minimum: 20 mm Maximum: 40 mm
Width	Minimum: beam flange with + 30 mm Maximum: column flange width
Material	From S235 to S355
Transverse column and beam stiffeners	According to requirements of EN 1993-1-8 and EN 1998-1.
Material	From S235 to S355
Supplementary web plates	According to requirements of EN 1993-1-8 and EN 1998-1. It is allowed to consider the full area of the supplementary web plates in computing the additional shear strength of column web panel.
Height	At least equal to the height of the end plate.
Material	From S235 to S355
Bolts	High strength structural bolting assemblies for preloading, according to EN 14399-3 (system HR) and EN 14399-4 (system HV). Bolts shall be fully preloaded according to EN 1090-2.
Size	M24 to M36

Table 2.4: **Limit values for prequalified data for haunched joints**

Grade	8.8 or 10.9
Holes	According to EN 1993-1-8
Haunch	
Angle	Haunch angle measured between the bottom flange of the beam and the flange of the haunch can range from 30° to 45°.
Welds	According to Figure 2.3.
End-plate to top beam flange and haunch flange	Reinforced full penetration groove welds
Continuity plates to column flanges	Full penetration groove welds
Supplementary web plates to column flanges	Full penetration groove welds
Other welds	Fillet welds both sides with a throat thickness greater than 0.55 time of the thickness the connected plates.

Note. Prequalification tests were performed on beams ranging from IPE360 to IPE600. The lower limit is extended to IPE330 as it represents less than 10% variation of the beam height, and smaller beam sizes were shown to be characterised by larger ductility in requalifying tests.

Table 2.5: **Initial choice of connection geometries and materials for haunched joints**

Connection elements	Beam sizes		
	Small (≈IPE360)	Middle (≈ IPE450)	High (≈ IPE600)
Bolt grade	10.9		
Bolt size	M27	M30	M36
Number of bolt rows	6	6	8
End-plate	*Thickness*: $t_{ep}=d_b$. *Dimensions*: The width should be larger than the beam flange width (by at least 30 mm in order to accommodate the weld) and smaller than the column flange. The extended part should be enough to position one bolt row, respecting the rules given in EN 1993-1-8 (§3.5).		
Haunch	Haunch flange width equal to beam flange width. Haunch flange thickness should be larger than γ_{ov} times the beam flange thickness. Haunch web thickness should be equal or larger than the beam web thickness. Haunch depth: h_h = 0.4*h_b for haunch angle of 30°≤ α <40°; h_h = 0.5*h_b for haunch angle of 40°≤ α ≤45°.		
Supplementary web plates	The thickness and the dimensions of the supplementary web plates should respect the rules given in EN 1993-1-8 (§ 6.2.6.1), otherwise plug welds should be used to guarantee the stability strength of the supplementary plates.		
Transverse stiffeners	Table 2.4		
Weld details	Table 2.4		
Note: t_{ep} is the thickness of the end-plate and d_b is the nominal diameter of the bolt.			

2.2 Extended stiffened end-plate beam-to-column joints

Stiffened end-plate connections (see
Table 2.6) cover three groups of specimens, as follows:

1. Exterior (TS) joint, stiffened end-plate connection, full-strength connection with strong web panel
2. Exterior (TS) joint, stiffened end-plate connection, equal strength connection with strong web panel
3. Interior (XS) joint, stiffened end-plate connection, equal strength connection with strong web panel

All specimens are made of S355 steel grade. Groups 1 and 2 serve for qualifying joints according to two alternative performance criteria applied to stiffened extended end-plate connections (full-strength and equal strength) for the considered range of beam sizes; the column web panel is designed to be over-strong respect to the connection zone in both cases. In addition, shot peening (Esp) will be investigated in Group 2. Group 3 investigates internal joints with strong column web panel (XS). There are 6 cyclic tests (2 per beam size) in each group. There are 6 cyclic tests (2 per beam size) in each group. In the first group there are 2 more monotonic tests in order to clearly evaluate the influence of the beam-to-column ratio. Also, there is one cyclic test with the alternative load protocol. Additionally, in Group 2 (TS configuration equal strength connections) there are three cyclic tests (one for each beam size) for specimens with shot-peening applied to welds. Connections in Group 2 are likely to have the largest demands in welds, so shot-peening may prove to be beneficial.

Table 2.6: **Specimen parameters and designations for stiffened end-plate beam-to-column connections**

Group	Connection type	Joint configuration	Connection strength	Loading protocol	Beam/column depth		
					1	2	3
1	ES	TS	F	M	ES1-TS-F-M	ES2-TS-F-CA	ES3-TS-F-M
	ES	TS	F	C1	ES1-TS-F-C1	ES2-TS-F-C1	ES3-TS-F-C1
	ES	TS	F	C2	ES1-TS-F-C2	ES2-TS-F-C2	ES3-TS-F-C2
2	ES	TS	E	C1	ES1-TS-E-C1	ES2-TS-E-C1	ES3-TS-E-C1
	ES	TS	E	C2	ES1-TS-E-C2	ES2-TS-E-C2	ES3-TS-E-C2
	ES	TS	Esp	C	ES1-TS-Esp-C3	ES2-TS-Esp-C3	ES3-TS-Esp-C3
3	ES	XS	E	C1	ES1-XS-E-C1	ES2-XS-E-C1	ES3-XS-E-C1*
	ES	XS	E	C2	ES1-XS-E-C2	ES2-XS-E-C2	ES3-XS-E-C2*

Notes:

- Connection type: stiffened end-plate beam-to-column connection (ES)
- Joint configuration: exterior joint and strong web panel (TS), interior joint and strong web panel (XS)
- Connection strength: full strength (F), equal strength (E), equal strength with shot-peening (Esp)
- Loading protocol: monotonic (M), cyclic (C1, C2, C3), alternative cyclic protocol (CA);
- Beam /column depths (see Table 2.2)
- * problems occurred due to unexpected premature failure of welds.

2.2.1 Description of the joint configuration

The joint configuration is described in Figure 2.4. Depending on the beam depth and the design criteria, 4 or 6 bolt rows can be adopted. The use of the additional plates is an option to reinforce the column web it is necessary, while the use of the continuity plates (transverse column stiffeners) is recommended for all cases.
Weld types prescribed in accordance with the design criteria are listed in Table 2.7, and depicted in Figure 2.5.

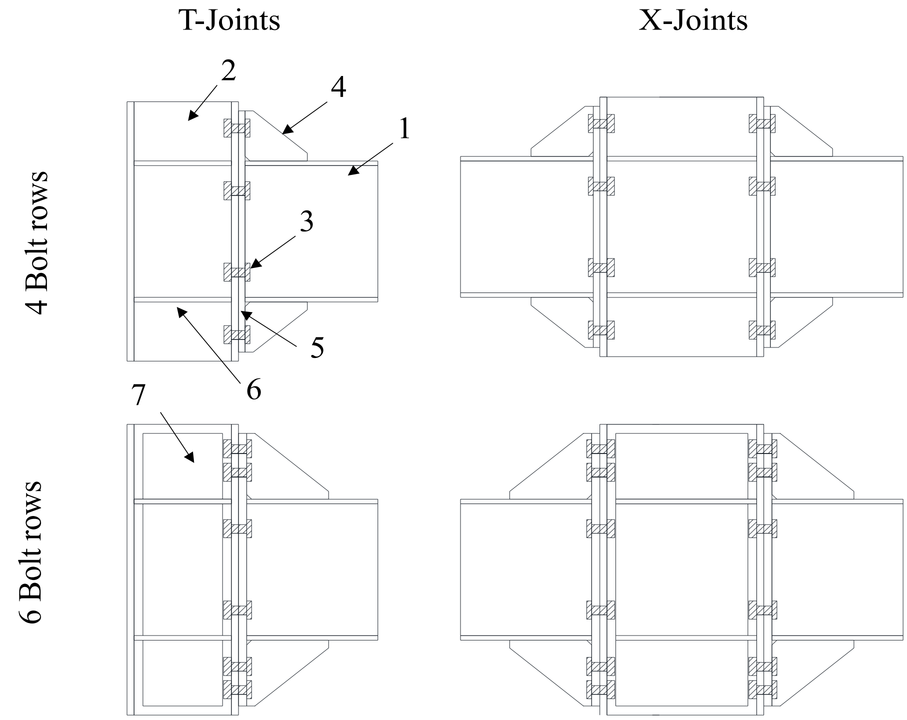

1: Beam	3: Bolts	5: End-plate	7: Supplementary
2: Column	4: Ribs	6: Continuity plates	plates

Figure 2.4: Description of stiffened extended end-plate joints

Table 2.7: **Weld types in accordance with the design criteria**

Welded Elements	Joint strength		
	Full	Equal	Partial
Beam flange to End-plate (bf-ep)	FPW	FPW	FPW
Beam web to End-plate (bw-ep)	FPW	FPW	FW
Continuity plates to column (cp-c)	FW	FW	FPW
Rib to End-plate (r-ep)	FPW	FPW	FPW
Rib to Beam flange (r-bf)	FPW	FPW	FPW
Supp. web plates to Column (Swp-c)	FPW+PW	FPW+PW	FPW+PW
Meaning of the acronyms: Fillet Weld (FW), Plug Weld (PW), and Full Penetration Weld (FPW)			

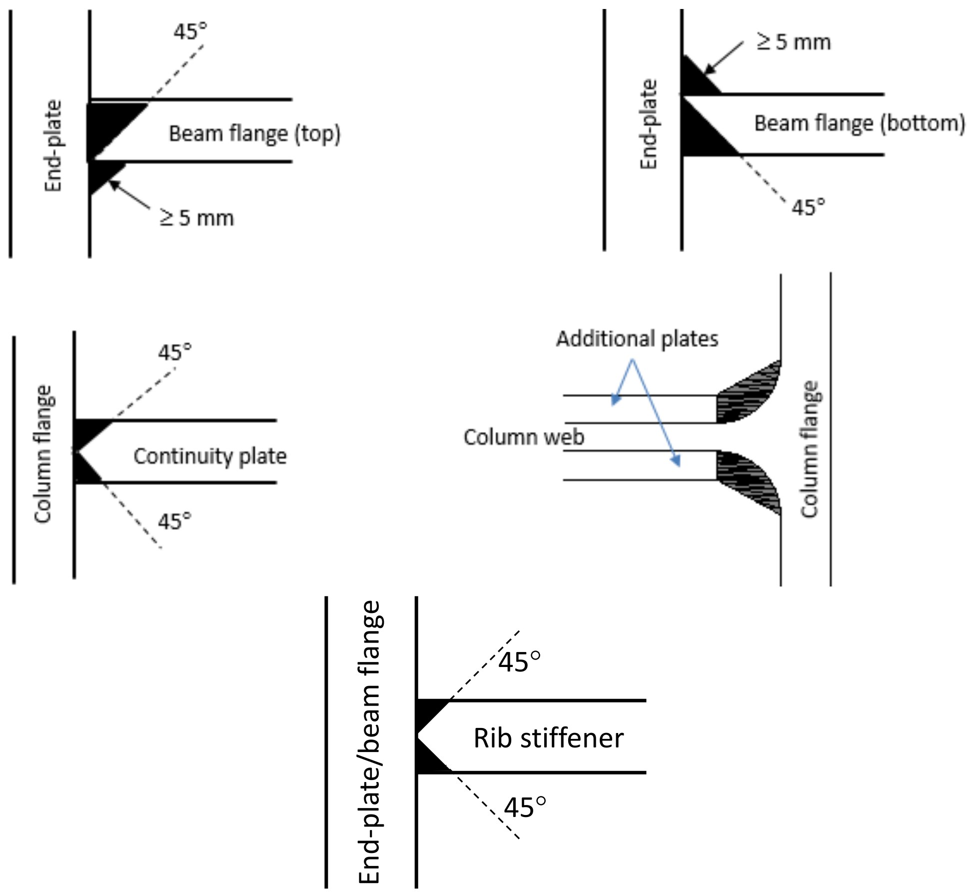

Figure 2.5: Joints Details of the groove full penetration welds

2.2.2 *List of systems for which connection is prequalified*

Extended stiffened end-plate bolted joints prequalified in this document can be used for the following structural systems:

- Moment Resisting Frames (MRFs);
- Dual Concentrically Braced Frames (i.e. MRF+ CBFs);
- Dual Eccentrically Braced Frames (i.e. MRF+ EBFs);

In addition, these joints should be used only in frames with perpendicular beam-column axis and regular span layout of the seismic resisting system, namely no sloped beam.

2.2.3 List of limit values for prequalified data

Limit values are listed in Table 2.8

Table 2.8: **Limit values for prequalified data**

Elements	Application range
Beam	
Depth	Maximum=600mm
Span-to-depth ratio	Maximum=23, Minimum=10
Flange thickness	Maximum=19mm
Material	From S235 to S355
Column	
Depth	Maximum=550mm
Flange thickness	Maximum=29mm
Material	From S235 to S355
Beam/column depth	0.65-2.15
End-plate	18-30mm
Thickness	Table 2.9
Material	From S235 to S355
Continuity plates	
Thickness	see Table 2.9
Material	From S235 to S355
Additional plates	
Thickness	see Table 2.9
Material	From S235 to S355
Bolts	Pre-loadable HV or HR
Size	see Table 2.9
Grade	10.9
Number of bolt rows	see Table 2.9
Washer	According to EN 14399-4
Holes	According to EN1993-1-8
Welds	See Table 2.7
End-plate to beam flanges	Reinforced groove full penetration (Figure 2.5)
Continuity plates to column flanges	Groove full penetration (Figure 2.5)
Additional plates to column flanges	Groove full penetration (Figure 2.5)
Other welds	Fillet welds: throat thickness greater than 0.55 time of the thickness the connected plates.

The recommendations given in Table 2.8 can be used for initiating the connection geometries and materials.

Table 2.9: **Initial choice of connection geometries and materials**

Connection elements	Beam sizes		
	Small (≈IPE360)	Middle (≈ IPE450)	High (≈ IPE600)
Bolt grade	HV 10.9		
Bolt size	M27	M30	M36
Number of bolt rows	4/6	4/6	6
End-plate	*Thickness*: t_{ep}=(2/3÷5/6) d_b for full joints it can be slightly larger than the column flanges; t_{ep}=(2/3÷5/6)d_b for equal joints; but should be less than the thickness of the column flanges. *Dimensions*: The width should be equal to or smaller than the column flange one. The extended part should be enough to position one or two bolt rows, respecting the rules given in EC3-1-8 (§3.5).		
Additional plates	The thickness and the dimensions of the additional plates should be respected the rules given in EC3-1.8 (§ 6.2.6.1), otherwise plug welds should be used to guarantee the stability strength of the supplementary plates.		
Continuity plates	Close to the thickness of the beam flanges		
Weld details	See Table 2.7		
Note: t_{ep} is the thickness of the end-plate and d_b is the nominal diameter of the bolt.			

2.3 Extended unstiffened end-plate beam-to-column joints

Unstiffened end-plate connections (see Table 2.10) are covered by three groups of specimens, as follows:

1. Exterior (TB) joint, unstiffened end-plate connection, equal strength connection with balanced web panel;
2. Exterior (TB) joint, unstiffened end-plate connection, 0.6 partial strength connection with balanced web panel;
3. Interior (XW) joint, unstiffened end-plate connection, 0.8 partial strength connection with weak web panel.

All joints are made of S355 steel grade elements. Groups 1 and 2 serve for qualifying joints according two alternative performance criteria applied to unstiffened extended end-plate connections (equal strength and 0.6 partial strength) for the considered range of beam sizes; the column web panel is designed to be balanced in comparison to the connection zone in both cases. In addition, shot peening (Psp) is investigated in Group 2. Group 3 investigates internal (XW) joints with weak column web panel.

There are at least 6 cyclic tests (2 per beam size) in each group as indicated in Table 2.10. In the first group there are also 2 monotonic tests in order to clearly evaluate the influence of cyclic loading on the joint response. Also, there is one cyclic test with the alternative load protocol. Additionally, in Group 2, there are three additional cyclic tests (one for each beam size) for specimens with shot-peening.

Table 2.10: **Specimen parameters and designations for unstiffened end-plate beam-to-column connections**

Group	Connection type	Joint configuration	Connection strength	Loading protocol	Beam/column depth		
					1	2	3
1	E	TB	E	M	E1-TB-E-M	E2-TB-E-M	E3-TB-E-CA
	E	TB	E	C1	E1-TB-E-C1	E2-TB-E-C1	E3-TB-E-C1
	E	TB	E	C2	E1-TB-E-C2	E2-TB-E-C2	E3-TB-E-C2
2	E	TB	$P_{(0.6)}$	C1	E1-TB-P-C1	E2-TB-P-C1	E3-TB-P-C1
	E	TB	$P_{(0.6)}$	C2	E1-TB-P-C2	E2-TB-P-C2	E3-TB-P-C2
	E	TB	$Psp_{(0.6)}$	C	E1-TB-Psp-C3	E2-TB-Psp-C3	E3-TB-Psp-C3
3	E	XW	$P_{(0.8)}$	C1	E1-XW-P-C1	E2-XW-P-C1*	E3-XW-P-C1
	E	XW	$P_{(0.8)}$	C2	E1-XW-P-C2	E2-XW-P-C2	E3-XW-P-C2

Notes:

- Connection type: unstiffened end-plate beam-to-column connection (E)
- Joint configuration: exterior joint and balanced web panel (TB), interior joint and weak web panel (XW)
- Connection strength: equal strength (E), 0.6 partial strength ($P_{(0.6)}$), 0.6 partial strength with shot-peening ($Psp_{(0.6)}$), 0.8 partial strength ($P_{(0.8)}$)
- Loading protocol: monotonic (M), cyclic (C1, C2, C3), alternative cyclic protocol (CA);
- Beam /column depths (see Table 2.2)
- As problems were encountered with the testing setup for this test, the results will not be discussed herein

2.3.1 Description of the joint configuration

The tested joint configuration is described in Figure 2.6. Depending on the beam depth, 4 or 6 bolt rows can be adopted. The use of the additional plates is an option to reinforce the column web when required, while the use of the continuity plates (transverse column stiffeners) is recommended for all cases. The welds to be used between the different joint components are given in Figure 2.7.

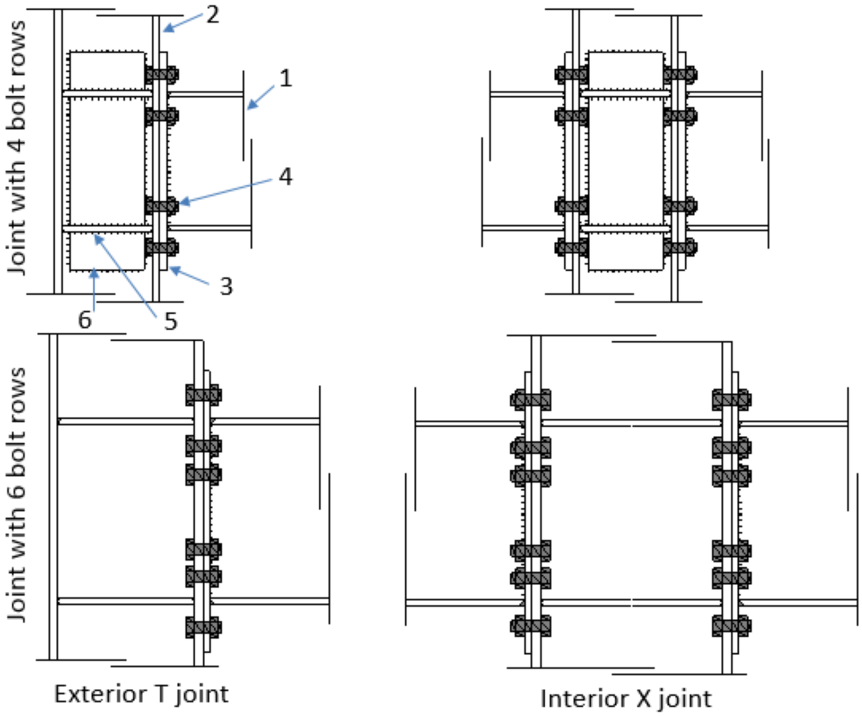

1: beam
2: column
3: end-plate
4: bolts
5: continuity plates
6: additional plates

Figure 2.6: Description of unstiffened extended end-plate joints

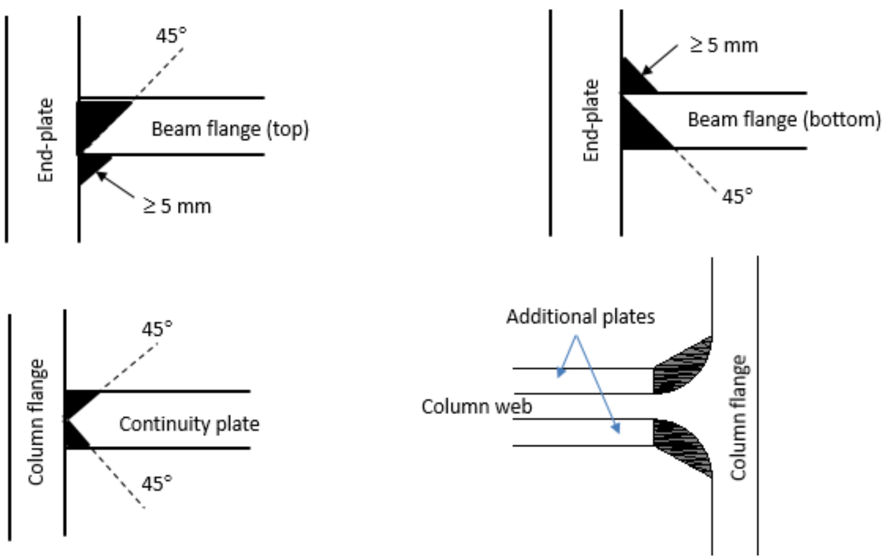

Figure 2.7: Details of the groove full penetration welds

2.3.2 *List of limit values for prequalified data*

Limit values are listed in Table 2.11.

Table 2.11: **Limit values for prequalified data**

Elements	Parameters	Application range
Beam		
	Depth	Maximum = 600mm
	Span-to-depth ration	Maximum = 23, Minimum = 10
	Flange thickness	Maximum = 19mm
	Material	From S235 to S355
Column		
	Depth	Maximum = 550mm
	Flange thickness	Maximum = 31mm
	Material	From S235 to S355
Beam/column depth		0.65-2.15
End-plate		
	Thickness	18-25mm
	Material	From S235 to S355
Continuity plates		
	Thickness	See Table 2.12
	Material	From S235 to S355
Additional plates		
	Thickness	See Table 2.12
	Material	From S235 to S355
Bolts	Pre-loadable	HV or HR
	Size	See Table 2.12
	Grade	10.9
	Number of bolt rows	See Table 2.12
	Washer	According to EN 14399-4
	Holes	According to EN1993:1-8
Welds		
	End-plate to beam flanges	Reinforced groove full penetration (see Figure 2.7)
	Continuity plates to column flanges	Groove full penetration (see Figure 2.7)
	Additional plates to column flanges	Groove full penetration (see Figure 2.7)
	Other welds	Fillet welds: throat thickness is greater than 0.55 times the thickness of the connected plates.

The recommendations given in Table 2.12 can be used as a good guess for the definition of the connection geometries and materials.

Table 2.12: **Initial choice of joint geometries and materials**

Connection elements	Beam sizes		
	Small (≈IPE360)	Middle (≈ IPE450)	High (≈ IPE600)
Bolt grade	HV 10.9		
Bolt size	M27	M30	M36
Number of bolt rows	4	4	6
End-plate	*Thickness*: t_p=(1/2÷2/3)d for partial joints; t_p=(2/3÷5/6)d for equal joints; but should be less than the thickness of the column flanges. *Dimensions*: The width should be equal to the column flange one. The extended part should be enough to position one bolt row, respecting the rules given in EC3-1-8 (§3.5).		
Additional plates	With HEB columns and IPE beams, the additional plates are only to be considered when the strong web panel is required. The thickness and the dimensions of the additional plates should be respected, so by following the rules given in EC3-1-8 (§ 6.2.6.1).		
Continuity plates	See Table 2.11		
Weld details			
Note: t_p is the thickness of the end-plate and d is the nominal diameter of the bolt.			

2.4 Dog-bone connections

The dog-bone joints experimental program consists by 2 connection tests, as summarized in Table 2.13:

Table 2.13: **Specimen parameters and designations for dog-bone connections**

Specimen	Beam	Column	Doubler plate (in)	RBS cut		
				A (mm)	B (mm)	C (mm)
SP2	W44×230	W14×342	None	200.66	708.406	68.326
SP4	W44×408	W40×503	None	304.8	949.96	85.344

All beams are made of US Grade 50 and all columns are made of US Grade 65, in order to make sure the plastic hinge occurs at the beam. In addition, all features are given in US metrics, since this section is mostly oriented to US pre-qualification and US practitioners.

The geometry of these two beam-to-column assemblies is representative of multi-storey buildings of American practice. Indeed, the size of members is extracted from a reference 15 storey tall square office tower, designed for high seismic accelerations in San Francisco. Structurally it is made of Special Moment Frames (SMF) with RBS connections used exclusively for the seismic-load-resisting system. Frames are located at the perimeter and are typically three bays wide, except at the lower levels. In these frames, members are sized to control drift to acceptable limits. Large members are required at the lower levels, many of which exceed current prequalification limits for RBS connections.

3 EXPERIMENTAL SETUP AND MEASUREMENT INSTRUMENTATION

3.1 Experimental setup

The experimental setups have been individually designed by the partners involved in the experimental activity (i.e. UNINA, UPT, ULiege, AM) compatibly with the facility of each laboratory and to assure loading procedure and data measurements consistent among all joint specimens. In detail, due to the specific need of the laboratories, haunched joints are tested vertically and the force is applied at the tip of the column (see Figure 3.1a), while the other ones are tested horizontally with the force applied at the tip of the beam(s) (see Figure 3.1b).

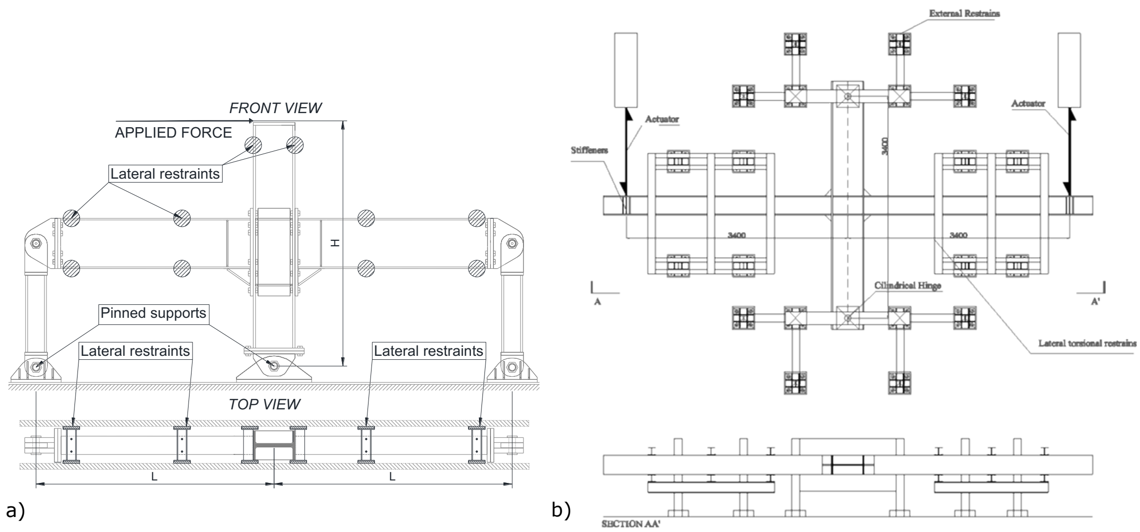

Figure 3.1: Test setups (a) joint tested vertically (b) joint tested horizontally

For what concerns the measuring instrumentation, displacement transducers have been used to record the deformation of the specimens during the tests. A representative transducers location is shown in Figure 3.2 for joint specimens tested in Naples.

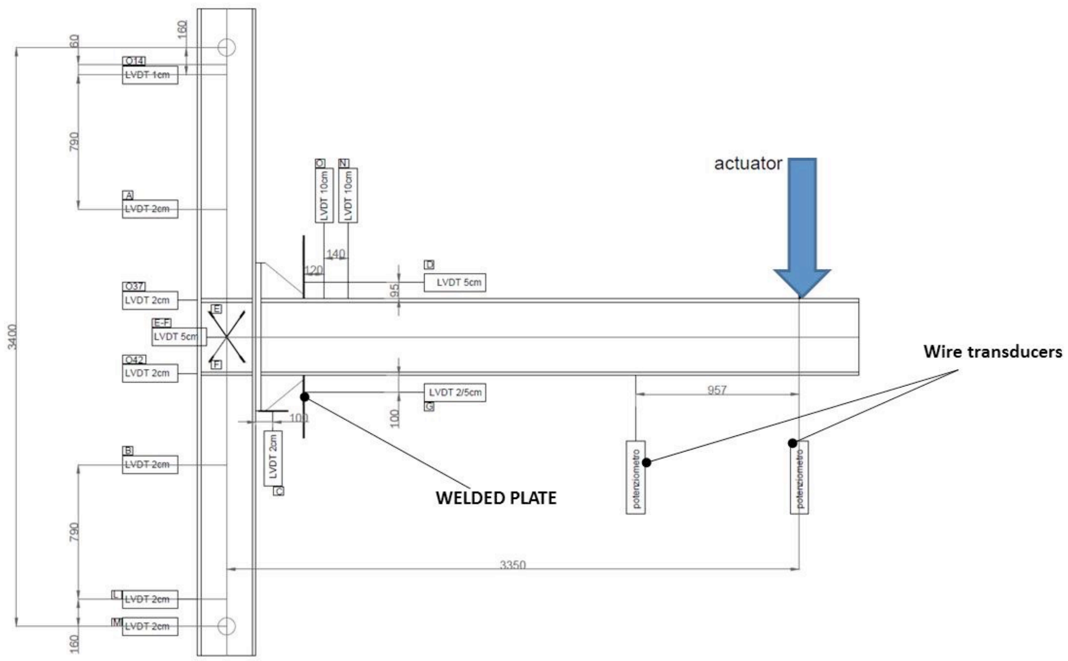

Figure 3.2: Measurement instrumentation used by the University of Naples

With this distribution of displacement transducers, the key deformations that are necessary to characterize the joint behaviour can be derived, in detail:

Transducers 1 e 2 are located at the cylindrical hinges in order to measure the column rigid rotation;

Transducers 3 e 4 are located along the column length in order to evaluate the displacement due to the column elastic rotation;

The panel zone rotation is given by transducers 5-6 diagonally fixed on the panel at the level of continuity plates

Transducers 7 is located at the end-plate upper tip in order to evaluate eventually slip of the end-plate.

The joint rotation is measured by transducers 8-9 fixed at the ribs tip.

Transducers 10-11 are located in the beam zone where the plastic hinge is expected in order to appreciate eventually plastic rotation of the beam.

In order to measure the girder displacements, two wire transducers have been located at beam ends as shown in Figure 3.2.

3.2 Loading procedure

Test control parameters:

Parameters used to control the tests on beam-to-column joints are interstorey drift θ of test assembly and bending moment *M* at the column centerline. It should be noted

that test control parameters θ and M are used primarily for load application, relating directly to lateral displacement at the tip of the column/beam δ and actuator force F which are usually used to control a test. Additional measurements and parameters are used in order to characterize response of the specimen.
For the test setups in which the actuator is applied at the tip of the column (namely for test setup of haunched joints), these parameters are defined by the following expressions (see Figure 3.3a):

$$\theta = \delta_{beam}/L_{beam} \tag{3.1}$$

$$M = F_{beam} \cdot L_{beam} \tag{3.2}$$

$$\delta_{beam} = \delta \cdot L_{beam}/L_{column} \tag{3.3}$$

$$F_{beam} = F \cdot L_{column}/L_{beam} \tag{3.4}$$

where:
θ is the interstorey drift of the test assembly;
M is bending moment at the column centerline;
δ is deformation of the beam-to-column joint assembly, defined as the lateral displacement at the tip of the column, "cleared" of any support displacements;
L_{beam} is beam length to column centerline;
L_{column} is column length;
F is force applied at the tip of the column;
δ_{beam} is deformation of the tip of the beam;
F_{beam} is reaction force at the tip of the beam.
Load is to be applied in displacement control. In the elastic range load can be applied in force control if needed.
For the test setups in which the actuator is applied at the tip of the beam(s)
Parameters used to control the tests are the joint rotation θ and bending moment M, defined as follows (see Figure 3.3b):

$$\theta = \delta/L_{beam} \tag{3.5}$$

$$M = F \cdot L_{beam} \tag{3.6}$$

Where:
θ is the joint rotation;
M is the bending moment at the column centerline;

δ is the deformation of the beam-to-column joint assembly, defined as the lateral displacement at the tip of the beam; eventually sources of deformability due to support displacements are deducted.
L_{beam} is beam length to column centerline;
F is force applied at the tip of the beam.

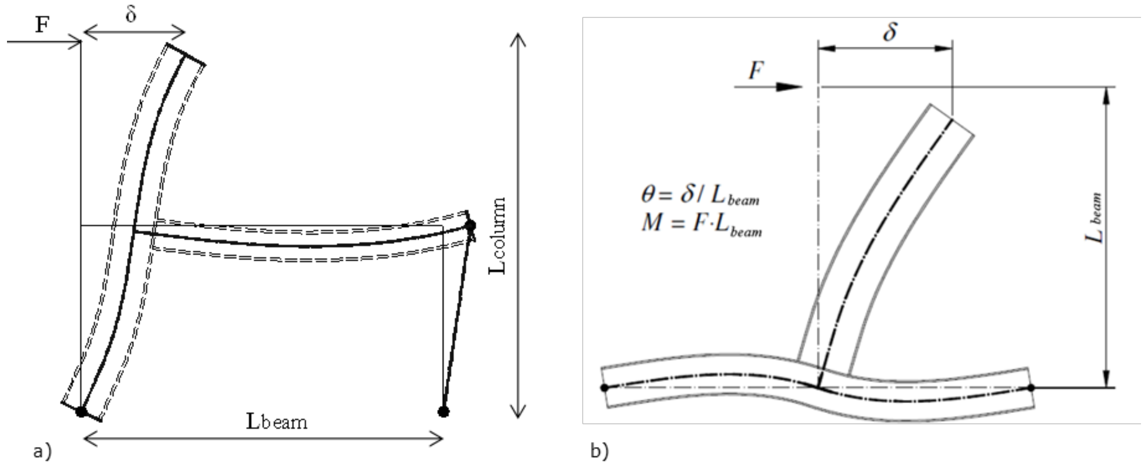

Figure 3.3 Definition of parameters for beam-to-column joints tested applying the force (a) at the tip of the column b) at the tip of the beam

3.2.1 Loading rate

A quasi-static loading should is used in the tests. Loading rate is small enough so that strain rate effects do not affect the results. It should be noted that apparently the loading rate to be used in test on beam-to-column joints is not properly addressed in current codes.
EN ISO 6892-1 (2009) provides the following values for tensile tests:
in the elastic range: 6-6.60 MPa/s (if stress control is used);
at yielding plateau: $\dot{\varepsilon}$ =0.00025 – 0.0025s^{-1} (if strain control is used);

3.2.2 Preloading

A few pre-test load cycles is applied to the test assembly before the test itself in order to stabilize the system and check the operation of the equipment. It is recommended to use two or three alternating cycles with a peak load of up to 25% of the expected yield load.

3.2.3 Monotonic loading

Monotonic loading is applied by progressively increasing the displacement at the tip of the column. Several unloading-reloading phases are applied in order to estimate the initial stiffness, even when the specimen is in the plastic range. It is recommended that the unloading correspond to specimen interstorey drift of θ = 0.02 rad and 0.03 rad

Loading could be paused several times during the test, by keeping the actuator displacement constant in order to assess the influence of strain rate, until the applied actuator force is stabilized. It is recommended that these "relaxation" phases be applied at the yield interstorey drift θ_y and subsequently in increments of 0.01 rad (θ_y + 0.01 rad, θ_y + 0.02 rad, etc.).

3.2.4 Cyclic loading protocol

Two cyclic loading protocols will be used in the experimental program: ANSI/AISC 341-16 (2016) loading procedure and a specific protocol developed with the EQUALJOINTS project are summarized in the following table:

Equaljoints protocol		ANSI/AISC 341-16 (2016)	
No. Cycles	Drift Angle θ,rad	No. Cycles	Drift Angle θ,rad
2	0.0040	6	0.00375
2	0.0045	6	0.005
2	0.0051	6	0.0075
2	0.0061	4	0.0100
2	0.0075	2	0.0150
2	0.0096	2	0.0200
2	0.0124	2	0.0300
2	0.0163	2	0.0400
2	0.0218		
2	0.0293		
2	0.0400		

The ANSI/AISC 341-16 loading protocol is selected due to its wide acceptance in the research community. It has been previously used in extensive pre-qualification programs on US-specific connection typologies (ANSI/AISC 358-16). Moreover, the large number of tests already performed worldwide using this protocol facilitates comparison of performance of joints with respect to alternative connection typologies tested in the past. On the other hand, the EQUALJOINTS protocol is developed within the project, specifically conceived for European qualification being more representative of European seismic input. In Figure 3.4 the loading protocol derived within the project (a) and the ANSI/AISC 341-16 loading protocol are compared, also showing the relevant cumulative demand functions (CDF) (c), which gives the cumulated rotation that is imposed cycle by cycle.

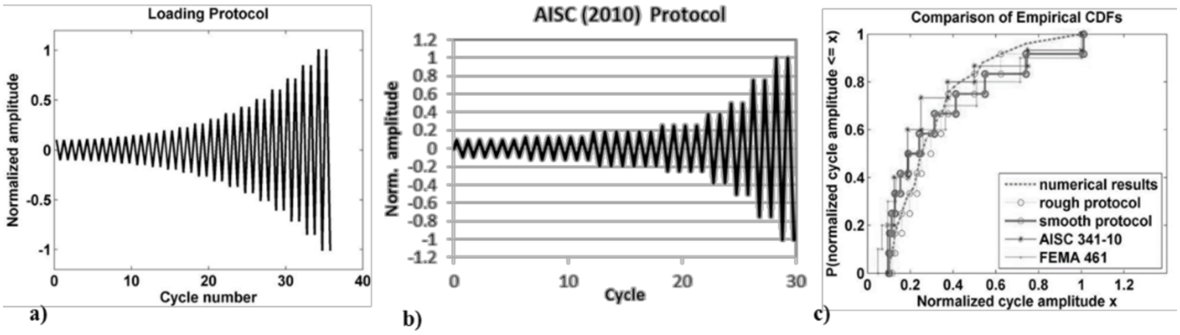

Figure 3.4 Loading protocol developed within EJ project (a) AISC 2010 loading protocol (b) comparison of CDF (c)

4 DESIGN PROCEDURE FOR QUALIFIED BOLTED JOINT TYPES

This Section provides design procedure developed within the Equaljoints project for the qualified bolted joint types.

4.1 General performance objectives

Strength criterion: According to EC8, the seismic design of steel structures is based on the concept of dissipative structures, where specific zones of the structures should be able to develop plastic deformation in order to dissipate the seismic energy. On the contrary, the non-dissipative parts should behave elastically under seismic action in order to avoid brittle collapse. The hierarchy of the resistances is the fundamental principle allowing this performance by detailing non-dissipative zones to resist the full plastic strength of the related dissipative members. The design criteria used within Equaljoints project aim at harmonizing the hierarchy requirements among the strengths of macro-components (e.g. the web panel, the connection, the beam and the column), and their sub-components (e.g. end-plate, bolts, welds, etc.), as well.

According to design procedure developed within the project, the joint is considered as made of three macro-components (i.e. the column web panel, the connection zone, and the beam zone, see Figure 4.1); each macro-component is individually designed according to specific assumptions and then simply capacity design criteria are applied, in order to obtain three different design objectives defined comparing the joint (i.e. web panel and connection) strength to the beam flexural resistance, namely (i) full strength, (ii) equal strength and (iii) partial strength joints.

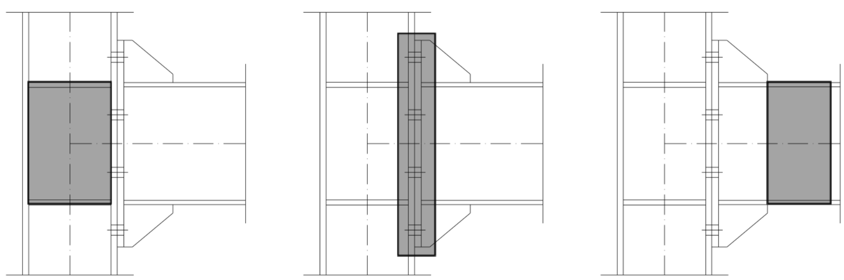

Figure 4.1: Plastic regions for the examined performance design objectives: a) web panel, b) connection and c) beam.

(i) Full strength connections are designed to guarantee the formation of all plastic deformations into the beam, which is consistent with EC8 strong column-weak beam capacity design rules.
(ii) Equal strength connections are theoretically characterized by the contemporary yielding of all macro-components (i.e. connection, web panel and beam).
(ii) Partial strength connections are designed to develop the plastic deformation only in the connection and web panel, in some cases.
It should be also noted that both EC3 and EC8 do not consider the case of equal strength joint, which is proposed within the project as an intermediate performance level. According to the current Eurocode classification, an equal strength joint falls on the category of partial strength.
The capacity design requirements to obtain the required joint behaviour can be guaranteed by satisfying the following inequality:

$$M_{wp,Rd} \geq M_{con,Rd} \geq M_{con,Ed} = \alpha \cdot \left(M_{\mathrm{B},Rd} + V_{B,Ed} \cdot s_h \right) \qquad (4.1)$$

Where $M_{wp,Rd}$ is the flexural resistance corresponding to the strength of column web panel; $M_{con,Rd}$ is the flexural strength of the connection; $M_{con,Ed}$ is the design bending moment at the column face; α depends on the design performance level. It is equal to $\gamma_{sh} \cdot \gamma_{ov}$ for the full strength joints (being γ_{ov} the overstrength factor due to the material randomness, and γ_{sh} the strain hardening factor corresponding to the ratio between the ultimate and the plastic moment of the beam), while equal to 1 for equal strength joints and smaller than 1 for partial strength joints. In order to avoid too severe damage concentration in the connection zone, the strength ratio for partial strength joints is assumed equal to 0.6 or 0.8. $M_{B,Rd}$ is the plastic flexural strength of the connected beam; s_h is the distance between the column face and the tip of the stiffener (rib or haunch); $V_{B,Ed}$ is the shear force corresponding to the occurring of the plastic hinge in the connected beam; it is given by:

$$V_{B,Ed} = V_{B,Ed,M} + V_{B,Ed,G} \qquad (4.2)$$

where $V_{B,Ed,M}$ is the shear force due to the formation of plastic hinges at both beam ends, spaced by the length L_h and calculated as:

$$V_{B,Ed,M} = \frac{2 \cdot M_{B,Rd}}{L_h} \qquad (4.3)$$

$V_{B,Ed,G}$ is the contribution due to the gravity loads; it should be noted that this amount does not account for the distance between the column face and plastic hinge and L_h is the approximate distance between plastic hinges.
Concerning both the overstrength factors, further considerations are necessary: γ_{ov} is assumed equal to 1.25, as recommended by EC8. The strain hardening factor γ_{sh} is assumed differently by EN1993-1-8 and EN1998-1. In particular, EN1993-1-8 recommends to consider an overstrength ratio equal to 1.2 for full strength joints, while EN1998-1 contradictorily assumes a value equal to 1.1. Several empirical equations are available in literature to estimate the flexural overstrength γ_{sh} developed by steel beams. Based on the main findings obtained by Mazzolani and Piluso (1992), D'Aniello et al (2012), Güneyisi et al (2013, 2014) it can be argued that γ_{sh} factor ranges within 1.1-1.2 for European profiles commonly used for beams (e.g. IPE), thus larger than the value recommended by EC8, but in line with AISC358-10 that assumes the following overstrength factor:

$$\gamma_{sh,AISC} = \frac{f_y + f_u}{2 \cdot f_y} \leq 1.20 \tag{4.4}$$

Therefore, in the current procedure γ_{sh} is conservatively assumed equal to 1.20, based also on the characteristic yield and ultimate strength of European mild carbon steel grades.

Moreover, in function of the resistance of the connection and column web panel for both equal and partial strength joint an addition classification can be introduced:

- Strong web panel: all the plastic demand is concentrated in the connection (partial strength joint) or in the connection and in the beam (equal strength joint);
- Balance web panel: the plastic demand is balance between the connection and the column web panel (partial strength joint), in the connection, in the web panel and in the beam (equal strength joint);
- Weak web panel: all the plastic demand is concentrated in the column web panel (partial strength joint) or in the web panel and in the beam (equal strength joint);

<u>Ductility criterion</u>: The joint ductility depends on the type of failure mode and the corresponding plastic deformation capacity of the activated component. Figure 4.2 concisely depicts the dependency of failure mode on geometric properties and end-plate to bolt strength ratio (Jaspart, 1997). In abscissa it is reported the ratio

β between the plastic moment ($M_{pl,Rd}$) of the transverse section of the plates or column flanges, and the axial strength of the bolts ($F_{t,Rd}$), while the vertical axis reports the ratio η between the T-stub strength (F) over $F_{t,Rd}$. The strength for mode 1 in case of non-circular pattern depends on the ratio $v = n/m$, where m is the distance between the bolt axis and the flange-to-web expected location of the plastic hinge, and n is the minimum of the distance between the edge of the flange and the bolts axis or 1.25m.

In line with Figure 4.2, two possible ductility criteria can be adopted to avoid mode 3, namely:

Level-1: $\beta \leq 1$ this condition imposes either a failure mode I or failure mode II (but very close to mode I), which provide very high ductility.

Level-2: $\beta < 2$ and $\eta \leq 0.95$, this condition imposes a failure mode II with limited ductility, but avoiding brittle failure.

The level of ductility to be guaranteed obviously depends on the design objectives: it is crucial providing the larger ductility for equal and partial strength, less for full strength joints.

According to the EN1993-1-8, the joint rotation capacity should be checked if M_{jRd} is less than 1.2 $M_{B,pl,Rd}$ and two alternative ways can be pursued: 1) performing experimental tests; 2) controlling the thickness t of either end-plate or column flange, provided that the joint design moment resistance is governed by those components, which should satisfy the following inequality:

$$t \leq 0.36d\sqrt{\frac{f_{ub}}{f_y}} \tag{4.5}$$

where d is the nominal bolt diameter, f_y is the yield strength of the relevant basic component and f_{ub} is the bolt ultimate strength.

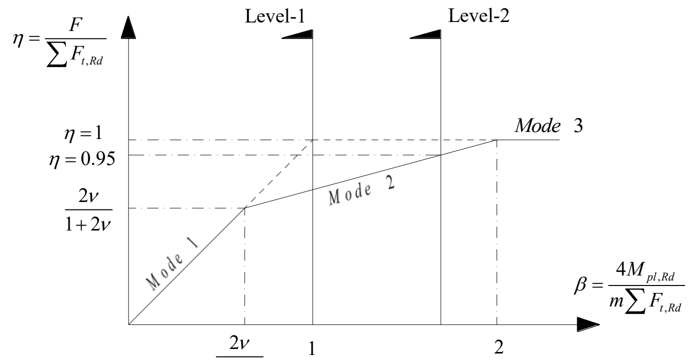

Figure 4.2: Ductility criterion: T-Stub resistance and corresponding failure mechanism

Eq. (4.5) would theoretically comply with the ductility Level-1 depicted in Figure 4.2, assuming that the resistance of each individual bolt ($F_{t,Rd}$) is greater than the resistance ($F_{p,Rd}$) of the connected plates (end-plate or column flange). In particular, the design resistance of a bolt in tension ($F_{t,Rd}$) is given as follows:

$$F_{t,Rd} = \frac{0.9 A_s f_{ub}}{\gamma_{M2}} \tag{4.6}$$

where A_s is the tensile stress area of the bolt and γ_{M2} is the relevant partial safety factor (i.e. Eurocode recommended value is equal to 1.25).
In addition, Eq. (4.5) uses the design resistance ($F_{p,Rd}$) corresponding to a circular mechanism, which can be assumed as follows:

$$F_{p,Rd} = \frac{\pi t^2 f_y}{\gamma_{M0}} \tag{4.7}$$

where t is the plate thickness and γ_{M0} is the relevant partial safety factor (recommended equal to 1).
It should be noted that Eq. (4.6 and 4.7) assume perfectly plastic behaviour of steel plates. However, in light of the considerations previously discussed, the ductility Level-1 for seismic resistant Partial strength joints should be expressed accounting for both the random variability of plate material and its relevant strain hardening, so that the following inequality can be used:

$$F_{t,Rd} \geq \gamma \cdot F_{p,Rd} = \gamma_{ov} \cdot \gamma_{sh} \cdot F_{p,Rd} \tag{4.8}$$

The overstrength factor γ in Eq. (4.8) can be taken equal to 1.5, since the Eurocode recommended value for γ_{ov} is equal to 1.25, the value for γ_{sh} is equal to 1.2 for European mild carbon steel, and the recommended partial safety factor γ_{M0} is equal to 1.0. Thus, rearranging the inequality (4.8) with Eq. (4.6), the ductility condition accounting for capacity design criteria can be expressed as following:

$$t \leq \frac{0.42 \cdot d}{\sqrt{\gamma_{ov} \cdot \gamma_{sh}}} \cdot \sqrt{\frac{\gamma_{M0} \cdot f_{ub}}{\gamma_{M2} \cdot f_y}} \cong 0.30 \cdot d \cdot \sqrt{\frac{f_{ub}}{f_y}} \tag{4.9}$$

Regarding full strength joints, even though either no or poor ductility should be exploited respectively, a local hierarchy criterion is advisable in order to avoid undesirable failure mode in the brittle components due to material variability. Hence, in line with ductility Level-2, the strength of bolts should satisfy the following inequality:

$$F_{t,Rd} \geq \gamma_{ov} \cdot F_{p,Rd} \tag{4.10}$$

Eq. (4.10), can be rearranged and after some algebraic manipulations it provides a similar criterion given by Eq. (4.5),
It is important to highlight that all criteria previously described require that failure of welds has to be unquestionably avoided, because of their brittle collapse mechanism.

4.2 Design assumptions for connection zone

The connection zone (see Figure 4.1b) includes the equivalent T-Stubs of the bolt rows belonging to end-plate, the column flange and the stiffeners if present (haunch/rib stiffeners).

4.2.1 Active bolt rows in tension

Differently from the component method implemented in EN1993:1-8, where all bolt rows in tension are rigorously obtained by imposing the equilibrium with compression internal resultant, the number of active bolt-rows in tension is assumed *a-priori* as shown, since the contribution of bolt rows below the central axis of the connection is reasonably negligible under pure bending condition (Maris et al., 2015, Stratan et al., D’Aniello et al, 2017; Tartaglia and D’Aniello, 2017).

4.2.2 Centre of compression and lever arm

For end-plate joints covered by EN 1993-1-8 provisions, the compression centre is located in the middle of thickness of beam flange, or at the tip of the haunch in case of haunched joints. Experimental and numerical results showed that the location of compression centre depends on both the joint type and the rotation demand due to the formation of plastic modes with different engagement of each joint component. According to the proposed design procedure and based on both experimental and numerical results from literature (Lee, 2002; Lee et al, 2005; Abidelah et al, 2012) and achieved within the project condition (Maris et al., 2015, Stratan et al., D’Aniello et al, 2017; Tartaglia and D’Aniello, 2017), the location of compression centre is assumed as follows: (i) in the middle of thickness of beam flange for unstiffened end-plate joints (see Figure 4.3a); (ii) at the centroid of the section made by the beam flange and the rib stiffeners, for the stiffened end-plate joints (see Figure 4.3b); (iii) at 0.5 the haunch height h_h, in case of haunched joints (see Figure 4.3c).

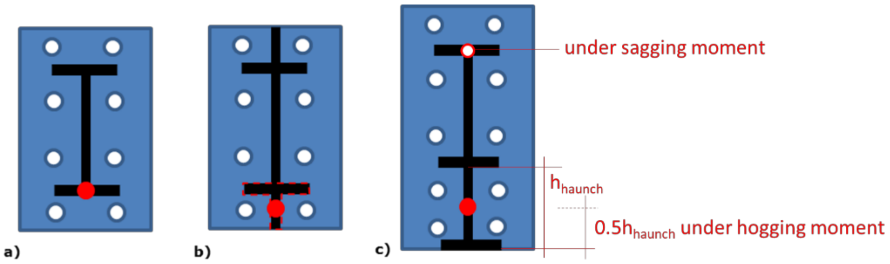

Figure 4.3: Location of compression centre (see the red circle) for different types of joint: (a) unstiffened end-plate (b) stiffened end-plate (c) haunched connections

4.2.3 Presence of rib stiffeners in ES joints

At current stage, the presence of the rib stiffener is not properly addressed by EC3. With this regard, analytical and semi-empirical formulations given by literature and validated by numerical simulations are assumed within the developed design procedure and described hereinafter. The design strength and stiffness of rib are assumed on the basis of the equivalent truss model provided by Lee (2002) (see Figure 1.2), which defines the equivalent strut area of the rib, A_e, as follows:

$$A_e = \eta \cdot h_e \cdot t \tag{4.11}$$

where η is the equivalent strut area factor and it is equal to 1.5; t is the rib thickness; h_e is the width perpendicular to the strut line (see Figure 1.2a) and it is defined as:

$$h_e = \frac{ab - c^2}{\sqrt{(a-c)^2 + (b-c)^2}} \tag{4.12}$$

Being a, b and c the dimensions of rib plate as shown in Figure 1.2. Based on the available experimental and analytical database (Lee, 2002; Lee et al, 2005; Abidelah et al, 2012; Tartaglia et al, 2016; D'Aniello et al, 2017) the slope θ of the rib can be assumed within the range 30°-40°. The lower limit of 30° is prescribed by AISC 358-10, while the upper limit of 40° is assumed in the present study in order to minimize the design bending moment acting on the connection.

The design forces acting on the rib stiffeners at the beam/column-to-rib interface (see Figure 1.2b) should be evaluated as follows:

$$N = \left(\frac{b}{a}\right) \cdot Q \tag{4.13}$$

$$Q = \frac{\dfrac{ad_b \cdot \left(0.21a + 0.51L^{'}\right)}{I_b}}{\dfrac{1}{\eta} \cdot \dfrac{0.6\sqrt{a^2+b^2}\sqrt{\left(a-c\right)^2+\left(b-c\right)^2}}{\left(ab-c^2\right)\cdot \mathrm{t}} + \dfrac{\left(0.81b+0.13d_b\right)\left(ad_b\right)}{I_b}} \cdot V_{B,Ed} \tag{4.14}$$

where d_b and I_b are the depth and second moment of area of the beam, respectively. $V_{B,Ed}$ is the design shear force.
The rib stiffener influences the shape of T-Stub mechanisms, which also depend on the number of bolt rows due to possible occurrence of group effect. Two configurations with either one or two bolt rows placed above the beam flange are addressed. In the first case, the effective length is assumed as that for the stiffened column flange. In the second case, due to the group effect the effective length is computed as given by the Green Book P398.
Finally, the presence of rib stiffeners also influences the beam web in compression capacity. According to EN1993-1-8, the design compression forces acting on beam web component is given by the following:

$$F_{c,fb,Rd} = \frac{M_{b,Rd}}{d_b - t_{fb}} \tag{4.15}$$

where $M_{b,Rd}$ is the bending moment capacity of the transverse section of the beam; d_b is the beam height; t_{fb} is the beam flange thickness.
Eq. (4.15) is conceived for extended unstiffened end-plate connections, where the maximum bending moment corresponds to the plastic strength of the beam $M_{b,Rd}$. In case of ES joints, the compression forces acting on beam web component can be more rationally obtained as follows:

$$F_{c,fb,Rd} = \frac{M_{j,Ed}}{z} = \frac{M_{con,Ed}}{d_b + \xi b - 0.5t_{fb}} \tag{4.16}$$

where ξb is the position of the compression centre as shown in Figure 4.3b.

4.2.4 Design assumption for column web panel zone

The design shear force acting ($V_{wp,Ed}$) on web panel depends on the position of the centre of compression and the lever arm z_{wp}, as well. As previously discussed, the location of compression centre and thus the level arm depends on the joint type and the plastic engagement of each component.
rib strut mechanism enlarges the lever arm z_{wp}. Consequently, the web panel zone involved by the bending transfer mechanism is deeper than the case of unstiffened joints, which implies reducing the design shear forces. Therefore, in this study $V_{wp,Ed}$ is computed as follows:

$$V_{wp,Ed} = \frac{\sum M_{con,Ed}}{z_{wp}} - V_c \tag{4.17}$$

Where $\Sigma M_{con,Ed}$ is the sum of bending moments in the beam at the column face; V_c is the shear force in the column; z_{wp} is the internal lever arm. It is worth noting that only for the haunched and the stiffened end-plate joints examined in the project the lever arm of the connection z_{wp} is close to that obtained according to Fig. 6.15 of EN1993:1-8, namely:

$$\begin{gathered} z_{wp} \simeq \left(d_b + \xi b - 0.5 t_{f,b}\right) \text{ for tested haunched and stiffened joints} \\ z_{wp} \neq \left(d_b - t_{f,b}\right) \text{ for tested unstiffened joints} \end{gathered} \tag{4.18}$$

This assumption depends on the fact that for the examined stiffened joints the inner bolt rows are not active (or very low engaged), so that the corresponding lever arm is consistent with that allowed by Fig. 6.15 of current EN1993-1-8 provided that the center of compression is properly accounted for. On the contrary, the tested unstiffened joints have more inner bolt rows and their interaction with the column web panel is very significant. Hence, for the examined unstiffened joints it's necessary to consider the coupled behavior of the web panel and the connection, namely the entire joint response for the estimation of the shear resistance and, consequently, the internal lever arm according to EN1993-1-8 (section 6.2.7.2).
The design shear strength $V_{wp,Rd}$ of column web panel deserves some considerations. According to EN1993-1-8 $V_{wp,Rd}$ is given by the following:

$$V_{wp,\mathrm{R}d} = \frac{0.9 \cdot A_v \cdot f_y}{\sqrt{3} \cdot \gamma_{M0}} + V_{wp,add,Rd} \tag{4.19}$$

where $V_{wp,add,Rd}$ is the contribution to the web panel shear resistance due to the plastic hinges, which can be developed in the column flanges or continuity plates. This requisite allows plastic deformation of the column web panel, which could be acceptable at ultimate limit state for non-seismic condition and for seismic applications where dissipative joints are considered, as well. Indeed, EN1998-1 (clause 6.6.4(4)) accepts that column web panel shear deformation could contribute up to 30% of the plastic rotation capacity of the joint provided that this requirement would be verified on the basis of experimental test. However, this requirement collides with the requirements stated at clause 6.6.1(1)P, which clearly mandates that plastic hinges should form in the beams or in the connections of the beams to the columns. In both cases the general rules of EC8 implies that for calculated joints (i.e. not experimentally qualified) the plastic deformations are accepted in the beam or in the connection, keeping elastic the column web panel. In line with this statement, according to current design procedure the shear overstrength ($V_{wp,add,Rd}$) might be neglected if the design purpose is to guarantee column free from damage, because the column flange contribution is fully reached when the panel zone is in the post-yield range at a shear distortion about 4 times the yield rotation of web panel (Brandonisio et al, 2012). Moreover, allowing web panel developing $V_{wp,add,Rd}$ may lead to considerable post-quake residual deformations with significant out-of-plumb for deep columns, thus corresponding to large repairing costs. It is clear that, in the most of cases, web column should be strengthened by means of supplementary steel plates in order to increase the web area. However, it could be difficult to fulfil this purpose following the requirements of EN1993-1-8, which mandates that the thickness of the supplementary web plate should be lesser of equal to the column web thickness, neglecting any increase of the shear area for thicker plates or if a further supplementary web plate is added on the other side of the column web. AISC358-16 does not have this requirement. Cyclic tests carried out by Ciutina and Dubina (2008) showed that shear strength of panel zone resistance increases proportionally to the shear area. Hence, the shear area can be increased by the total section of the supplementary plates. Moreover, the web panel strengthened by means of supplementary web plates proves very stable behaviour with good ductility and rotation greater than 0.035 rad.

In line with such consideration, according to design procedure developed within the project, the contribution $V_{wp,add,Rd}$ is neglected for both full and equal strength joints. Moreover, the resisting shear area A_v is assumed as the sum of column shear area $A_{v,c}$ and the gross area of eventual additional web plates $A_{v,p}$.

4.3 Technological requirements

The construction of a structure undergoes several stages, each of which must be thoroughly thought. In structures that may be subject to seismic actions at some point of their use life, these considerations are especially significant. Joints between steel elements in this type of structures should always be designed, fabricated and erected such that fragile failure is avoided and a ductile mode of failure governs the collapse.

Designers must always bear in mind design requirements set by the relevant design standards. In Europe, EN1998 must be observed for the seismic design of structures, with significant reference to EN1993 for the design of steel structures and EN1993-1-8 in particular for the design of steel joints.

EN1993-1-8 defines all parameters relevant to the design of connections with respect to their strength and stiffness. Connections may be welded, bolted or combinations of bolts and welds may be used.

Bolted connections must be designed in accordance with EN1993-1-8, Section 3. Table 3.1 of the standard defines the bolt classes and their nominal yield and ultimate stresses. Table 3.3 of the same document sets out the minimum and maximum pitch, end and edge distances in order to ensure enough bearing capacity.

Connections are designed following the component resistance method. When the capacities of each component are calculated, a ductile failure mode (such as bolt bearing, bearing on the supporting element or on the plates) must be the governing criterion.

The design criteria for welded joints are described in EN1993-1-8, Section 4. In seismic design, welds are usually designed to be full strength and thus avoid weld failure (fragile failure mode).

When specifying the materials and dimensions, the engineer should always consider the standard available element dimensions and characteristics of the raw elements. For example, the fabricator can source standard plates of 10 or 12 mm thickness, designers should not specify 11mm thick plates, in order to avoid unnecessary machining as far as possible.

Material toughness and through-thickness properties are given in EN 1993-1-10. EN 1993-1-10 contains design guidance for the selection of steel for fracture toughness and for through-thickness properties of welded elements where there is a significant risk of lamellar tearing during fabrication, for constructions executed in accordance with EN 1090-2.

Detailed information on toughness oriented rules in EN 1993-1-10 is available in Nussbaumer et al (2011). According to this design manual, the $\sigma_{Ed} = 0.75\, f_y(t)$ value corresponds to the maximum possible “frequent stress”, where for the ultimate limit state verification yielding of the extreme fibre of the elastic cross section has been assumed ($\sigma_{Ed} = fy(t)$ /1.35 = 0.75 $fy(t)$). Consequently, the value $\sigma_{Ed} = 0.75\, fy(t)$ given by EN 1993-1-10 would correspond to the case of yielded cross section, and it can be presumably used for selection of material toughness and thickness in the seismic design situation.

The guidance given in Section 2 of EN 1993-1-10 shall be used for the selection of material for new construction. The rules shall be used to select a suitable steel grade from the European Standards for steel products listed in EN 1993-1-1.

The choice of Quality Class shall be selected from Table 3.1 EN 1993-1-10 depending on the consequences of lamellar tearing.

Depending on the Quality Class selected from Table 3.1, either: through thickness properties for the steel material shall be specified from EN 10164, or post-fabrication inspection shall be used to identify whether lamellar tearing has occurred.

Guidance on the avoidance of lamellar tearing during welding is given in EN 1011-2.

National choice is allowed through clauses listed in the Foreword to EN 1993-1-10.

Designers and fabricators must work closely together to ensure the accuracy and clarity of the drawings, which should indicate the details of connections, sizes and qualities of bolts and welds as well as the steel grades of the members as specified by EN 1998-1. On occasions, the designer fails to recognize situations where what has been drawn cannot actually be executed, for example due to a lack of adequate space for welding. Often several meetings are required before both parties are satisfied that the graphic representation of the design is correct and can be fabricated.

The fabrication of the elements, including assembly, transportation and erection on site, must all be carefully managed in order to ensure the final quality of the structure is appropriate.

Structures must be executed in accordance with the relevant execution standards, namely EN1090-2 in Europe and AISC 303-10 in the USA, which set minimum quality requirements. Based on experience some fabricators may choose to exceed these requirements, and thus avoid known issues that often arise during erection on site.

5 NON-LINEAR MOMENT-ROTATION RESPONSE ACCORDING TO EN1993-1-8

5.1 Generality

The flexural response curve of joints can be predicted by means of the component method implemented in EN1993:1-8. This methodology consists of identifying the sources of strength and deformability, which are generally known as joint components. Each component is schematized as an extensional spring characterized by an elastic perfectly plastic force-deformation (F-Δ) response and then combined into a mechanical model made up of those springs and rigid links. All components should be assembled in order to derive the joint moment-rotation response in terms of stiffness and resistance, being the latter governed by the resistance of the weakest component. The centre of compression is assumed in the mid-thickness of the beam compression flange. As it can be noted, according to the model adopted in EN 1993-1.8, the hardening and the geometrical nonlinearity effects are neglected.
In details, the strength calculation according to EN1993:1-8 of a bolted moment resisting joint involves three distinct steps:
1. Calculating the resistance of each bolt rows in the tension zone;
2. Checking if the total tension resistance can be realised, as it may be limited by either the shear resistance of the column web panel, or the resistance of the connection in the compression zone (i.e. the beam flange in compression of the crushing or buckling of column web).
3. Calculating the moment resistance $M_{j,Rd}$ as the sum of the tension forces multiplied by their respective lever arms, namely as follows.

$$M_{j,Rd} = \sum_r h_r F_{tr,Rd} \tag{5.1}$$

where $F_{tr,Rd}$ is the effective design tension resistance of bolt-row r; h_r is the distance from bolt-row r to the centre of compression; r is the bolt row number.
Since the tension strength of a bolt-row may be limited by the effects of forces in other rows in the bolt group, the effective design tension resistance of the bolt row as alone is considered as a potential resistance. The potential design tension resistance $F_{tr,Rd}$ for each bolt row should be determined in sequence, starting from the bolt row with the maximum lever arm up to the equilibrium with compressive strength is achieved. Moreover, the effective design tension resistance $F_{tr,Rd}$ at each bolt row in the tension zone should satisfy the following criterion:

$$F_{tr,Rd} = min\left(F_{t,fc,Rd}\,;\,F_{t,wc,Rd}\,;\,F_{t,ep,Rd}\,;\,F_{t,wb,Rd}\right) \tag{5.2}$$

being $F_{t,fc,Rd}$ the column flange bending and bolt strength; $F_{t,wc,Rd}$ the resistance of column web in transverse tension; $F_{t,ep,Rd}$ the end-plate bending and bolt strength; $F_{t,wb,Rd}$ the resistance of beam web in tension.

Moreover, in order to guarantee the internal equilibrium of plastic distribution of forces at each bolt-row the total design resistance $\sum_r F_{tr,Rd}$ should satisfy the following criterion:

$$\sum_r F_{tr,Rd} \leq min\left(V_{wp,Rd}\,;\,F_{c,wc,Rd}\,;\,F_{c,fb,Rd}\right) \tag{5.3}$$

where $V_{wp,Rd}$ is the column web panel strength; $F_{c,wc,Rd}$ is the design resistance of the column web in compression; $F_{c,fb,Rd}$ is the design resistance of the beam flange and web in compression.

Generally speaking, in case of semi-rigid bolted end-plate joints the rotational response is mostly governed by the deformation of the tension zone of the connection, which is formed by the column flange and the end-plate under tension and elongation of the bolts. The tension zone is modelled by means of "equivalent T-stubs" concept, which corresponds to two T elements connected through the flanges by means of one or more bolt rows. The mechanical equivalence between the T-Stub and the corresponding element at bolt row is obtained by means the effective length (l_{eff}) which converts the real yield line patterns (both circular and non-circular) into an equivalent T-stub. Depending on the geometry of the joint, different yield line patterns are possible, each of them characterized by an effective length of the equivalent T-stub. The shortest length corresponds to the minimum strength and is taken as the resistance of that bolt row. The bolt-to-stiffener (i.e. the beam flange or web, or the rib stiffener, etc.) distance significantly influences the strength of the equivalent T-stub. The closest is the bolt to the stiffener the larger is the T-Stub strength. Conversely, bolts adjacent to an unstiffened free edge result in a shorter length of equivalent T-stub, namely a smaller strength. In all cases, EC3 provides effective lengths of equivalent T-stubs for individual bolt rows and for bolt-rows as part of a group. However, EC3 does not clearly provide the effective lengths for the bolt-rows above beam flange in case of extended stiffened connections.

Once the effective length has been determined, the resistance of the T-stub can be calculated as the minimum of that corresponding to three failure modes, as illustrated in Figure 5.1, which are described as follows:

Mode 1 – it is characterized by the complete plasticization of the flange whereas the bolts are not involved in the failure mechanism (see Figure 5.1a).

Mode 2 – it is characterized by a combined mechanism of flange plasticization and failure of the bolts (see Figure 5.1b).
Mode 3 – it is characterized by the failure of the bolts and it does not involve any plastic engagement of the T-stub flange (see Figure 5.1c).
EC3 provides also criteria to predict the joint initial stiffness $S_{j,ini}$ that can be assessed by combining the stiffness of all basic components according to the following:

$$S_{j,ini} = \frac{Ez^2}{\mu \sum_i \frac{1}{k_i}} \tag{5.4}$$

where E is the steel Young modulus; k_i is the stiffness coefficient for basic joint component i; z is the lever arm; μ is a stiffness ratio that depends on the ratio of the applied moment to the moment resistance of the joint.

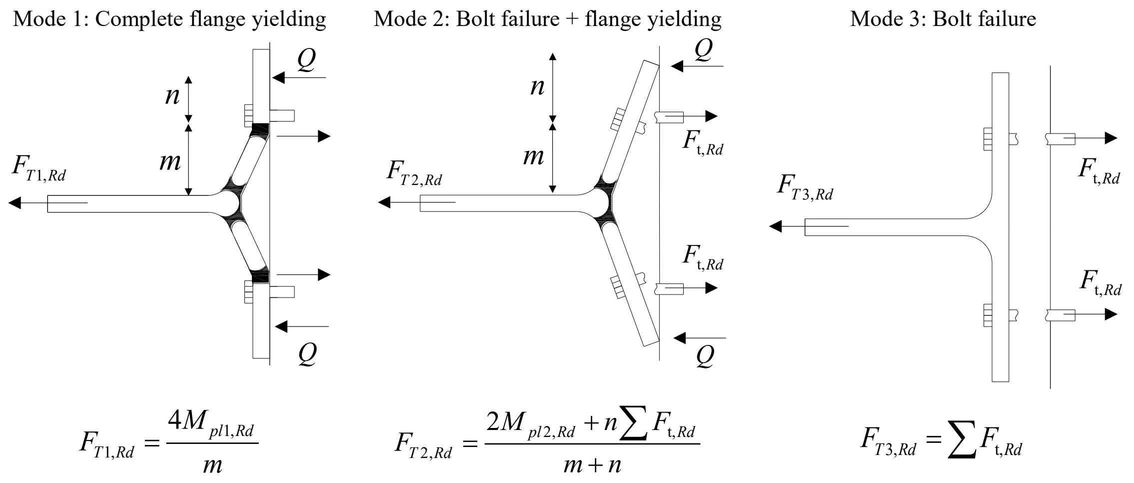

Figure 5.1: T-stub failure modes

5.2 Moment-rotation curves of haunched joints according to EN1993-1-8

The moment rotation curves used for the comparison with the experimental tests are computed according to EN1993-1-8. Additionally, based on the results of the EQUALJOINTS project, a modified approach based on EN 1993-1-8 was used. The main differences between the two approaches concern:

- the position of the center of compression
- the number of active bolts
- the resistance of the column web panel in shear

- the resistance of the beam flange and web component in compression

EN 1993-1-8 assumes that under hogging bending moment, for bolted extended end-plate connection with haunches, the center of compression is located at the middle of the haunch flange. According to the recent numerical simulations (Maris et al., 2015 and Stratan et al., 2016) it has been observed that the compression centre is located much higher, approximately at 50% from the haunch height. Therefore, in the modified design approach, the centre of compression under hogging moments was assumed to be at the mid-depth of the haunch. In the case of sagging bending moment, centre of compression is assumed to be located at the middle of the upper beam flange.

The second difference concern active bolt rows. In the modified design approach, it was assumed that only the bolt rows which are above the mid-depth of the beam cross-section (without haunch) are active under hogging moment. Under sagging moment, only bolt rows located beyond mid-depth of the beam cross-section including haunch we assumed active.

In what concerns the column web panel in shear, according to section 6.2.6.1 (6) from EN 1993-1-8, in the case of stiffened column web panel it is stated that the shear area A_{vc} may be increased with b_s t_{wc} (where b_s is the width of the supplementary plate and t_{wc} the thickness of the column web). Moreover, the resistance remains the same even if another web plate is added on the other side. According to the procedure from EQUALJOINTS, for the shear resistance of the web panel, the entire area corresponding to the added supplementary web plates was considered.

For haunched beams, EN 1993-1-8 determines the resistance of the beam flange and web in compression as the one corresponding to the cross-section of the beam (including the haunch) at section 1-1 in Figure 5.2, neglecting the intermediate beam flange. However, this assumption disregards the resistance of the beam at the end of the haunch (section 2-2 in Figure 5.2), which is the intended location of the plastic hinge. Therefore, instead of $M_{c,Rd}$ defined in in section 6.2.6.7 in EN1993-1-8, the modified procedure considered the plastic moment of the beam, projected at the column face, $M^*_{pl,Rd}$, determined according to the following expressions:

$$M_{con,Ed} = M^*_{pl,Rd} + V^*_{Ed} \cdot s_h$$

$$M^*_{pl,Rd} = \gamma_{sh} \cdot \gamma_{ov} \cdot W_{pl,beam} \cdot f_{y,beam}$$

$$V^*_{Ed} = \frac{2M^*_{pl,Rd}}{L_h} + V_{Ed,G}$$

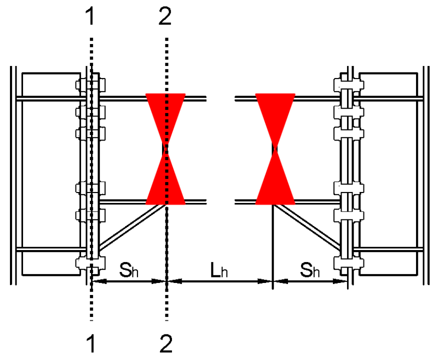

Figure 5.2 Plastic hinge location in haunched joints

As a simplification, the position of the plastic hinge (s_h) may be assumed to be located at the end of the haunch. However, tests indicate that the actual location of the plastic hinge is located at roughly 0,3 times the beam depth away from the end of the haunch.

Considering that for haunched joints the response of the connection and web panel was elastic, comparison of analytical results with the response of the experimental envelopes for each of these components may be done in terms of stiffness only. Therefore, it was decided to compare the analytical prediction to the experimental results in terms of moment – interstorey drift (M_{cf}-θ) curves. The analytical interstorey drift was obtained by adding the joint rotation (as determined by the EN 1993-1-8 approach) and the elastic rotation of the tests assembly due to flexural and shear stiffness of the members. Moment resistance of the joint was obtained using the EN 1993-1-8 design rules, using measured geometry and material characteristics. Partial factors for materials were assumed equal to 1.0.

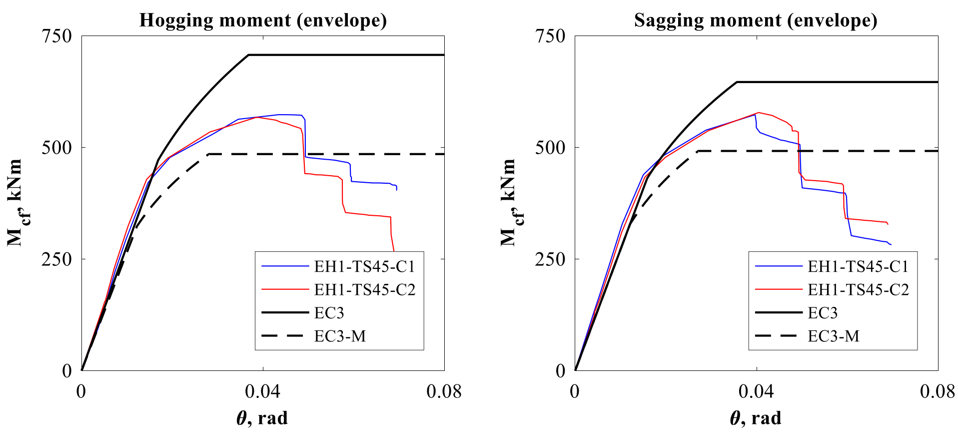

Figure 5.4 and Figure 5.5 present experimental envelopes vs. analytical predictions for EH2-TS35 and EH2-TS45 specimens. It can be observed that the EN 1993-1-8 model ("EC3") overestimates to a large extent the resistance of the joint, both under hogging and sagging moment. This is owing to the fact that EN 1993-1-8 does not account for the resistance of the beam in bending at the end of the haunch. The modified approach

based on EN 1993-1-8 ("EC3-M") provides a fairly good agreement with the experimental envelopes in terms of moment resistance. For initial stiffness, good agreement could be observed for both models. However, the degradation of stiffness for moments between $2/3M_{j,Rd}$ and $M_{j,Rd}$ is obviously not well suited for full-strength joints.

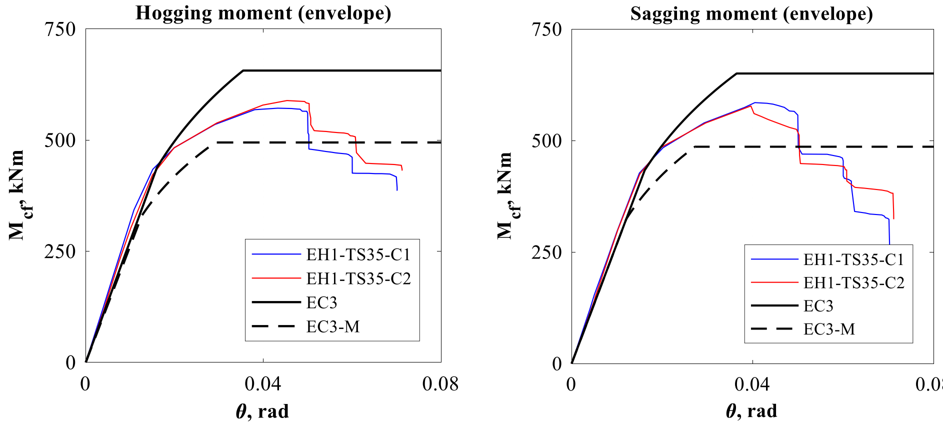

Figure 5.3: Experimental envelopes vs. analytical predictions for EH1-TS35 specimens

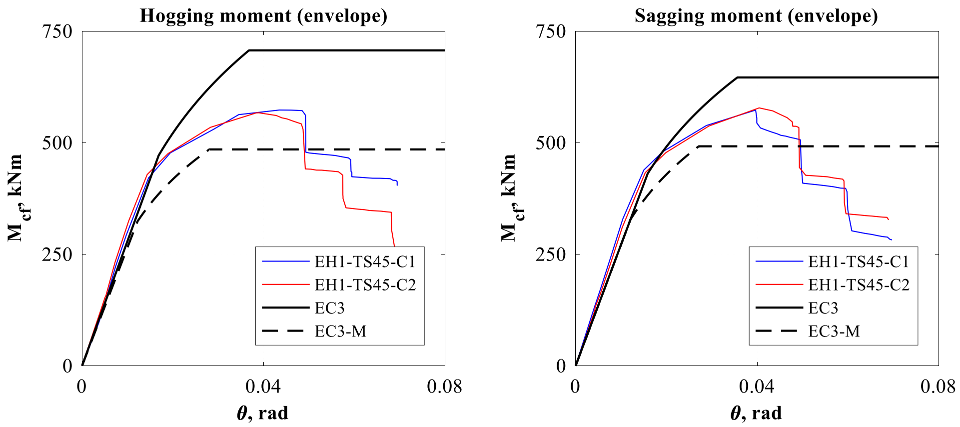

Figure 5.4: Experimental envelopes vs. analytical predictions for EH1-TS45 specimens

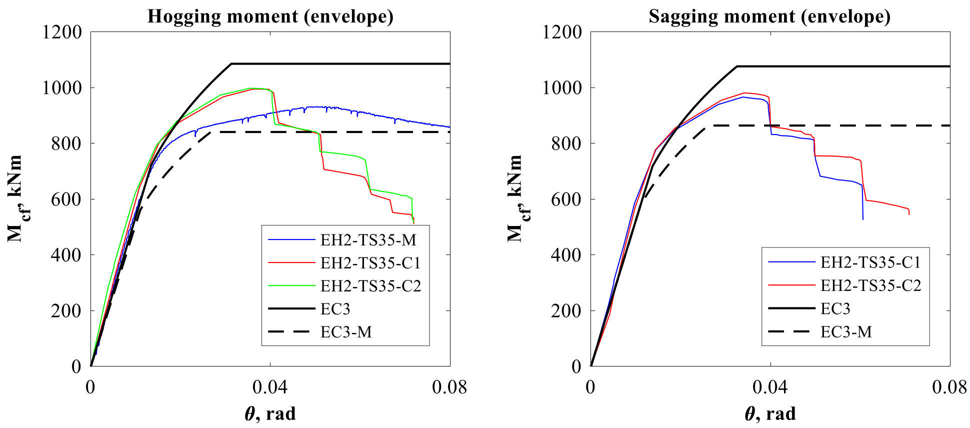

Figure 5.5: Experimental envelopes vs. analytical predictions for EH2-TS35 specimens

5.3 Moment-rotation curves of extended stiffened joints according to EN1993-1-8

The tests were carried out on both single and double sided joint configurations, namely involving one or two connection(s). The analytical predictions of the response curves of the joints has been compared to that experimentally measured in terms of overall moment-interstorey drift ratio (or chord rotation) curves. The moment is the one at the interface between the column flange and the endplates. The connection resistance is calculated considering as active all bolt rows above the horizontal symmetry axis of the connection (namely all rows out of the beam and a single inner row close to the beam flange). Besides that, another main source of joint deformability is associated to the shear of the column web panel, which was calculated as reported in Section 4.2.4. The joint response ($M_{b,Ed}$-φ_j curve), according to the definition provided in Eurocode 3 Part 1-8, was obtained by adding φ_c and γ rotations so as to get the φ_j one. Finally, the "assembly response" characterising the tested specimens are reported in the form of a $M_{b,Ed}$-θ curve in which -θ designates the interstorey drift ratio (also called "chord rotation") obtained by dividing the deflection under the applied load at beam end by the physical length of the beam. In this case the analytical prediction is obtained by adding the beam rotation and the elastic rotation of the column to the joint rotation φ_c. In all cases the resistance of the beam at the end of the rib stiffener (which is the section where plastic hinge is intended to occur) has been considered as projected at the column face, $M^*_{pl,Rd}$, as done for the haunched joints.

The analytical response curves of the assemblies satisfactory predict the stiffness and the strength of the connections that were experimentally measured, as shown in the following:

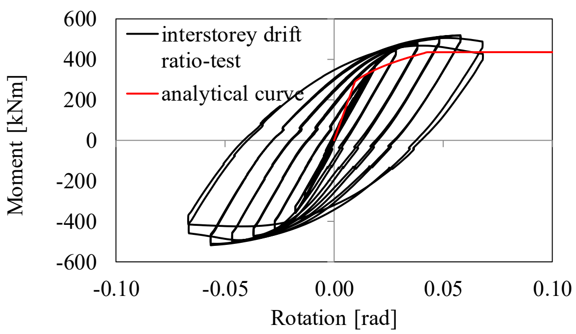

Figure 5.6: Experimental response vs. EC3:1-8 moment-rotation curves of ES1-TS-E joints - test C1

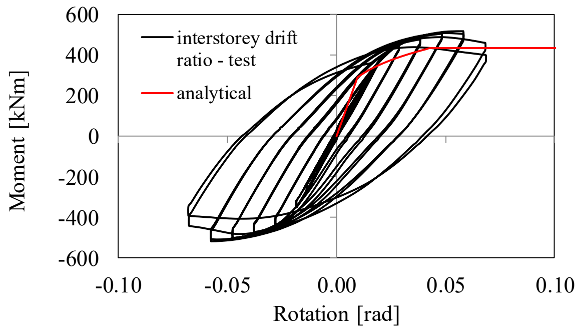

Figure 5.7: Experimental response vs. EC3:1-8 moment-rotation curves of ES1-TS-E joints - test C2

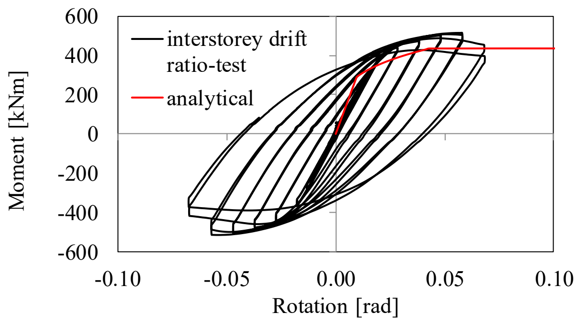

Figure 5.8: Experimental response vs. EC3:1-8 moment-rotation curves of ES1-TS-Esp joints-test C

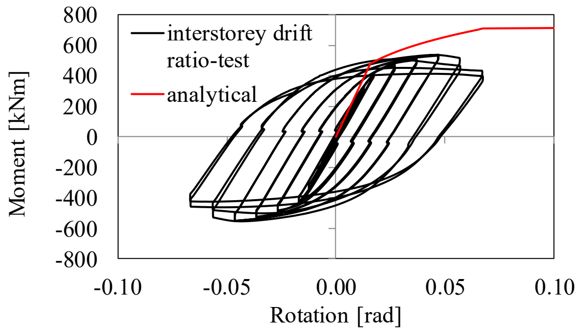

Figure 5.9: Experimental response vs. EC3:1-8 moment-rotation curves of ES1-TS-F joints - test C1

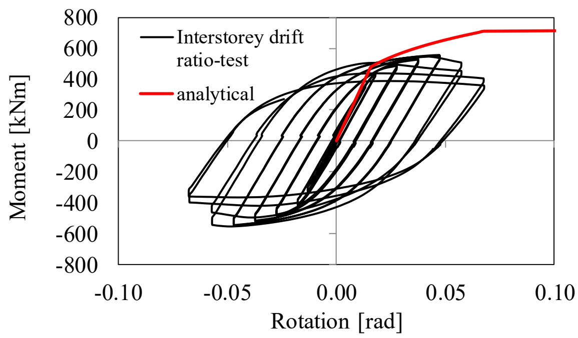

Figure 5.10: Experimental response vs. EC3:1-8 moment-rotation curves of ES1-TS-F joints-test C2

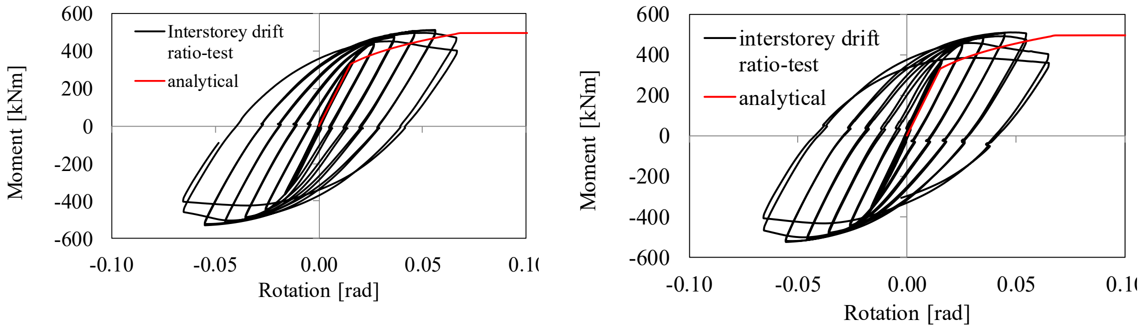

Left side Right side

Figure 5.11: Experimental response vs. EC3:1-8 moment-rotation curves of ES1-XS-E joints-test C1

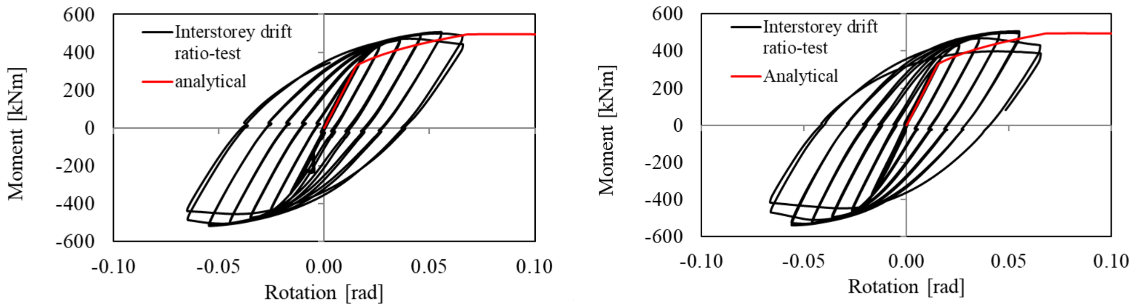

left side right side

Figure 5.12: Experimental response vs. EC3:1-8 moment-rotation curves of ES1-XS-E joints-test C2

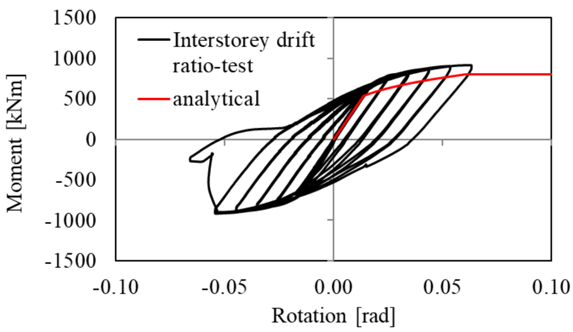

Figure 5.13: Experimental response vs. EC3:1-8 moment-rotation curves of ES2-TS-E joints-test C1

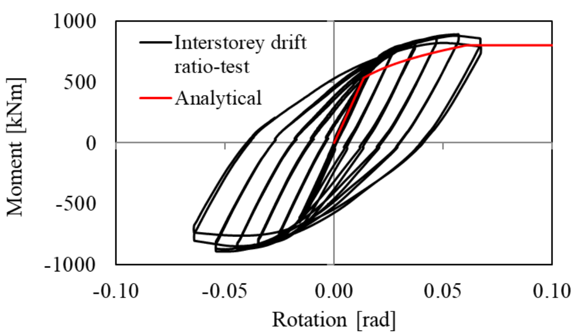

Figure 5.14: Experimental response vs. EC3:1-8 moment-rotation curve of ES2-TS-E joints-test C2

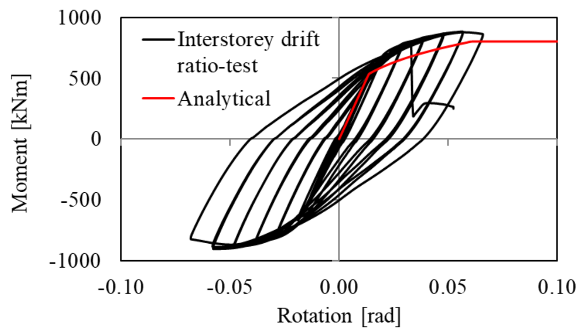

Figure 5.15: Experimental response vs EC3:1-8 moment-rotation curve of ES2-TS-Esp joints-test C

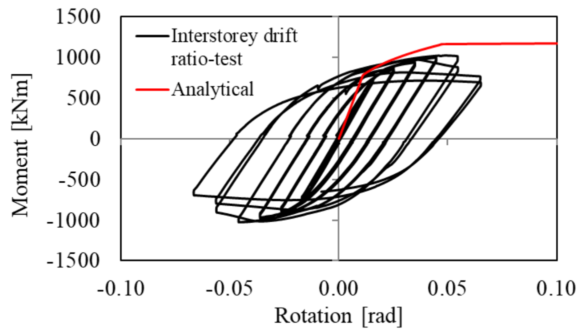

Figure 5.16: Experimental response vs. EC3:1-8 moment-rotation curve of ES2-TS-F joints - test C1

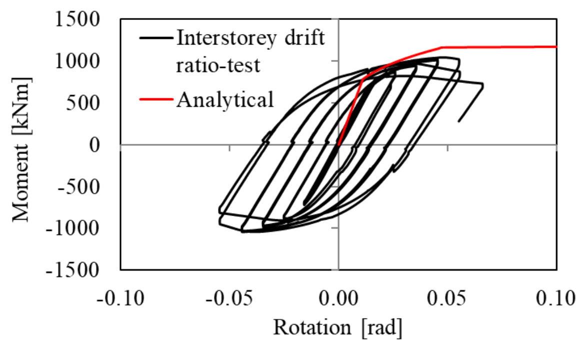

Figure 5.17: Experimental response vs. EC3:1-8 moment-rotation curve of ES2-TS-F joints - test C2

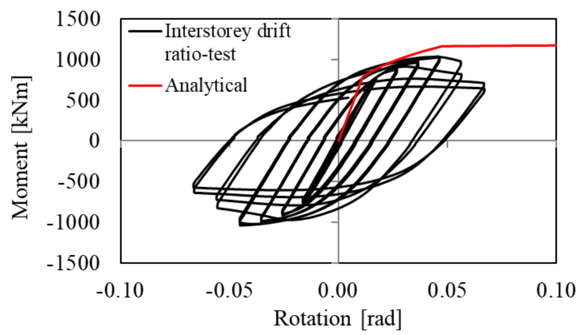

Figure 5.18: Experimental response vs. EC3:1-8 moment-rotation curve of ES2-TS-F joints - test CA

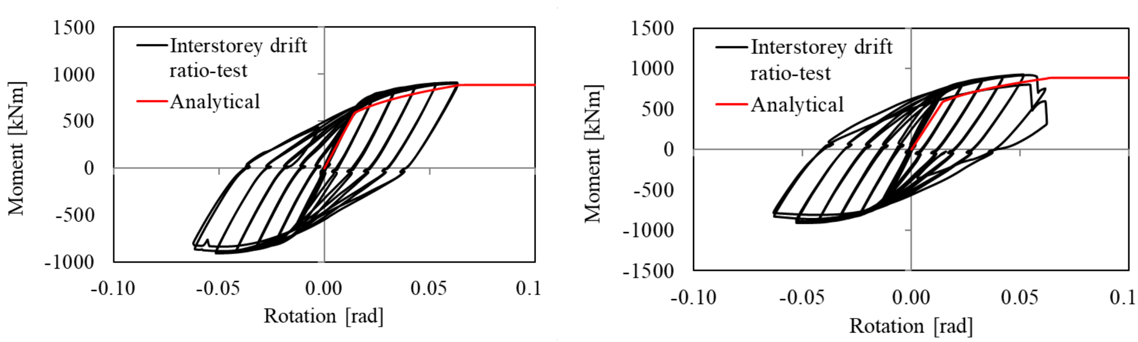

Left side

Right side

Figure 5.19: Experimental response vs. EC3:1-8 moment-rotation curve of ES2-XS-E joints - test C1

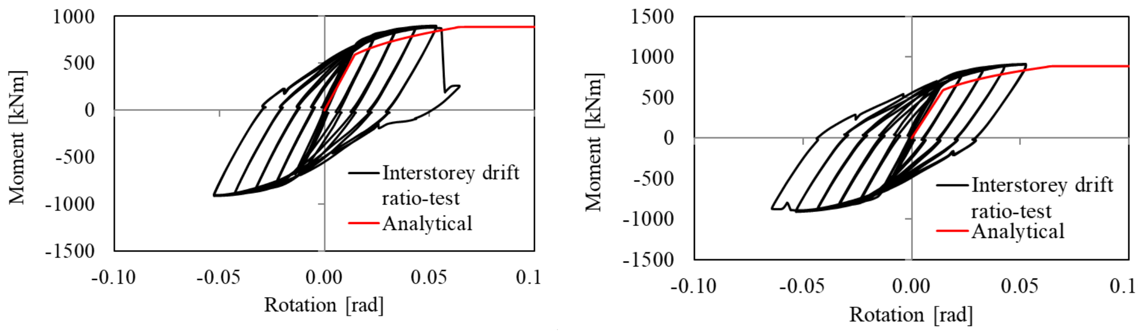

Left side

Right side

Figure 5.20: Experimental response vs. EC3:1-8 moment-rotation curve of ES2-XS-E joints - test C2

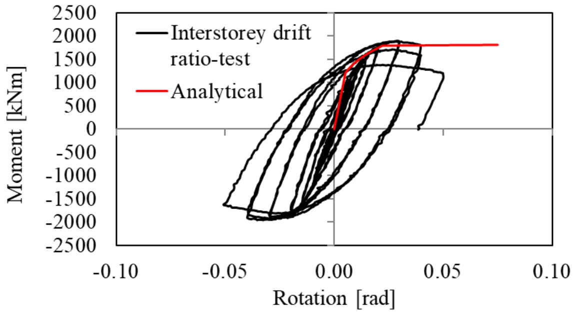

Figure 5.21: Experimental response vs. EC3:1-8 moment-rotation curve of ES3-TS-E joints - test C1

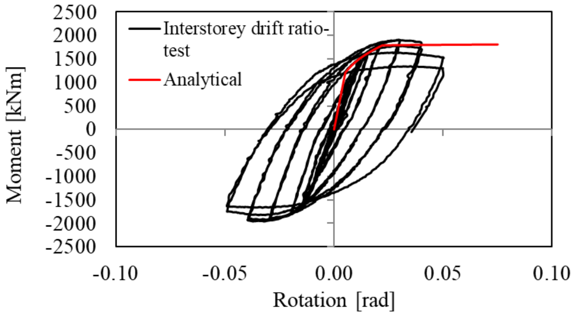

Figure 5.22: Experimental response vs. EC3:1-8 moment-rotation curve of ES3-TS-E joints - test C2

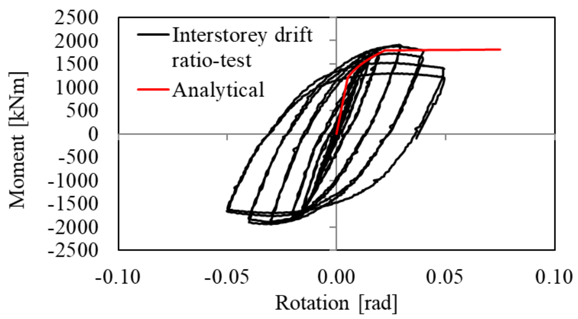

Figure 5.23: Experimental response vs. EC3:1-8 moment-rotation curve of ES3-TS-Esp joints-test C

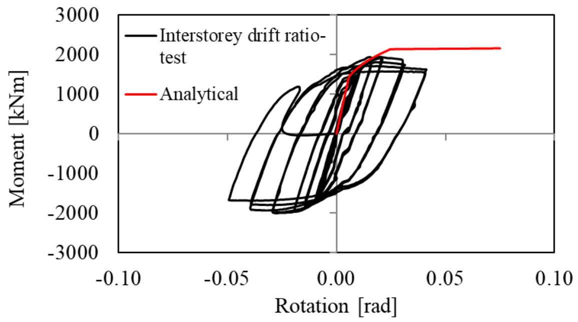

Figure 5.24: Experimental response vs. EC3:1-8 moment-rotation curve of ES3-TS-F joints - test C1

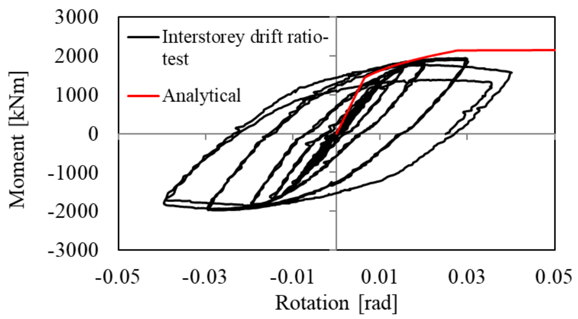

Figure 5.25: Experimental response vs. EC3:1-8 moment-rotation curve of ES3-TS-F joints - test C2

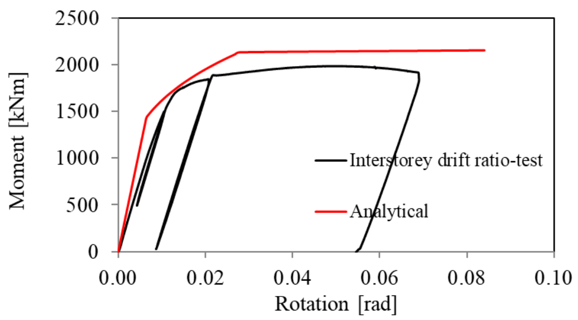

Figure 5.26: Experimental response vs. EC3:1-8 moment-rotation curves of ES3-TS-F joints - test M

5.4 Moment-rotation curves of extended unstiffened joints according to EN1993-1-8

The tests were carried out on both single and double sided joint configurations, namely involving one or two connection(s). The analytical predictions of the response curves of the joints has been compared to that experimentally measured in terms of overall moment-interstorey drift ratio (or chord rotation) curves. The moment is the one at the interface between the column flange and the endplates. The joint (connection + column web panel) resistance is calculated according to EN1993-1-8 (section 6.2.7.2). The joint rotation was calculated according to EN1993-1-8 (section 6.3.1). Finally, the “assembly response” characterising the tested specimens are reported in the form of a $M_{b,Ed}$-θ curve in which θ designates the interstorey drift ratio (also called “chord rotation”) obtained by dividing the deflection under the applied load at beam end by the physical length of the beam. In this case the analytical prediction is obtained by adding the beam deflection and the elastic rotation of the column to the joint rotation φ_c.
The analytical response curves of the assemblies satisfactory predict the stiffness and the strength of the connections that were experimentally measured, as shown in the following:

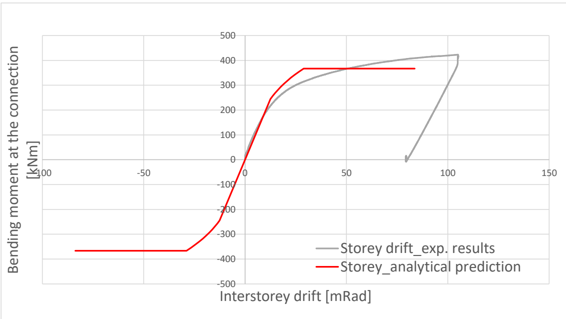

Figure 5.27 Experimental response vs. EC3:1-8 moment-rotation curves of E1-TB-E joints – monotonic test

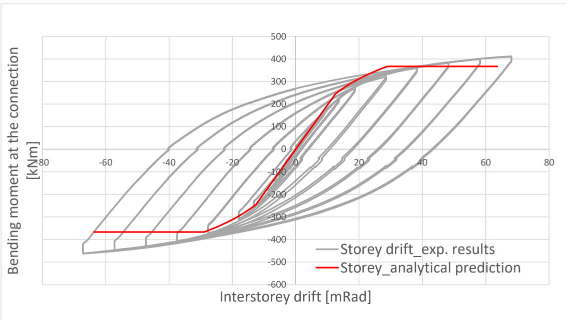

Figure 5.28 Experimental response vs. EC3:1-8 moment-rotation curves of E1-TB-E joints – cyclic test 1

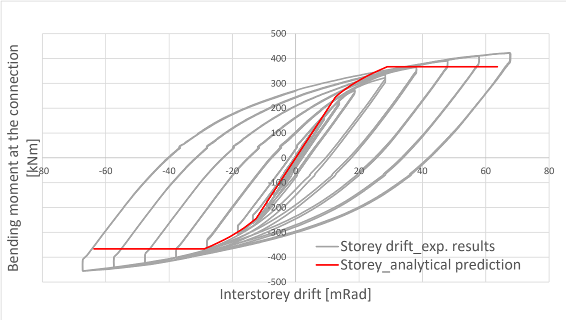

Figure 5.29: Experimental response vs. EC3:1-8 moment-rotation curves of E1-TB-E joints – cyclic test 2

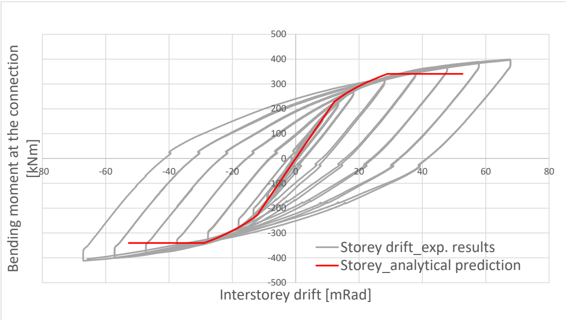

Figure 5.30: Experimental response vs. EC3:1-8 moment-rotation curves of E1-TB-P joints – cyclic test 1

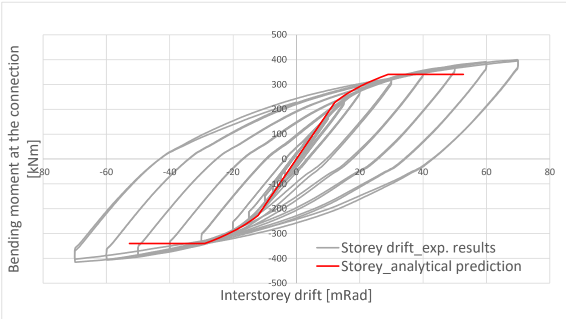

Figure 5.31: Experimental response vs. EC3:1-8 moment-rotation curves of E1-TB-P joints – cyclic test 2

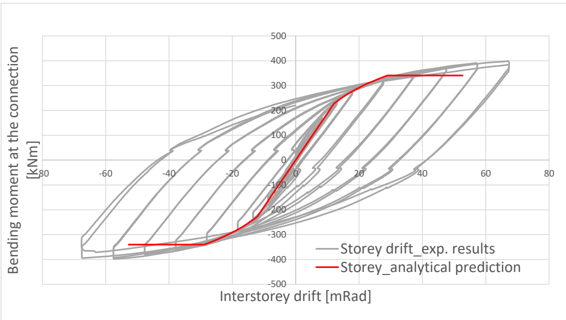

Figure 5.32: Experimental response vs. EC3:1-8 moment-rotation curves of E1-TB-PP joints – cyclic test

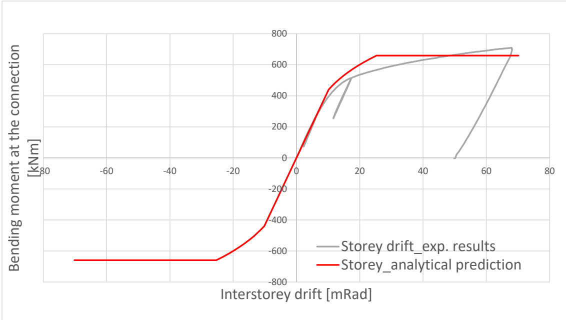

Figure 5.33: Experimental response vs. EC3:1-8 moment-rotation curves of E2-TB-E joints – Monotonic test

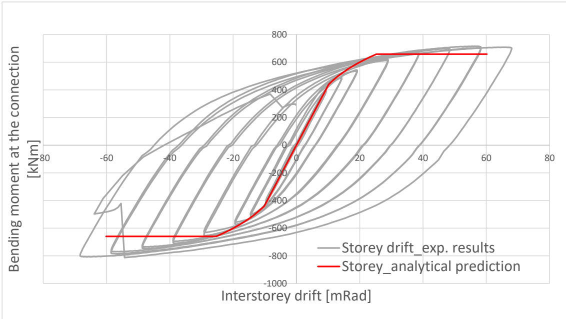

Figure 5.34: Experimental response vs. EC3:1-8 moment-rotation curves of E2-TB-E joints – cyclic test 1

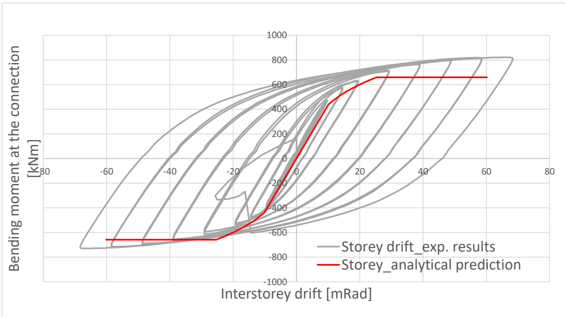

Figure 5.35: Experimental response vs. EC3:1-8 moment-rotation curves of E2-TB-E joints – cyclic test 2

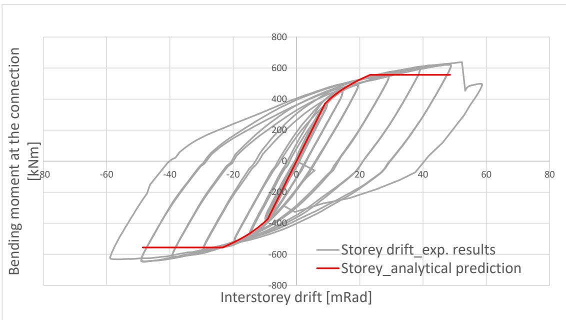

Figure 5.36: Experimental response vs. EC3:1-8 moment-rotation curves of E2-TB-P joints – cyclic test 1

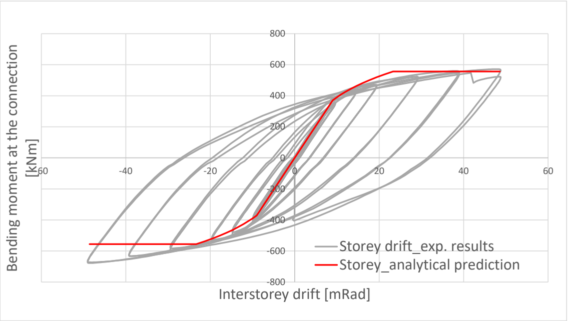

Figure 5.37: Experimental response vs. EC3:1-8 moment-rotation curves of E2-TB-P joints – cyclic test 2

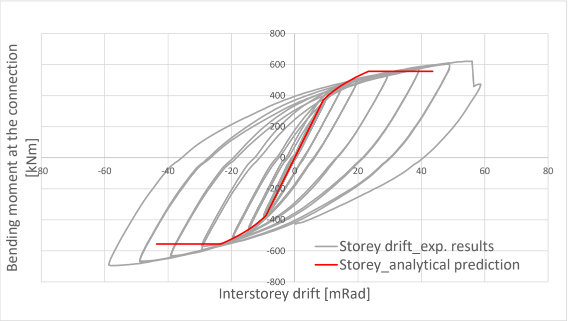

Figure 5.38: Experimental response vs. EC3:1-8 moment-rotation curves of E2-TB-P joints – cyclic test – shot peening

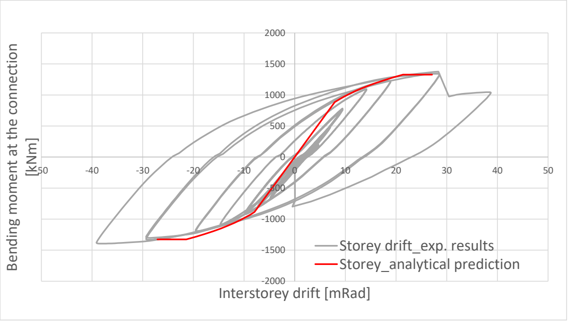

Figure 5.39: Experimental response vs. EC3:1-8 moment-rotation curves of E3-TB-E joints – cyclic test 1

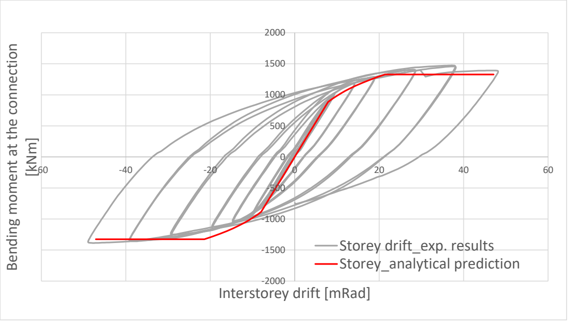

Figure 5.40: Experimental response vs. EC3:1-8 moment-rotation curves of E3-TB-E joints – cyclic test 2

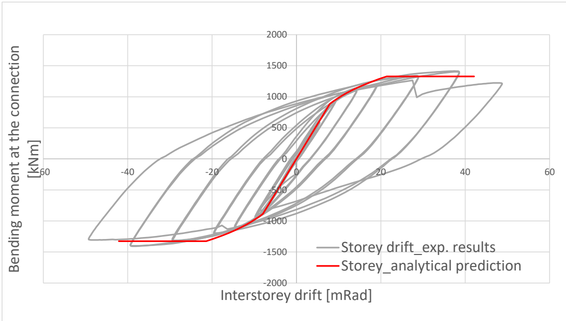

Figure 5.41: Experimental response vs. EC3:1-8 moment-rotation curves of E3-TB-E joints – Equaljoint cyclic test protocol

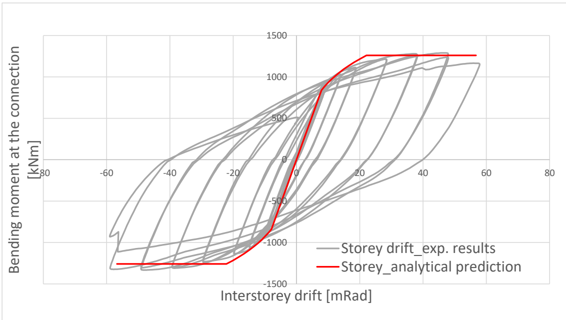

Figure 5.42: Experimental response vs. EC3:1-8 moment-rotation curves of E3-TB-P joints – cyclic test 1

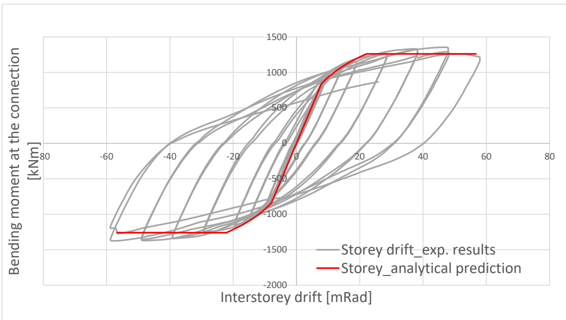

Figure 5.43: Experimental response vs. EC3:1-8 moment-rotation curves of E3-TB-P joints – cyclic test 2

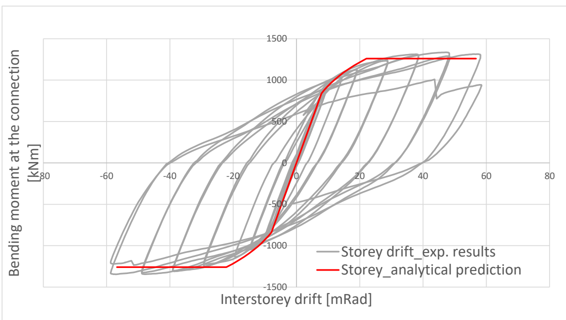

Figure 5.44: Experimental response vs. EC3:1-8 moment-rotation curves of E3-TB-P joints – cyclic test – shot peening

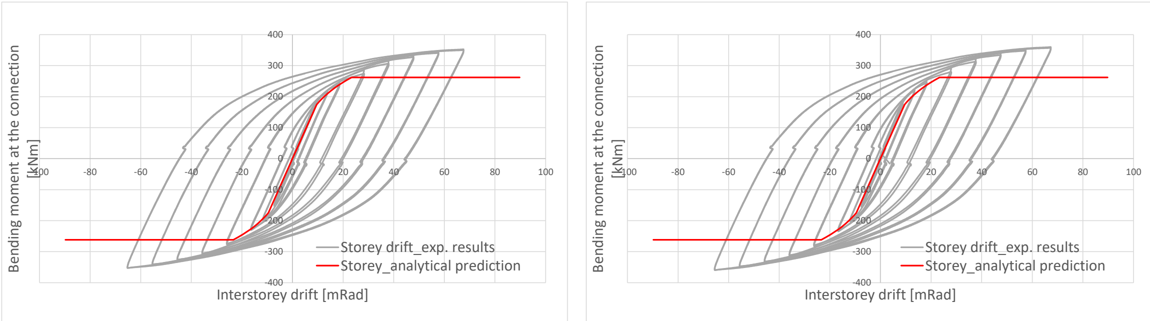

Left side Right side

Figure 5.45: Experimental response vs. EC3:1-8 moment-rotation curves of E1-XW-P joint – Cyclic test 1

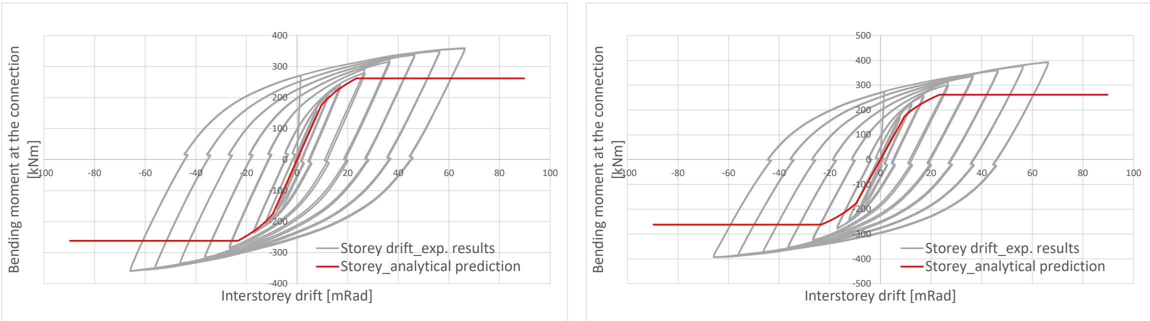

Left side Right side

Figure 5.46: Experimental vs. EC3:1-8 moment-rotation curves of E1-XW-P joint – Cyclic test 2

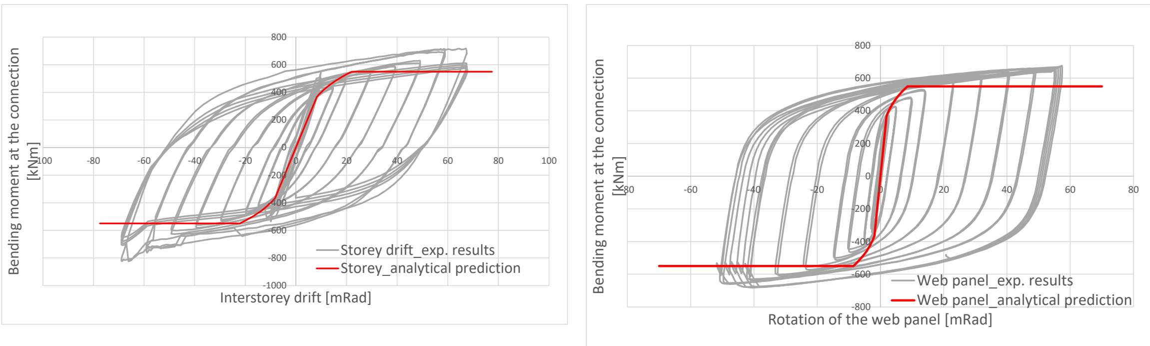

Left side Right side

Figure 5.47: Experimental vs. EC3:1-8 moment-rotation curves of E2-XW-P joints – cyclic test 2

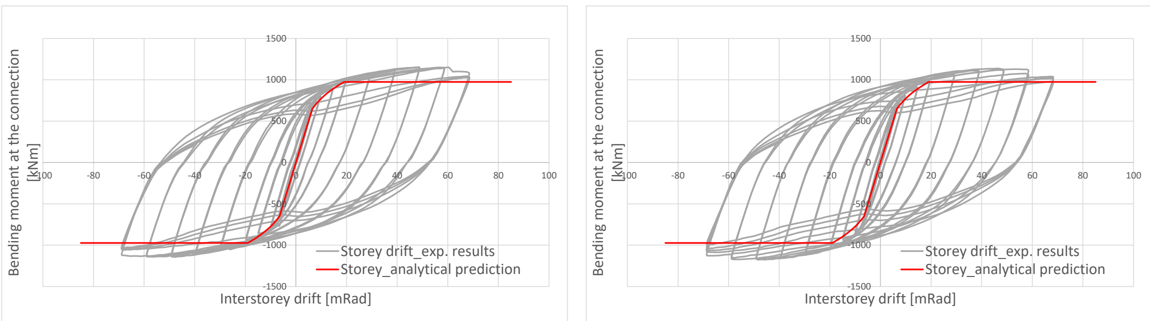

Left side Right side

Figure 5.48: Experimental response vs. EC3:1-8 moment-rotation curves of E3-XW-P joints – cyclic test 1

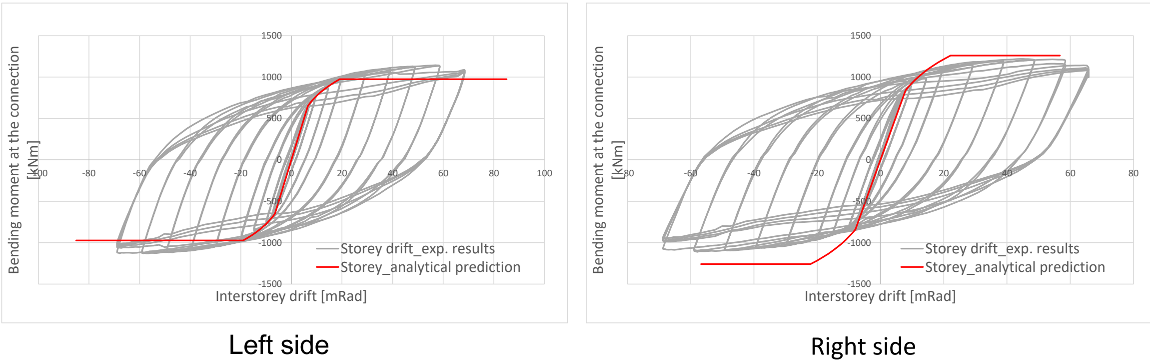

Figure 5.49: Experimental response vs. EC3:1-8 moment-rotation curves of E3-XW-P joints – cyclic test 2

Globally, it can be observed that the analytical predictions obtained by EC3 Part 1-8 in terms of resistance and stiffness agree quite well with the experimental results, for all the connections and for the joints. A similar conclusion is drawn for the column web panels as far as the panels are assumed to have depth equal to the “maximum shear” height resulting from the application of the Part 1-8 assembly procedure (section 6.2.7.2). On the contrary, an unsafe estimation of the web panel resistance is obtained when the height of the panels is taken as equal to the distance between the centres of gravity of the beam flanges (according to Eurocode 3 Part 1-8 Figure 6.15). This result highlights that for joints where the contribution of the inner bolt rows is significant the simplified approach given by Fig. 6.15 of EC3:1-8 should be avoided.

5.5 Moment-rotation curves of dog-bone joints

As noted before, the dog-bone or RBS (reduced beam section) joints were considered as part of examining the use of European steel for large beam-column assemblies incorporating this type of dissipative connection. Accordingly, they represent a special case which is not directly related to the other connection configurations discussed above (i.e. haunched, extended stiffened and extended unstiffened). However, in order to illustrate the typical moment-rotation response of the two large scale RBS connections, Figure 5.50 and Figure 5.51 depict the moment versus rotation response of Specimens SP2 and SP4, represented by the column centreline moment against the total storey drift (as a percentage of the storey height).
For SP2, a maximum total force of 293 kips (1.303,33 kN) was reached during the 4% storey drift cycles. The elastic stiffness of the specimen was approximately 75 k/in (13.13 kN/mm). The specimen exhibited largely linear elastic response up to a

drift exceeding 1%, and notable inelastic behaviour started to occur at a drift of 2%. Local buckling of the web was initiated around 3% drift, with visible flange local buckling occurring at a drift of about 4%. Following the two cycles at 4% that completed the prequalification test, five complete cycles were performed at 5% story drift, with strength degradation being notable with more severe local buckling in the flanges and web, until failure occurred due to low-cycle fatigue. During the final cycle, the beam experienced fracture in both its top and bottom flanges at the location of the RBS, due to the concentration of severe local buckling.

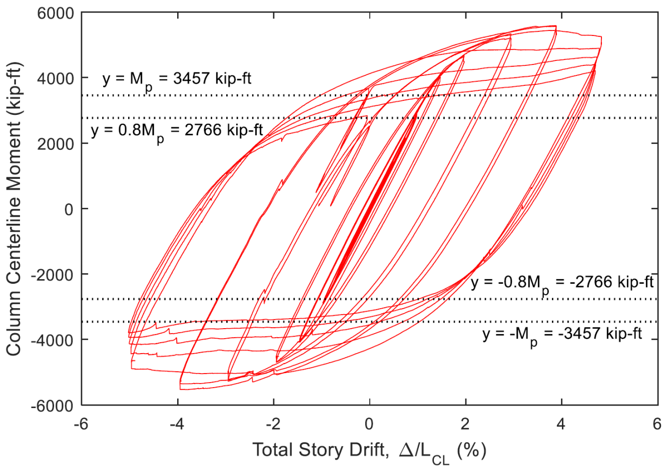

Figure 5.50: Moment-rotation response of RBS (dog-bone) joint – Specimen SP2

As shown in the response of SP2, at 4% storey drift cycles, the moment undergone by the specimen beam well exceeded 80% of the nominal plastic flexural strength, M_p. The same holds true for story drifts of 5%. This satisfies the acceptance criteria for special moment frames as described in Section E3.6 of AISC 341-10 (2010). After early cycles in the testing, inelastic deformation contributes the majority to story drift. As the RBS begins to yield with subsequently larger deformations, a hinge forms at the RBS, and most of the rotation in the connection occurs within the reduced section. Also, at the start of the test, when the response is largely elastic, the panel zone contribution is significant. However, this reduces gradually with increasing levels of inelasticity as the dissipation becomes more concentrated within the RBS.

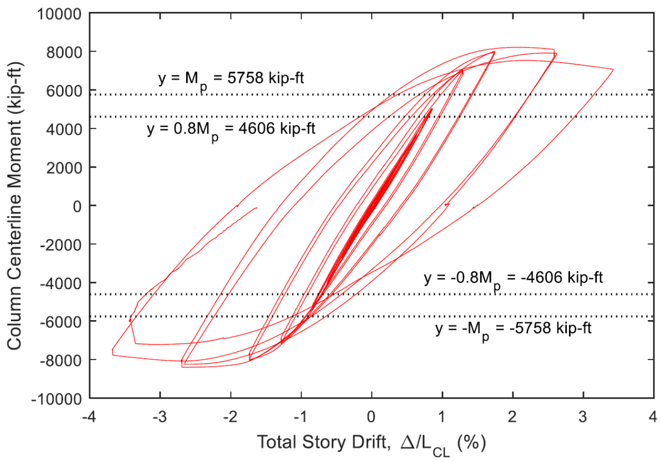

Figure 5.51: Moment-rotation response of RBS (dog-bone) joint – Specimen SP4

A broadly similar response was obtained for SP4, for which the same procedure as that adopted for SP2 was utilised, based on AISC341-10 (2010). The test was performed up to a drift approaching 4% and was subsequently terminated due to limitations with lateral stability, which results in significant out of plane deformation and significant torsional deformations within the deep column profile adopted.

The specimen exhibited largely linear elastic response up to a drift exceeding 1%, and notable inelastic behaviour started to occur at a drift of 2%. Yielding and local buckling of the web was initiated around 3% drift, with visible flange local buckling occurring at a drift of about 4%, with significant strength degradation and more severe web buckling. The test was terminated at a drift approaching 4% due to the limitation of the lateral bracing system used.

As for SP2, the strength of the SP4 connection was above 80% of the nominal plastic flexural capacity of the beam at the 4% story drift cycles. However, it should be noted that in the figure, the moment is calculated at the column centreline in accordance with AISC 341-10, hence it appears to be significantly exceeding M_p whilst the margin of over-strength is in reality lower. The ratio between the applied moment at the RBS to the nominal moment capacity of the RBS, is still greater than the 80% nominal plastic capacity.

It is worth noting that in Section K2.8 of AISC 341-10 (2010), the acceptance criteria for the prequalification of beam-to-column connections states that requirements must be satisfied for both strength and storey drift angle. For a special moment frame, the storey drift requirement is that the specimen must complete at least one full cycle with at least a 4% storey drift. The strength requirement is that at the drift angle of 4%, the connection must be able to withstand a moment that is at least as great as $0.80M_p$. Based on the results discussed above, the response of SP2 complies with these requirements, thus satisfying the acceptance criteria for the prequalification of beam-to-column connections.

It is worth noting that the inclusion of lateral bracing at the RBS location may have had previously unconsidered adverse effects on the qualification of the specimen section. AISC 358-10 discusses prequalification limitations on the beam for RBS connections and addresses these limitations as they concern lateral bracing in Section 5.3.1(7). According to this section, there is an exception to the requirement of lateral bracing at the RBS, stemming from systems that utilize a concrete structural slab supported by the beam section.

6 PERFORMANCE PARAMETERS OF THE TESTED JOINTS (I.E. HYSTERETIC BEHAVIOUR OF ELEMENTS TO CYCLIC LOADING, STIFFNESS AND STRENGTH DEGRADATION)

The performance parameters of joints reported in the following Sections are obtained according to the procedure described in Figure 6.1. In particular, for both haunched and extended stiffened joints the performance parameters are reported according to Fig.6.1a, which is in line with EN1998-1. Indeed, for these types of joints the main source of dissipation is the beam that is influenced by the shape and the details of the stiffeners (i.e. haunches and ribs) and the performance parameters are reported to evaluate the performance of the beam-to-column assembly equipped within the structure. For Unstiffened joints the main source of deformation are the connection and column web panel. Hence, the performance parameters are reported only in terms of joint rotation in line with EN1993-1-8, as shown in Fig. 6.1b. This aspect also explains the different symbols adopted to identify consistently different response parameters.

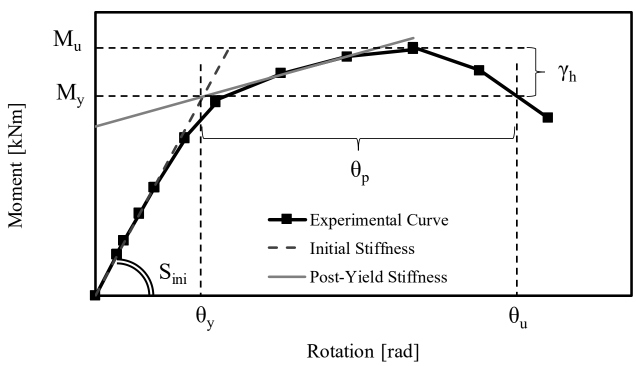

a)

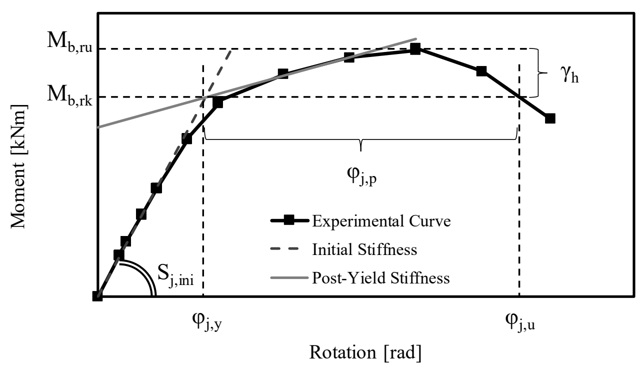

b)

Figure 6.1: Definition of performance parameters: a) in terms of overall chord rotation (interstorey drift ratio) according to AISC341-16 and EN1998-1; b) in terms of joint (i.e. connection + web panel) rotation according to EN1993-1-8

6.1 Haunched joints

The proposed modelling for haunched joints (type a) is presented in the schematics that follow. Three cases are presented: (a1) exterior joints, (a2) interior moment joints for Moment-resisting frames and (a3) interior braced joints for dual frames (i.e. Moment-resisting frames + Concentrically Braced frames or Moment-resisting frames + Eccentrically Braced frames). The height of the panel zone is assumed equal to h_b + h_h (see Fig. 6.2 for the meaning of the symbols). The moment-resisting beams have stiff elastic elements at their ends, at a length of s_h from the column face. The brace is connected to the pivot point of the scissors assembly, namely to the connecting point between the two rigid segments simulating the dimensions of the column web panel.

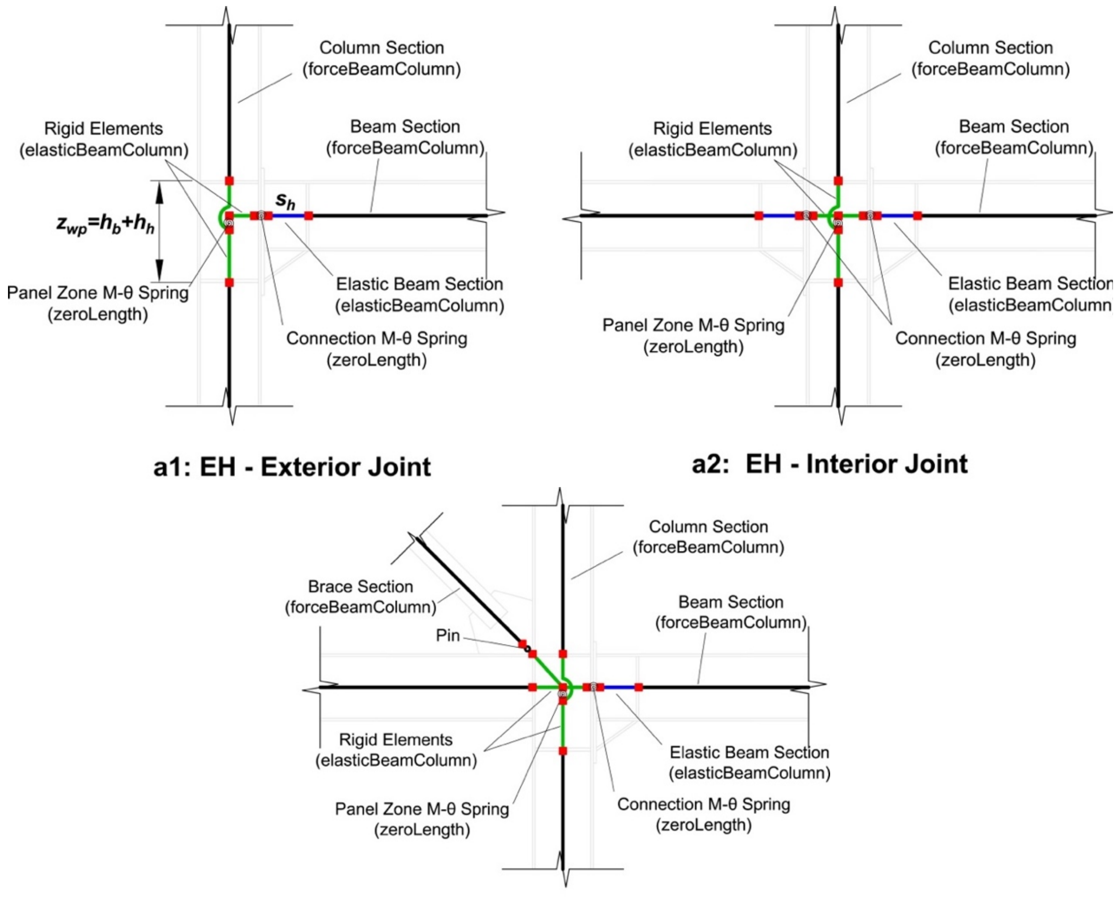

a1: EH - Exterior Joint **a2: EH - Interior Joint**

a3: EH - Braced Interior Joint

Figure 6.2: Modelling of joints with haunched connections

A “good guess” estimation of strength-stiffness characteristics of the haunched joints is given hereinafter. The proposed values have been obtained on the basis of numerical simulations and experimental data on the pre-qualified joints for a set of building archetypes. The validity of these data is limited to the considered assumptions, namely building frames with span length within the range [6m – 8m] and interstorey height within [3.5m – 4m] and beam profiles varying from IPE360 to IPE600. However, once designed the actual geometry of the joint, the mechanical features should be reevaluated to achieve a more accurate prediction of the structural response.

The normalisation of strength is with respect to the expected beam plastic strength calculated at the column face, $M^{e}_{pl,b,cf,Rd}$, and the normalisation of stiffness is with respect to the beam flexural stiffness parameter, $s_b = EI_b/L_b$. The normalised strength values are consistent with the capacity design principles and the normalised stiffness values are averages for each joint design group.

Joint Type	Geometry	Strength		Stiffness	
		Connection:	Panel Zone:	Connection:	Panel Zone:
EH-S: Full-strength with strong panel zone	$h_h/h_b = 0.45$ $s_h/h_b = 0.65$ $z_{wp} = h_b + h_h$	$\frac{M^{n}_{j.Rd}}{M^{e}_{pl,b,cf,Rd}} = 1.3$	External nodes: $\frac{V^{n}_{wp.Rd} \cdot z_{wp}}{M^{e}_{pl,b,cf,Rd}} = 1.65$ Internal nodes: $\frac{V^{n}_{wp.Rd} \cdot z_{wp}}{2 \cdot M^{e}_{pl,b,cf,Rd}} = 1.65$	$\frac{s_{con,ini}}{s_b} = 80$	Ext. nodes: $\frac{s_{wp,ini}}{s_b} = 55$ Int. nodes: $\frac{s_{wp,ini}}{2 \cdot s_b} = 55$
EH-B: Full-strength with balanced panel zone	$h_h/h_b = 0.45$ $s_h/h_b = 0.65$ $z_{wp} = h_b + h_h$	$\frac{M^{n}_{j.Rd}}{M^{e}_{pl,b,cf,Rd}} = 1.3$	External nodes: $\frac{V^{n}_{wp.Rd} \cdot z_{wp}}{M^{e}_{pl,b,cf,Rd}} = 1.0$ Internal nodes: $\frac{V^{n}_{wp.Rd} \cdot z_{wp}}{2 \cdot M^{e}_{pl,b,cf,Rd}} = 1.0$	$\frac{s_{con,ini}}{s_b} = 65$	Ext. nodes: $\frac{s_{wp,ini}}{s_b} = 31$ Int. nodes: $\frac{s_{wp,ini}}{2 \cdot s_b} = 31$
Notes: i) Elasto-plastic behaviour is assumed for the connection springs, with 1% post-yield hardening. The assumed pre-capping plastic rotation capacity of the component is 18 mrad (ASCE 41-13, Table 9-6, yield of bolts). The connection behaviour can be implemented e.g. by assigning a Bilin material (modified Ibarra-Medina-Krawinkler model) to the rotational DOF of the spring. ii) The spring for the column web panel zone is modelled according to the established tri-linear model by Krawinkler (see Gupta and Krawinkler, 1999). The proposed strength value corresponds to the **first** yield point (panel). A post-yield hardening of 1.5% is assumed. In OpenSEES the panel zone behaviour can be implemented by assigning Hysteretic or Steel02 material to the rotational DOF of the spring. iii) When modelling the panel zone using (a) a parallelogram of rigid elements and pins or (b) the Joint2D macromodel, the kinematics are identical and the properties of the rotational spring are the same. In this case the elastic spring stiffness is: $s_{wp} = (V_{wp}/\gamma) z_{wp}$ iv) If the panel zone is modelled according to the "scissors" model, the strength and stiffness values of the rotational spring (calculated per Krawinkler's approach) have to be modified (see Charney and Downs, 2004).					

6.1.1 Performance parameters of tested joints

In order to achieve a set of joint performance parameters, envelopes of specimens tested under cyclic loading were constructed firstly. Up to the maximum bending moment, the envelope was obtained by connecting the points of peak moments for each cycle of loading, while beyond the maximum moment points of largest moment at a given deformation were used. Figure 6.3a, shows the positive and negative envelopes constructed for the EH2-TS35-C1 single-sided joint assembly and Figure 6.4a shows the positive and negative envelopes constructed for the EH2-XB35-C1 double-sided joint assembly. The initial stiffness (S_{ini}) was obtained by a linear fit of points on the envelope corresponding to values of the bending moment below 0.7 times the maximum one (M_{max}). The yield bending moment (M_y) was determined at the intersection of the initial and tangent stiffness lines (Figure 6.3b and Figure 6.4b). The latter was defined by a linear fit of data points on the M_{cf}-θ curve located between 0.8M_{max} and M_{max}. Lastly, ultimate deformation θ_u was determined as point on the M_{cf}-θ envelope corresponding to a drop of moment of 0.8 times the maximum one (Figure 6.3b and Figure 6.4b). For each cyclic test, the parameters defined above were computed for positive and negative envelopes, which were close to each over. For initial stiffness (S_{ini}), yield moment (M_y) and maximum moment (M_{max}) the average of the positive and negative values were then computed, while for ultimate drift (θ_u) – the minimum one. The parameters obtained in this manner are reported in Table 6.1. Additionally the strain hardening coefficient (γ_h) was computed as the ratio between the maximum (M_{max}) and yield moment (M_y), as well as the plastic ultimate drift ($\theta_{pl,u}$), defined as subtracting from the total ultimate drift (θ_u), the elastic drift, corresponding to the yield moment (M_y), obtained using the initial stiffness as computed above.

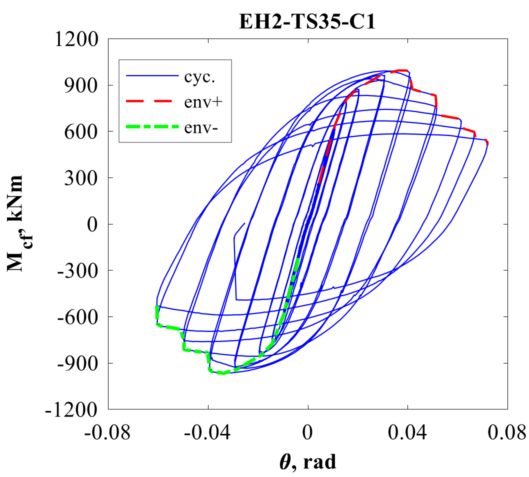

(a)

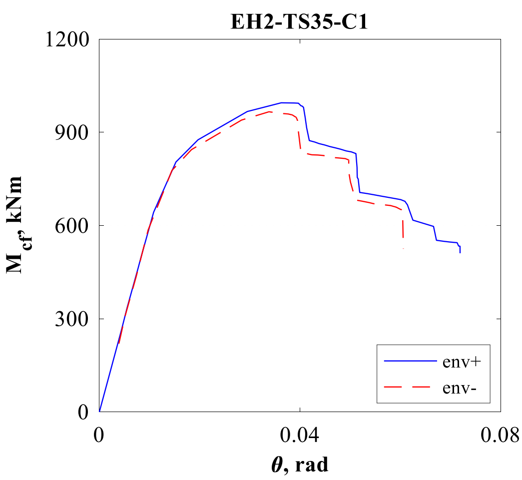

(b)

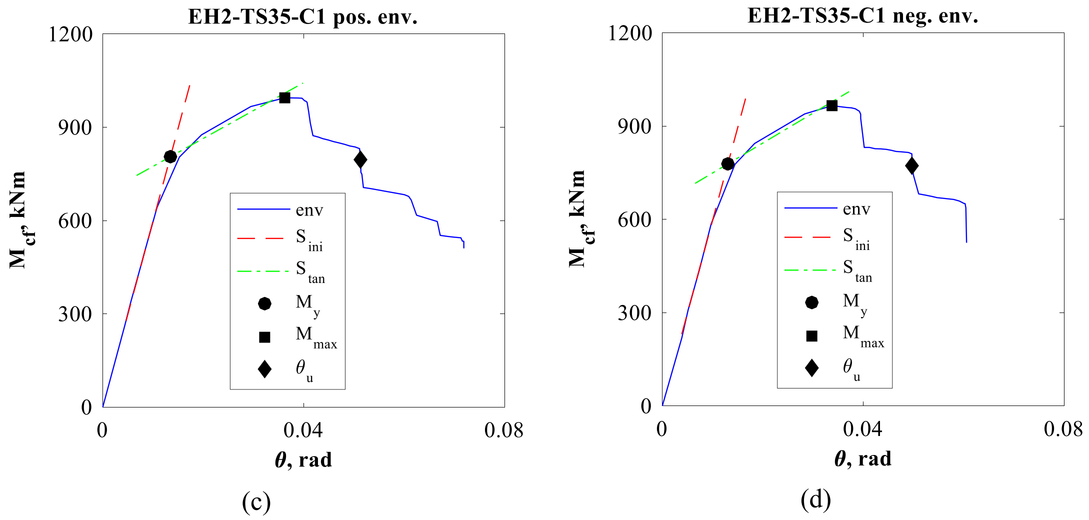

Figure 6.3: EH2-TS35-C1: a) Hysteretic loops and envelope; b) positive vs. negative envelope c); characteristic M_{cf} - θ curve for positive envelope; d) characteristic M_{cf} - θ curve for negative envelope

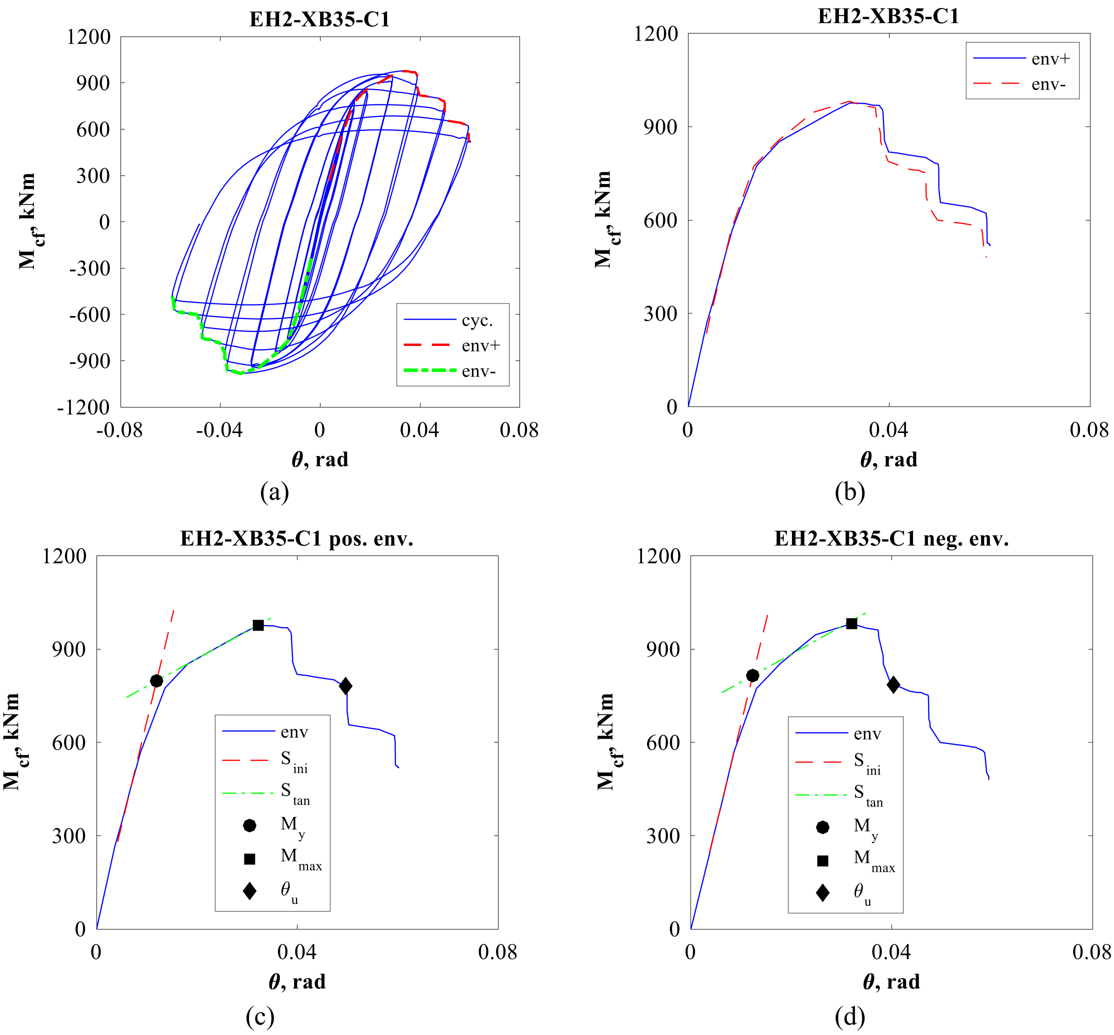

Figure 6.4: EH2-XB5-C1: a) Hysteretic loops and envelope; b) positive vs. negative envelope c); characteristic M_{cf} - θ curve for positive envelope; d) characteristic M_{cf} - θ curve for negative envelope

It can be observed that the strain hardening coefficient is relatively uniform across specimens, averaging at about γ_h =1.21. Ultimate inter-storey drift (θ_u) is generally larger than 0.04 rad (the minimum requirement specified in ANSI/AISC 341-16, for special steel moment frames). The ultimate inter-storey drift reduces gradually with increasing the beam depth. Moreover, for larger beam sizes with 45° haunch (EH3-TS45-C1 and EH3-TS45-C2) the ultimate drift (θ_u) falls below the minimum requirements, being about 0.037 rad. Similarly, the plastic drift (θ_p) is generally larger than 0.03 rad, except for larger beam specimens with 45° haunch (EH3-TS45-C1 and EH3-TS45-C2), for which 0.027 rad was attained. Moreover, the EH2-XB35-C1 specimen (double sided joint with IPE450 beam and 35° haunch) showed smaller ultimate rotations (θ_u=0.040 rad and θ_p =0.038 rad). This attributed to larger column size and smaller beam depth to span ratio, resulting in larger influence of the shear force.

Table 6.1: **Performance parameters of tested haunched joints (EN 1998-1)**

Specimen	S_{ini} [kNm/rad]	M_y [kNm]	M_{max} [kNm]	γ_h	θ_u [rad]	θ_p [rad]
EH1-TS35-C1	30674.5	468.1	578.4	1.24	0.057	0.041
EH1-TS35-C2	29377.0	471.6	583.3	1.24	0.050	0.034
EH1-TS35-CA	30585.9	472.4	586.5	1.24	0.052	0.036
EH1-TS45-C1	30537.6	468.1	573.1	1.22	0.050	0.035
EH1-TS45-C2	30618.6	461.8	572.4	1.24	0.049	0.034
EH1-TSO-35-C	30629.2	541.2	650.1	1.20	0.057	0.041
EH2-TS35-M	56741.9	795.5	931.7	1.17	0.118	0.105
EH2-TS35-C1	59699.5	792.0	980.2	1.24	0.050	0.037
EH2-TS35-C2	60740.4	831.5	989.1	1.19	0.050	0.036
EH2-TS35-CA	59540.6	814.5	995.5	1.22	0.049	0.034
EH2-TS45-C1	60290.7	801.8	963.5	1.20	0.042	0.029
EH2-TS45-C2	59986.7	800.4	987.0	1.23	0.049	0.035
EH2-TS45-M	60969.3	798.6	957.2	1.20	0.123	0.110
EH3-TS35-C1	149595.3	1886.5	2232.3	1.18	0.045	0.033
EH3-TS35-C2	142546.6	1956.3	2240.7	1.15	0.044	0.033
EH3-TS35-CA	146423.8	1971.4	2217.9	1.13	0.046	0.034
EH3-TSO35-C	140557.6	1962.9	2376.9	1.21	0.050	0.036
EH3-TS45-C1	153141.9	1554.7	1939.4	1.25	0.037	0.027
EH3-TS45-C2	144779.7	1560.2	1956.3	1.25	0.038	0.028
EH1-XB35-C1	27229.1	469.6	562.5	1.20	0.070	0.052
EH1-XB35-C2	29290.7	436.3	557.5	1.28	0.056	0.041
EH2-XB35-C1	66494.3	806.5	979.3	1.21	0.040	0.028
EH2-XB35-C2	65565.3	809.9	987.0	1.22	0.045	0.033
EH2-XB35-M	62344.2	807.2	952.2	1.18	0.112	0.100

In Table 6.1, average values of positive and negative envelope were computed for initial stiffness (S_{ini}), yield bending moment (M_y) and maximum bending moment (M_{max}). The minimum values of ultimate inter-storey drift (θ_u) and the plastic drift (θ_p) for positive and negative envelope was computed in Table 6.1. Further in
Table 6.2 are presented the values of ultimate inter-storey drift (θ_u) and the plastic drift (θ_p) for positive and negative envelope. The ultimate rotations under negative cycles are in general slightly smaller than for the positive ones.

Table 6.2: **Performance parameters of tested haunched joints**

Specimen	θ_u [rad]			θ_u [rad]		
	sagging	hogging	min	sagging	hogging	min
EH1-TS35-C1	0.060	0.057	0.057	0.046	0.041	0.041
EH1-TS35-C2	0.061	0.050	0.050	0.045	0.034	0.034
EH1-TS35-CA	0.052	0.065	0.052	0.036	0.050	0.036
EH1-TS45-C1	0.059	0.050	0.050	0.044	0.035	0.035
EH1-TS45-C2	0.049	0.049	0.049	0.035	0.034	0.034
EH1-TSO-35-C	0.057	0.060	0.057	0.041	0.042	0.041
EH2-TS35-C1	0.118	-	0.118	0.105	-	0.105
EH2-TS35-C2	0.051	0.050	0.050	0.038	0.037	0.037
EH2-TS35-CA	0.051	0.050	0.050	0.039	0.036	0.036
EH2-TS35-M	0.057	0.049	0.049	0.045	0.034	0.034
EH2-TS45-C1	0.049	0.042	0.042	0.037	0.029	0.029
EH2-TS45-C2	0.050	0.049	0.049	0.038	0.035	0.035
EH2-TS45-M	0.123	-	0.123	0.110	-	0.110
EH3-TS35-C1	0.048	0.045	0.045	0.036	0.033	0.033
EH3-TS35-C2	0.044	0.049	0.044	0.033	0.036	0.033
EH3-TS35-CA	0.048	0.046	0.046	0.035	0.034	0.034
EH3-TSO35-C	0.050	0.050	0.050	0.036	0.037	0.036
EH3-TS45-C1	0.040	0.037	0.037	0.029	0.027	0.027
EH3-TS45-C2	0.040	0.038	0.038	0.029	0.028	0.028
EH1-XB35-C1	0.070	0.070	0.070	0.055	0.052	0.052
EH1-XB35-C2	0.056	0.060	0.056	0.041	0.045	0.041
EH2-XB35-C1	0.050	0.040	0.040	0.038	0.028	0.028
EH2-XB35-C2	0.050	0.045	0.045	0.038	0.033	0.033
EH2-XB35-M	0.112	-	0.112	0.100	-	0.100

6.1.2 Influence of beam depth

The influence of the member size on joint response can be observed in Figure 6.5 for single-sided joints 35° haunch angle and in Figure 6.6 for single-sided joints 45° haunch angle. Buckling occurs earlier and the post-peak curve has a steeper slope with increasing the beam depth. The same response is observed for the member size parameter in case of the specimens with a 45˚ slope of the haunch. As mentioned above, the ultimate inter-storey drift reduces gradually with increasing beam depth.

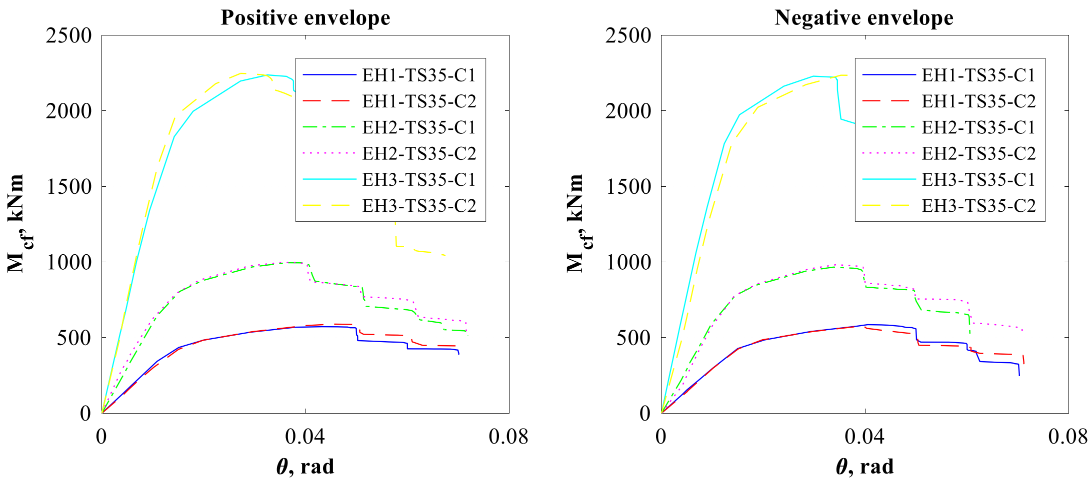

(a) (b)

Figure 6.5: Influence of the beam depth for single-sided joints 35° haunch: a) positive envelopes; b) negative envelopes

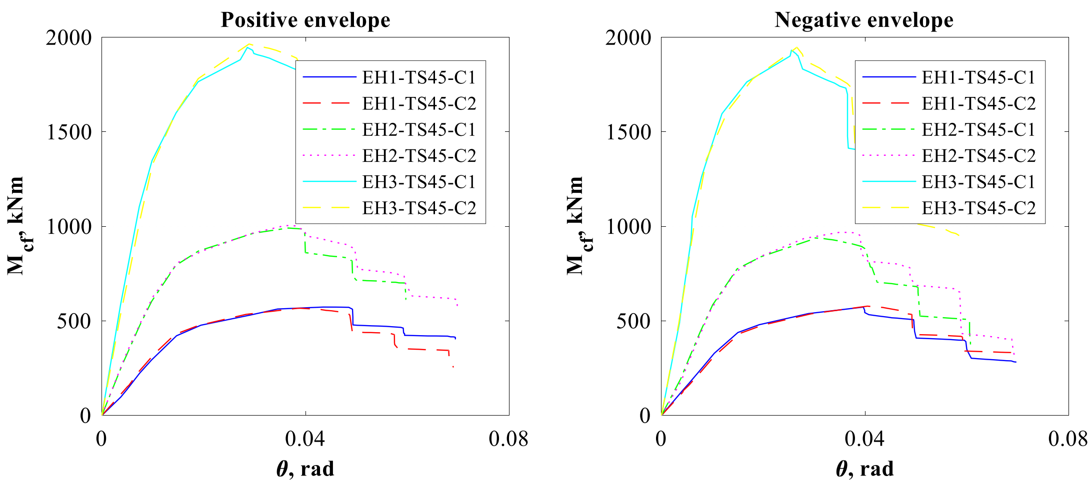

(a) (b)

Figure 6.6: Influence of the beam depth for single-sided joints 45° haunch: a) positive envelopes; b) negative envelopes

6.1.3 Influence of haunch depth

The influence of haunch depth was emphasized by comparing the response of specimens from groups 1 and 2 (Table 2.3). From envelopes plotted in Figure 6.7 and Figure 6.8 and parameters reported in Table 6.1 it can be observed that specimens with 45˚ are prone to more rapid strength degradation after peak bending moment, as well as smaller ultimate drifts. Though this difference is rather small in the case of the specimens with IPE360 beams, it becomes important for larger beam sizes (IPE450 and IPE600). The larger strength of EH3-TS35 specimens with respect to the EH3-TS45 that can be observed in Figure 6.9 occurs due to the fact that the two series were fabricated from different batches, and the yield strength of the material is larger in the case of the former.

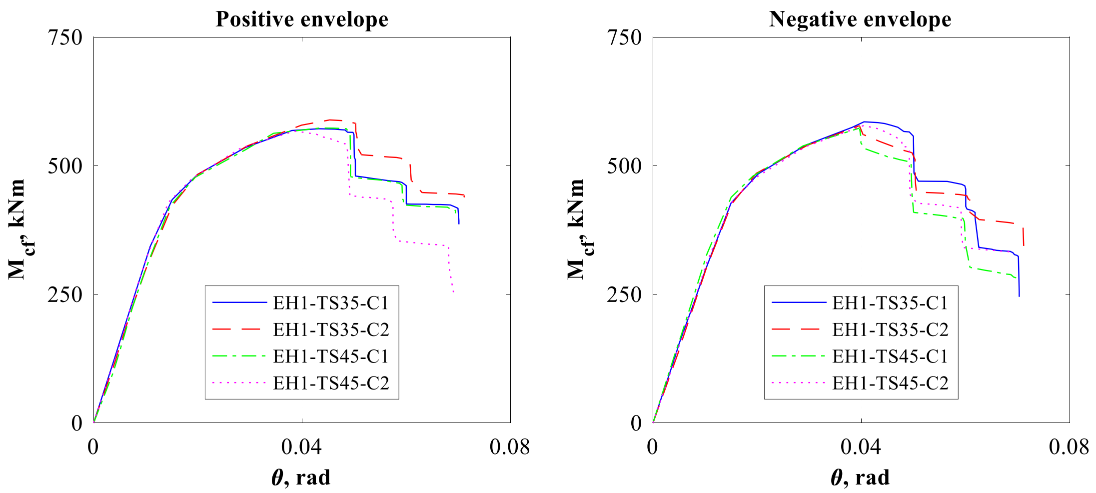

(a) (b)

Figure 6.7: Influence of the haunch depth for IPE360 specimens: a) positive envelopes; b) negative envelopes

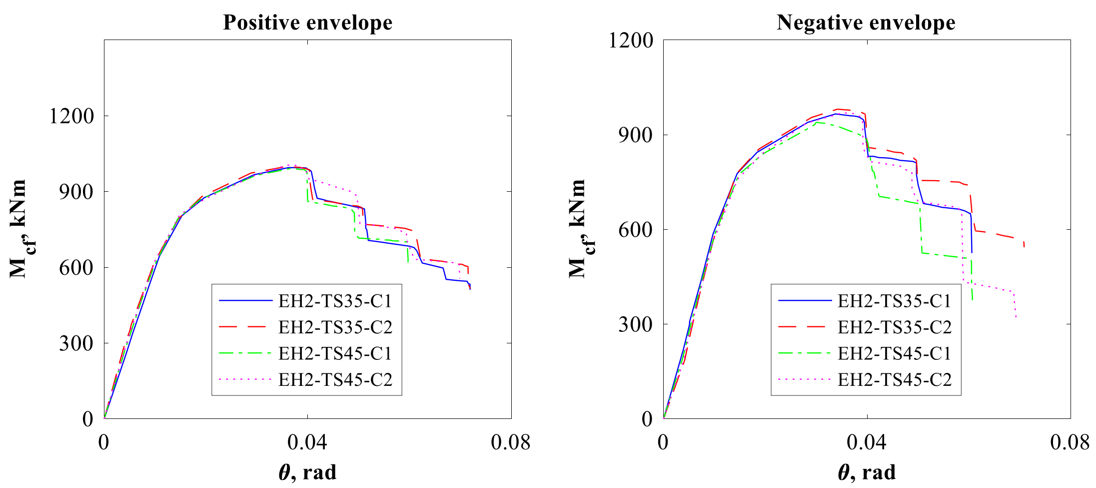

(a) (b)

Figure 6.8: Influence of the haunch depth for IPE450 specimens: a) positive envelopes; b) negative envelopes

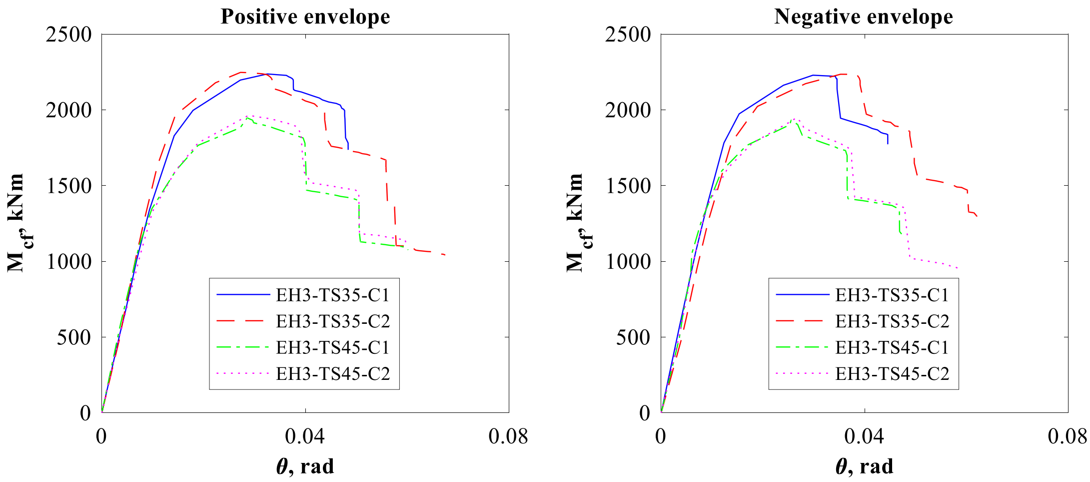

(a) (b)

Figure 6.9: Influence of the haunch depth for IPE600 specimens: a) positive envelopes; b) negative envelopes

6.1.4 *Influence of loading protocol*

Figure 6.10 shows a comparison between the monotonic and cyclic response of the EH2-TS35 specimens. An increase of the maximum moment (due to isotropic strain hardening) and reduction of ultimate deformation capacity can be observed due to cyclic loading. The initial stiffness remains the same for both monotonic and cyclic loading.

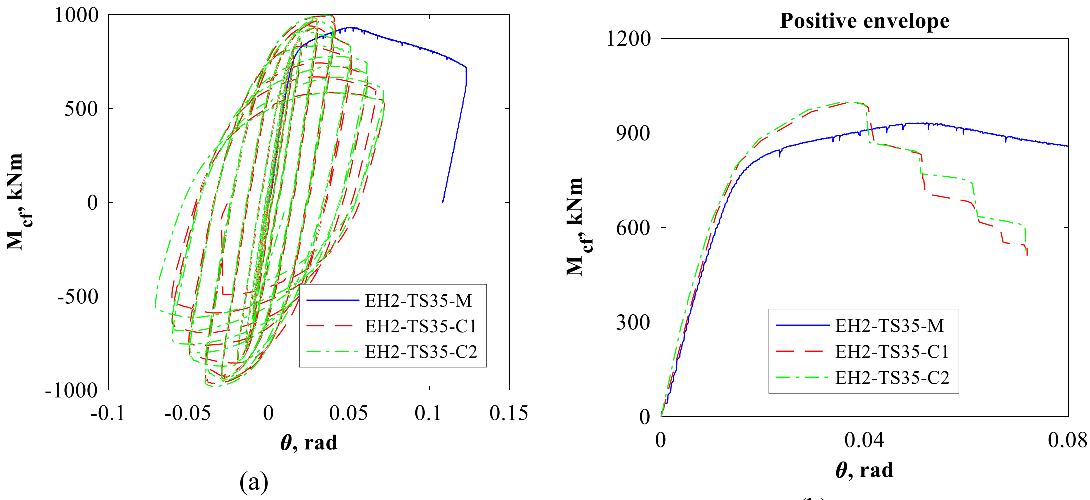

(a) (b)

Figure 6.10: Cyclic and monotone loading: a) hysteretic curves and monotone curve; b) positive envelopes and monotone curve

There is negligible influence between the cyclic loading protocol ANSI/AISC 341 and alternative protocol suggested by EQUALJOINTS project (see Figure 6.11), due to the fact that the difference between the two concerns merely less elastic cycles in the case of the latter.

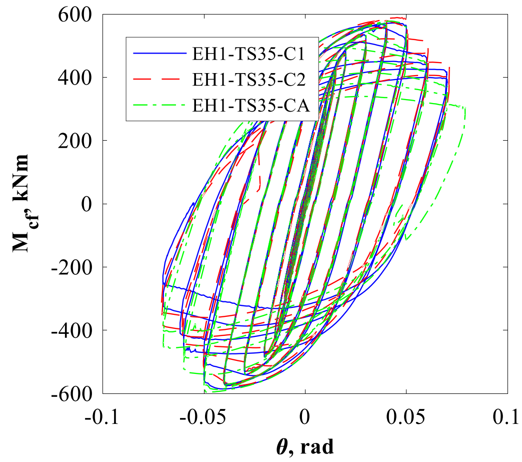

(a)

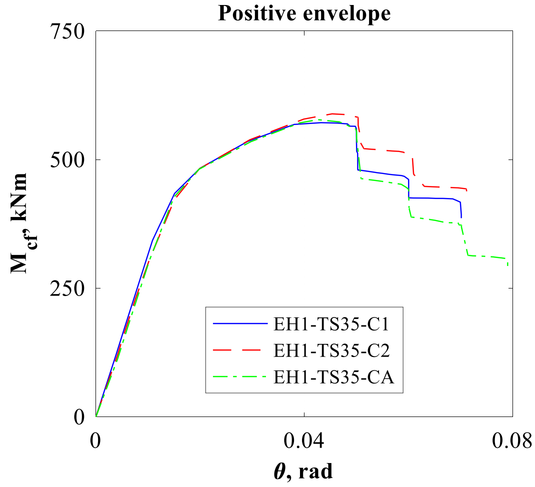

(b)

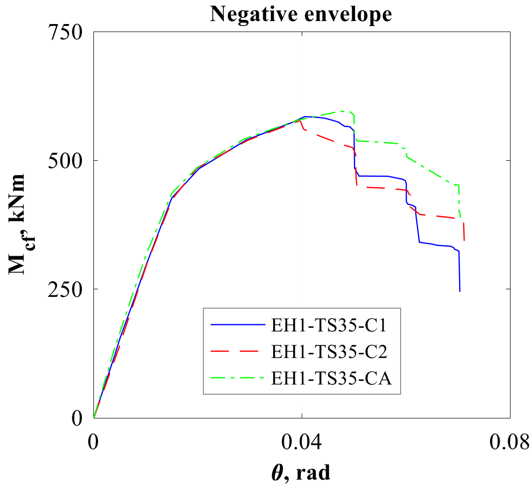

(c)

Figure 6.11: ANSI/AISC 341 loading protocol (EH1-TS35-C1 and EH1-TS35-C2 specimens), alternative protocol (EH1-TS35-CA specimen): a) hysteretic curves for two cyclic loading protocols; b) comparison between positive envelopes; c) comparison between negative envelope

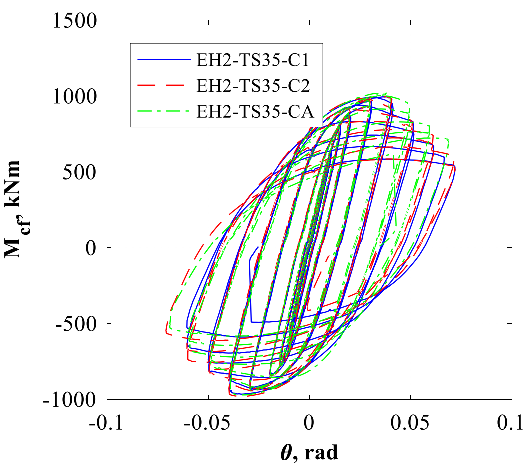

(a)

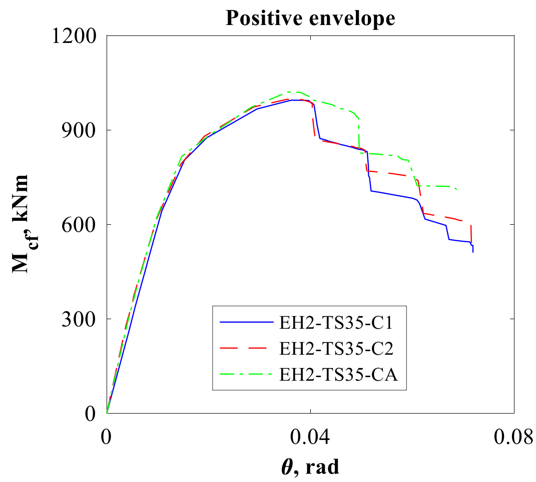

(b)

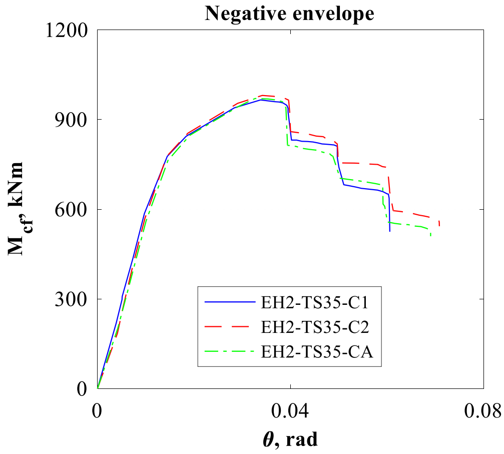

(c)

Figure 6.12: ANSI/AISC 341 loading protocol (EH2-TS35-C1 and EH2-TS35-C2 specimens), alternative protocol (EH2-TS35-CA specimen): a) hysteretic curves for two cyclic loading protocols; b) comparison between positive envelopes; c) comparison between negative envelope

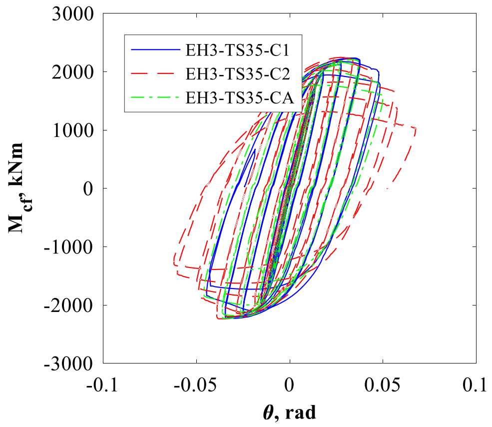

(a)

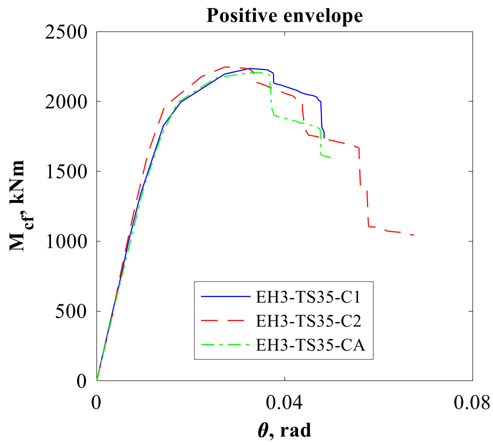

(b)

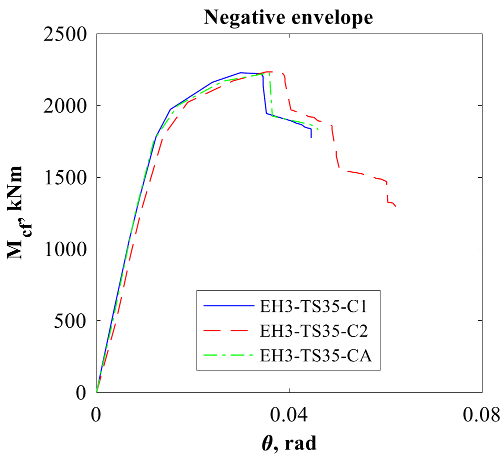

(c)

Figure 6.13: ANSI/AISC 341 loading protocol (EH3-TS35-C1 and EH3-TS35-C2 specimens), alternative protocol (EH3-TS35-CA specimen): a) hysteretic curves for two cyclic loading protocols; b) comparison between positive envelopes; c) comparison between negative envelope

6.1.5 Influence of steel beam over-strength

In order to assess the possible effect of beam over-strength that could potentially trigger a brittle failure mode in the connection, two specimens (TSO series) were fabricated with a beam made of S460 steel grade, instead of S355. In the case of EH1 series of specimens (IPE360 beams) S460 steel grade provided an effective over-strength of 1.3 times the S355 grade. However, in the case of the EH3 series of specimens (IPE600 beams) S460 steel grade provided only negligible over-strength over S355 grade. Thus, beam over-strength was effectively attained only in the case of the EH1 specimens. (IPE360 beams). Despite a larger yield and maximum moments, beam over-strength did not results in a reduction of ultimate drift, nor a change in failure mode of the specimen. Figure 6.14(a, b), shows the M_{cf} - θ envelopes for the EH1 (IPE360 beams) and Figure 6.14 (c, d) for EH3 (IPE600 beams).

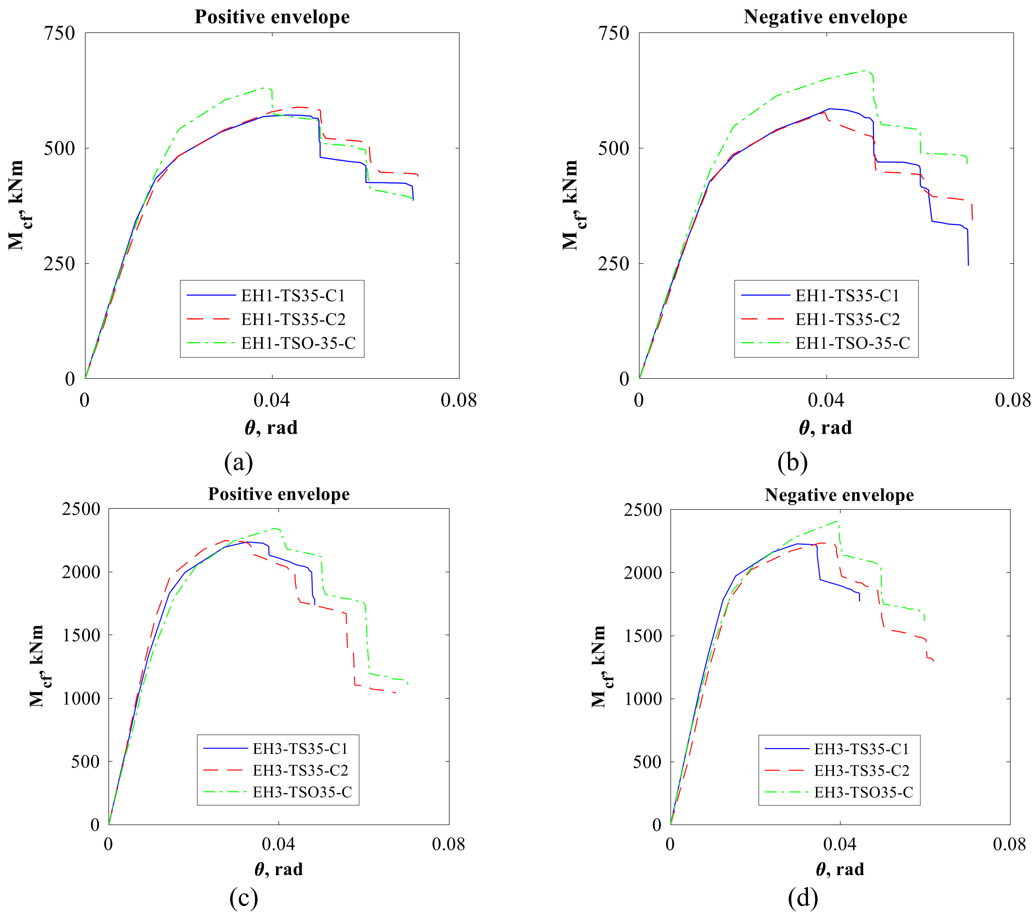

Figure 6.14: Influence of beam steel over-strength: a) EH1 series – positive envelops; b) EH1 series – negative envelops; c) EH3 series – positive envelops; d) EH3 series – negative envelops

6.1.6 Contribution of joint components to total rotation

Figure 6.15 to Figure 6.21 show the contribution of joint components - beam (θ_{bhd}), connection (θ_{cd}), distortion of column web panel (γ_d) and elastic rotation of the assembly (θ_e) – to the interstorey drift (θ). Rotation of the plastic hinge in the beam has the major contribution to the interstorey drift.

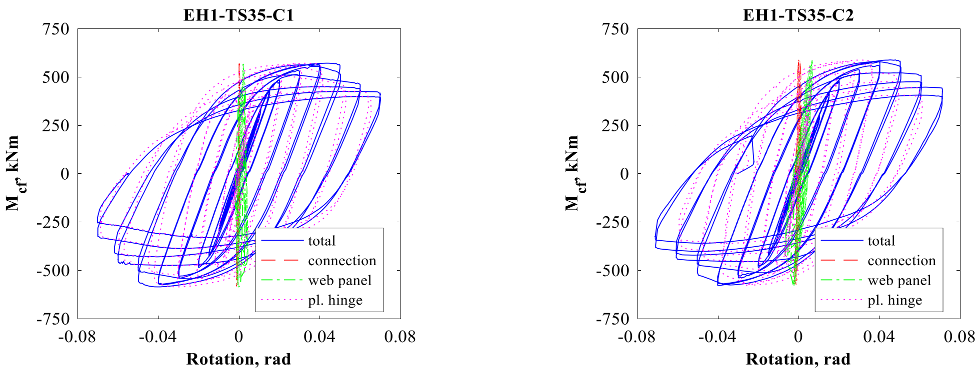

(a) (b)

Figure 6.15: Contribution of component rotations to the interstorey drift of specimens EH1-TS35-C1 and C2

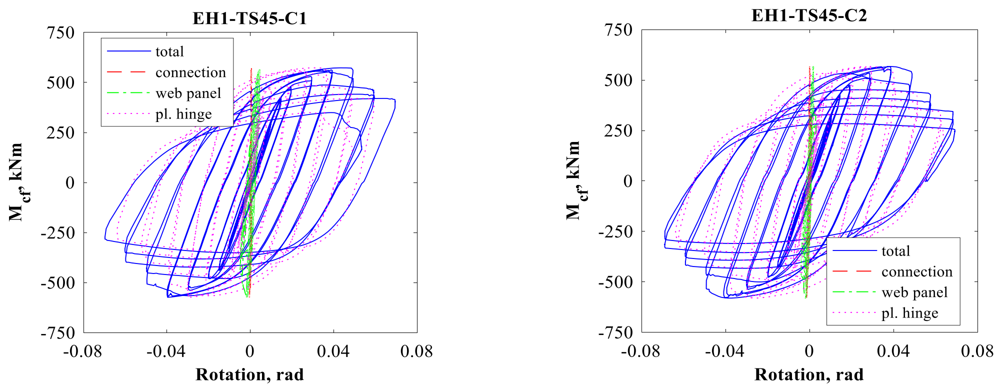

(a) (b)

Figure 6.16: Contribution of component rotations to the interstorey drift of specimens EH1-TS45-C1 and C2

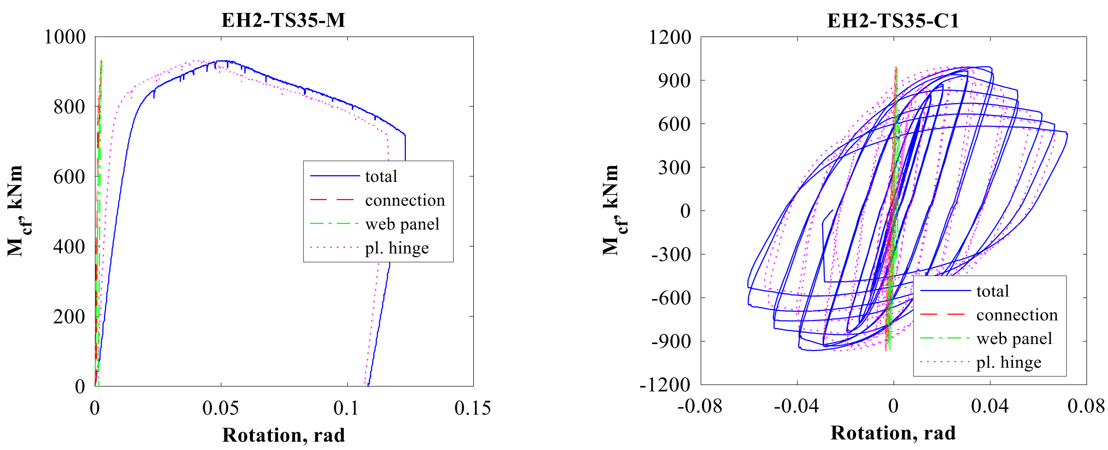

(a) (b)

Figure 6.17: Contribution of component rotations to the interstorey drift of specimens EH2-TS35-M and C1

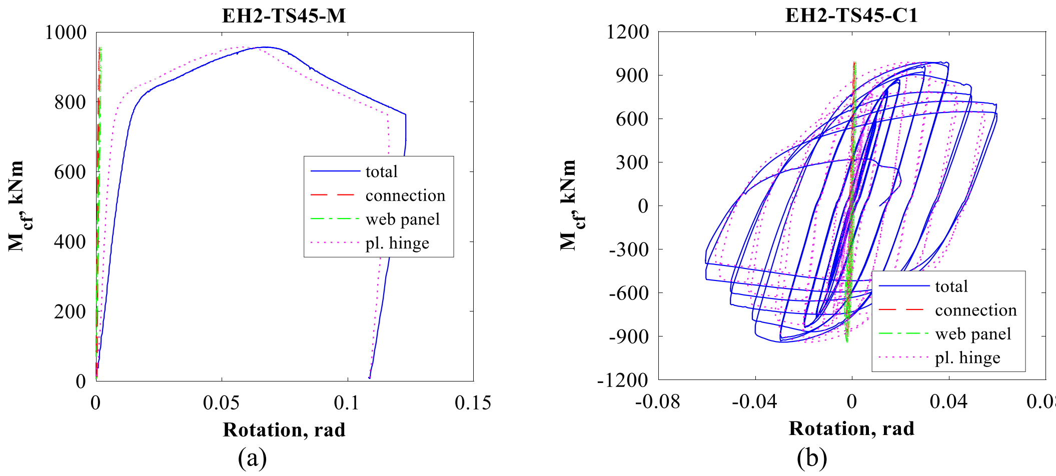

Figure 6.18: Contribution of component rotations to the interstorey drift of specimens EH2-TS45-M and C1

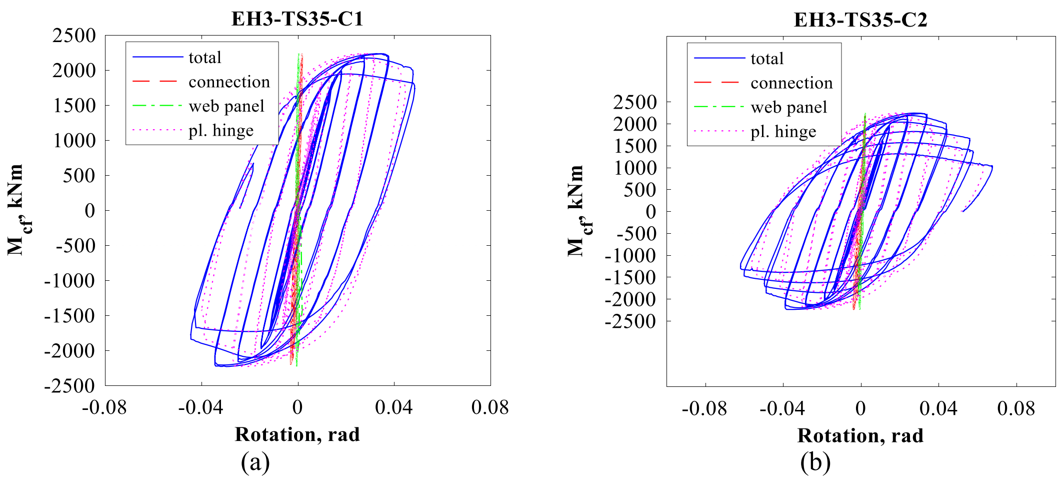

Figure 6.19: Contribution of component rotations to the interstorey drift of specimens EH3-TS35-C1 and C2

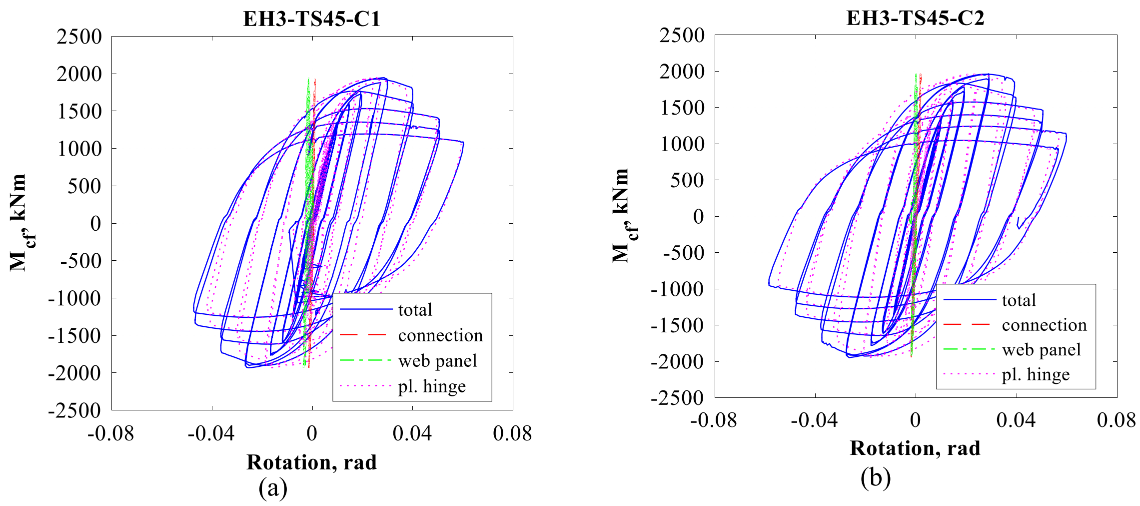

Figure 6.20: Contribution of component rotations to the interstorey drift of specimens EH3-TS45-C1 and C2

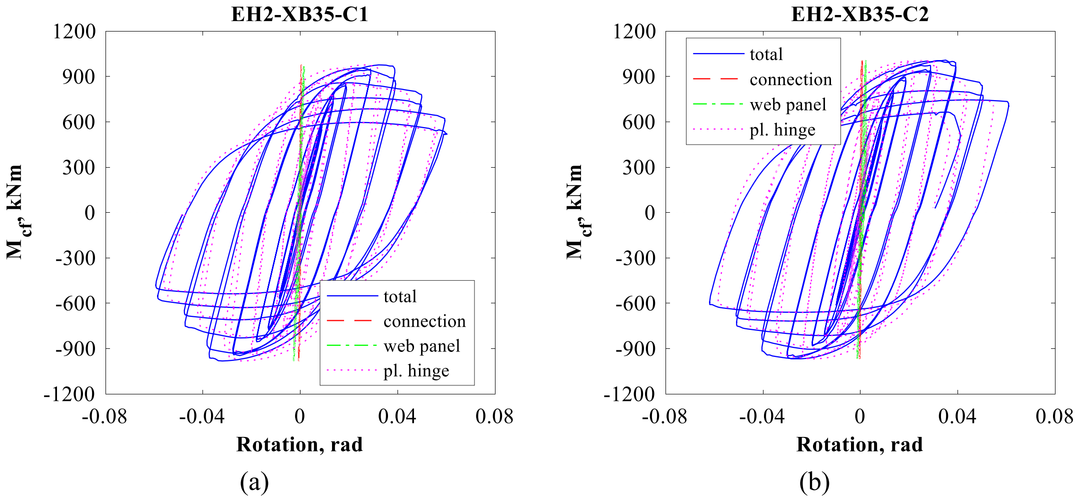

Figure 6.21: Contribution of component rotations to the interstorey drift of specimens EH2-XB35-C1 and C2

6.1.7 Overall remarks on haunched joints

The tests outlined an experimental program for seismic prequalification of bolted beam to column joints with haunches. All specimens showed a stable hysteretic response, with plastic deformation concentrated in the beam next to the haunch. Failure mode was characterized by gradual strength degradation due local buckling of the beam. No significant contribution of column web panel or connection rotation was recorded for the tested specimens. Extensive local buckling triggered eventually cracking of beam flange and web, due to low-cycle fatigue.

All specimens tested under cyclic loading fulfilled the qualification criteria according to ANSI/AISC 341-16 for application in high ductile structural systems. Thus, all joints (1) were capable of accommodating a story drift angle of at least 0.04 rad and (2) the measured flexural resistance of the connection, determined at the column face, was equal to least 0.80Mp of the connected beam at a story drift angle of 0.04 rad.

Performance of joints was quantified also in terms of ultimate interstorey drift, corresponding to 20% drop of the maximum moment. Almost all joints developed ultimate drifts in excess of 0.04 rad under cyclic loading. Ultimate storey drifts were less than 0.04 rad (but larger than 0.03 rad) in the case of joints with large (IPE600) beams with steep (45°) haunches.

6.2 Extended stiffened end-plate joints

The proposed modelling for stiffened extended end-plate joints is depicted in Figure 6.22. Three cases are presented: (b1) exterior joints, (b2) interior moment joints for Moment-resisting frames and (b3) interior braced joints for dual frames (i.e. Moment-resisting frames + Concentrically Braced frames or Moment-resisting frames +

Eccentrically Braced frames). The height of the panel zone is assumed equal to z_{wp}=(h_b+0.3hr_{ib}), see Fig. 6.22 for the meaning of the symbols. The moment-resisting beams have stiff elastic elements at their ends, at a length of s_{rib} from the column face. The brace is connected to the pivot point of the scissors assembly.

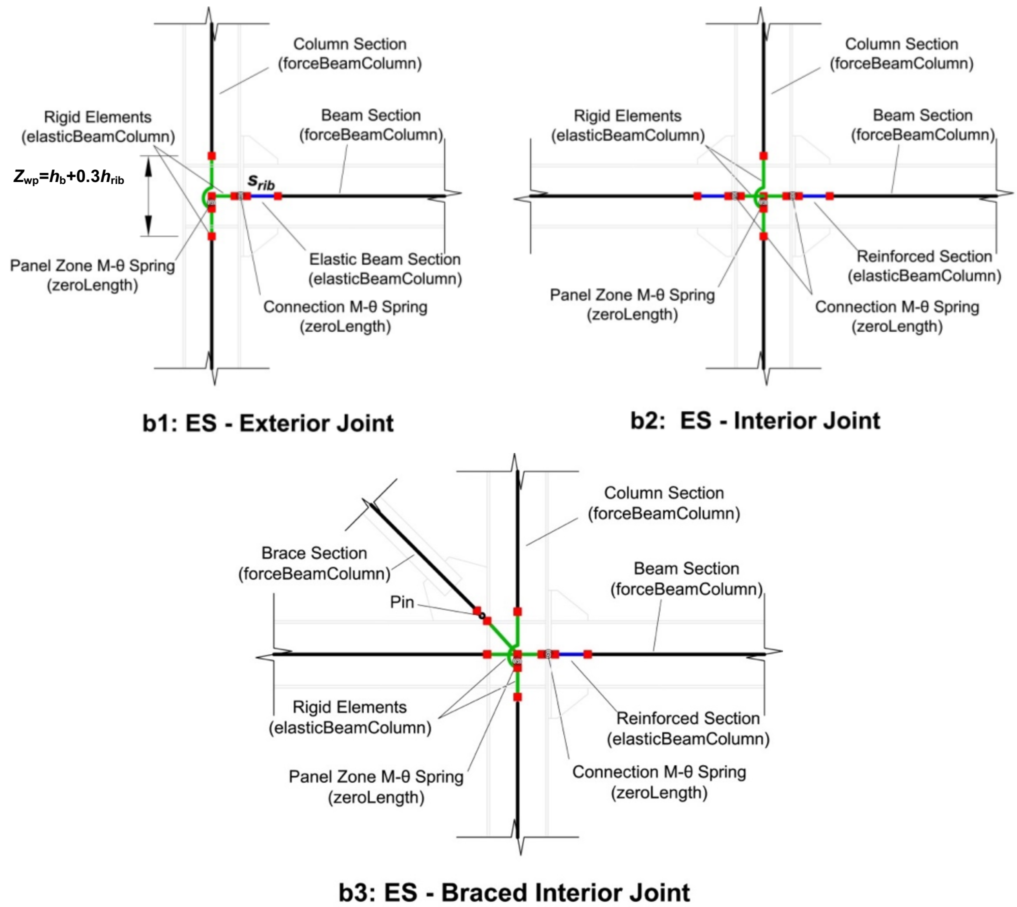

Figure 6.22 Modelling of joints with stiffened extended end-plate connections

A “good guess” estimation of strength-stiffness characteristics of the extended stiffened end-plate joints is given hereinafter. The proposed values have been obtained on the basis of numerical simulations and experimental data on the pre-qualified joints for a set of building archetypes. The validity of these data is limited to the considered assumptions, namely building frames with span length within the range [6m – 8m] and interstorey height within [3.5m – 4m] and beam profiles varying from IPE360 to IPE600. However, once designed the actual geometry of the joint, the mechanical features should be reevaluated to achieve a more accurate prediction of the structural response. The normalisation of strength is with respect to the expected beam plastic strength calculated at the column face, $M^{e}_{pl,b,cf,Rd}$, and the normalisation of stiffness is with respect to the beam flexural stiffness parameter, s_b = EI_b/L_b. The normalised strength values are consistent with the capacity design principles and the normalised stiffness values are averages for each joint design group.

Joint Type	Geometry	Strength		Stiffness	
		Connection:	Panel Zone:	Connection:	Panel Zone:
ES-S-E: Equal strength with strong panel zone	h_{rib}/h_b = 0.35 s_{rib}/h_b = 0.45 $z_{wp} = h_b + 0.3h_{rib}$	$\frac{M^n_{j.Rd}}{M^e_{pl,b,cf,Rd}} = 1.0$	External nodes: $\frac{V^n_{wp.Rd} \cdot z_{wp}}{M^e_{pl,b,cf,Rd}} = 1.15$ Internal nodes: $\frac{V^n_{wp.Rd} \cdot z_{wp}}{2 \cdot M^e_{pl,b,cf,Rd}} = 1.15$	$\frac{s_{con,ini}}{s_b} = 34$	Ext. nodes: $\frac{s_{wp,ini}}{s_b} = 35$ Int. nodes: $\frac{s_{wp,ini}}{2 \cdot s_b} = 35$
ES-S-F: Full-strength with strong panel zone	h_{rib}/h_b = 0.45 s_{rib}/h_b = 0.55 $z_{wp} = h_b + 0.3h_{rib}$	$\frac{M^n_{j.Rd}}{M^e_{pl,b,cf,Rd}} = 1.5$	External nodes: $\frac{V^n_{wp.Rd} \cdot z_{wp}}{M^e_{pl,b,cf,Rd}} = 1.65$ Internal nodes: $\frac{V^n_{wp.Rd} \cdot z_{wp}}{2 \cdot M^e_{pl,b,cf,Rd}} = 1.65$	$\frac{s_{con,ini}}{s_b} = 68$	Ext. nodes: $\frac{s_{wp,ini}}{s_b} = 56$ Int. nodes: $\frac{s_{wp,ini}}{2 \cdot s_b} = 56$
ES-B-E: Equal strength with balanced panel zone	h_{rib}/h_b = 0.35 s_{rib}/h_b = 0.45 $z_{wp} = h_b + 0.3h_{rib}$	$\frac{M^n_{j.Rd}}{M^e_{pl,b,cf,Rd}} = 1.0$	External nodes: $\frac{V^n_{wp.Rd} \cdot z_{wp}}{M^e_{pl,b,cf,Rd}} = 1.0$ Internal nodes: $\frac{V^n_{wp.Rd} \cdot z_{wp}}{2 \cdot M^e_{pl,b,cf,Rd}} = 1.0$	$\frac{s_{con,ini}}{s_b} = 37$	Ext. nodes: $\frac{s_{wp,ini}}{s_b} = 30$ Int. nodes: $\frac{s_{wp,ini}}{2 \cdot s_b} = 30$

Notes:

i) Elasto-plastic behaviour is assumed for the connection springs, with 1% post-yield hardening. The assumed pre-capping plastic rotation capacity of the connection component is 42 mrad (ASCE 41-13, Table 9-6, yield of bolted end-plate). In OpenSEES the connection behaviour can be implemented e.g. by assigning a Bilin material (modified Ibarra-Medina-Krawinkler model) to the rotational DOF of the spring.

ii) The spring for the column web panel zone is modelled according to the established tri-linear model by Krawinkler (see Gupta and Krawinkler, 1999). The proposed strength value corresponds to the **first** yield point (panel). A post-yield hardening of 1.5% is assumed. In OpenSEES the panel zone behaviour may be implemented by assigning Hysteretic or Steel02 material to the rotational DOF of the spring.

iii) When modelling the panel zone using (a) a parallelogram of rigid elements and pins or (b) the Joint2D macromodel, the kinematics are identical and the properties of the rotational spring are the same. In this case the elastic spring stiffness is: $s_{wp} = (V_{wp}/\gamma) z_{wp}$

iv) If the panel zone is modelled according to the “scissors” model, the strength and stiffness values of the rotational spring (calculated per Krawinkler’s approach) have to be modified (see Charney and Downs, 2004)

6.2.1 Performance parameters of tested joints

The performance parameters that are usually adopted for the seismic pre-qualification (see Figure 6.1a) obtained for ES joints are reported in Table 6.3. For equal strength joints that are characterized by response curves without significant

loss of strength the ultimate deformation Θ_u is determined as the minimum value between the positive and negative peak chord rotation.
It can be observed that the strain hardening coefficient is relatively uniform across specimens, averaging at about $\gamma_h = 1.30$. Ultimate inter-storey drift (Θ_u) is generally larger than 0.04 rad (the minimum requirement specified in ANSI/AISC 341-16 for special steel moment frames), as well as the plastic rotation is larger than 0.035 rad (the minimum requirement specified in EN1998-1 for ductility class high). Therefore, both full strength and equal strength extended stiffened end-plate joints can be used in high ductile structures and can be considered qualified with the only exception of the ES3-XS-E-C1 and ES3-XS-E-C2 specimens.

Table 6.3: **Performance parameters of tested extended stiffened beam-to-column joints**

Specimen	S_{ini}, kNm/rad	M_y, kNm	M_{max}, kNm	γ_h	Θ_y, rad	Θ_u, rad	Θ_p, rad
ES1-TS-E-C1	23000	433.33	505.78	1.17	0.019	0.068	0.049
ES1-TS-E-C2	22800	411.11	489.67	1.19	0.018	0.068	0.05
ES1-TS-Esp-C	21500	444.44	503.84	1.13	0.021	0.064	0.043
ES1-TS-F-C1	27800	444.44	518.64	1.17	0.016	0.064	0.048
ES1-TS-F-C2	27800	433.33	524.82	1.21	0.016	0.062	0.046
ES1-TS-F-M	27600	461.11	577.52	1.25	0.017	0.094	0.077
ES1-TS-E-C1_L	27100	413.33	505.67	1.22	0.015	0.066	0.051
ES1-TS-E-C1_R	26800	427.78	504.56	1.18	0.016	0.062	0.046
ES1-TS-E-C2_L	27100	413.33	509.03	1.23	0.015	0.066	0.051
ES1-TS-E-C2_R	27300	433.33	502.67	1.16	0.016	0.061	0.045
ES2-TS-E-C1	45500	738.89	897.19	1.21	0.016	0.063	0.047
ES2-TS-E-C2	45500	733.33	856.66	1.17	0.016	0.066	0.05
ES2-TS-Esp-C	47500	724.44	879.92	1.21	0.015	0.064	0.049
ES2-TS-F-C1	55600	822.22	991.85	1.21	0.015	0.062	0.047
ES2-TS-F-C2	52000	844.44	1002.93	1.19	0.016	0.061	0.045
ES2-TS-F-CA	52000	844.44	985.52	1.17	0.016	0.061	0.045
ES2-TS-E-C1_L	54300	722.22	912.04	1.26	0.015	0.063	0.048
ES2-TS-E-C1_R	58000	755.56	927.00	1.23	0.013	0.042	0.029
ES2-TS-E-C2_L	54600	744.44	900.62	1.21	0.014	0.053	0.039
ES2-TS-E-C2_R	57000	755.56	908.46	1.20	0.013	0.043	0.03
ES3-TS-E-C1	135000	1811.11	2081.54	1.15	0.013	0.051	0.038
ES3-TS-E-C2	135000	1866.67	2127.01	1.14	0.014	0.049	0.035
ES3-TS-Esp-C	135000	1888.89	2084.26	1.10	0.014	0.05	0.036
ES3-TS-F-C1	215000	1888.89	2202.29	1.17	0.009	0.049	0.04
ES3-TS-F-C2	170000	1833.33	2107.21	1.15	0.011	0.04	0.029
ES3-TS-F-M	165000	1700.00	1987.60	1.17	0.01	0.068	0.058
ES3-TS-Esp-C	136029	1621.19	2090.09	1.29	0.012	0.05	0.038
ES3-XS-E-C1**	116025	1501.22	1882.25	1.25	0.013	0.03	0.017
ES3-XS-E-C2***	-	-	-	-	-	-	-

** this test was characterized by the unexpected brittle failure of the beam, which damaged the test setup
***owing to the damage of the test setup due to the unexpected failure of the beam, this test was not performed.

6.2.2 Failure mechanisms

The failure modes of extended stiffened joints depend on the design performance level. Indeed, those designed as full strength joints exhibit a failure mode similar to haunched joints (i.e. plastic hinge of the beam with progressive deterioration due to local buckling and fracture of the beam due to low cycle fatigue), as it can be observed in Figure 6.23. On the contrary, the joints designed as equal strength with full strength web panel show a more complex failure mechanism with the plastic deformations in both beam (i.e. local buckling of the flanges) and connection (i.e. end-plate in bending), as it can be observed in Figure 6.24. All tested double-sided (or internal) joints were designed as equal strength connection with strong web panel and their relevant experimental failure mode is fully consistent with the design criteria and in line with the corresponding external joints. An example of failure mode of internal joint is depicted in Figure 6.25.

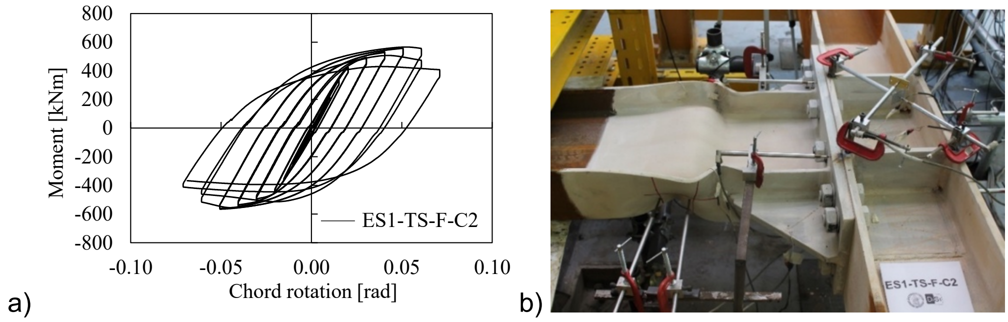

Figure 6.23: Full strength single-sided extended end-stiffened joints: experimental response (a) and failure mode (b) of ES1-TS-F-C2

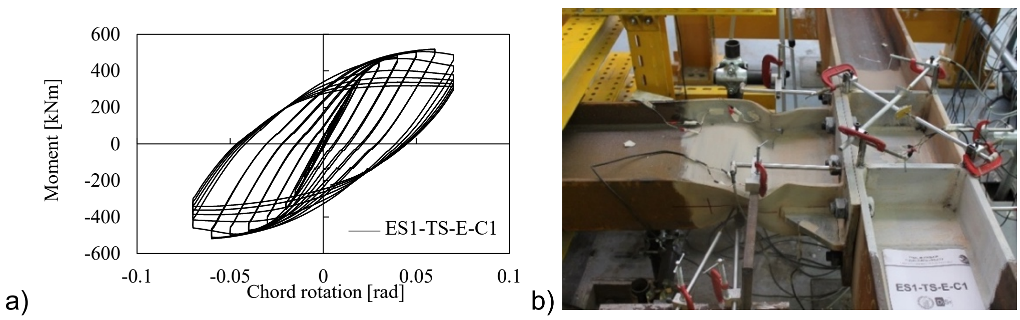

Figure 6.24: Equal strength single-sided extended end-stiffened joints: experimental response (a) and failure mode (b) of ES1-TS-E-C1

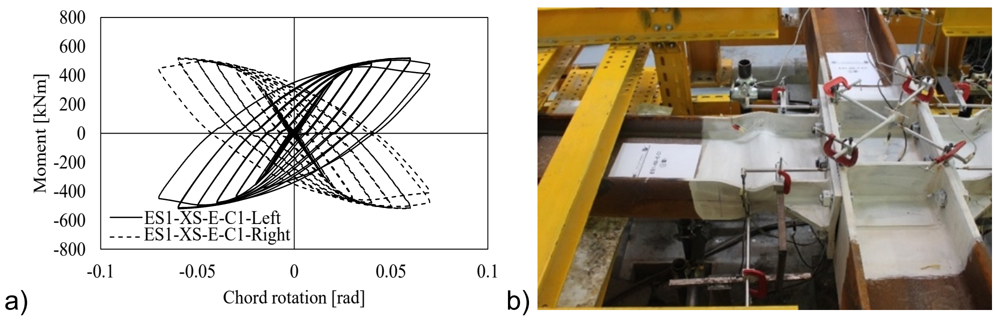

Figure 6.25 Equal strength double-sided extended end-stiffened joints: experimental response (a) and failure mode (b) of ES1-XS-E-C1

It is important to highlight that in all cases the column web panel behave in elastic range. As general remark it can be also observed that the performance of the most of extended end-plate joints is stable without appreciable degradation up to 0.04 rad. However, there are two exceptions, namely ES3-XS-E-C joints. Indeed, the test on ES3-XS-E-C1 has been prematurely stopped because an unexpected big and brittle crack appeared at the level of the beam flange in tension before the development of significant yielding in the specimen. The value of the applied moment at the level of the beam when the crack appeared is just equal to the plastic bending moment of the beam computed using the actual properties of the steel material.

6.2.3 Influence of beam depth

The influence of the member size on response curves of full strength extended stiffened joint is very similar to that exhibited by haunched joints, namely increasing the beam depth the rotation capacity decreases. However, in case of equal strength joints there is only an increase of the yield rotation, but no appreciably influence can be observed for the ultimate rotation, as it can be recognized on the data reported in Table 6.3. It should be highlighted that increasing the beam depth of equal strength joints increases the tendency to brittle failure into the beam when plastic hinge form. The fracture starts from the toe of the weld at the rib tip and propagates into the beam web, see Figure 6.26. This phenomenon occurs only for ES2-E and ES3-E assemblies. However, in the ES2-E assemblies the failure occurs at large rotation demand (i.e. about 6%), while in the ES3-E assemblies rather soon (i.e. about 3%).

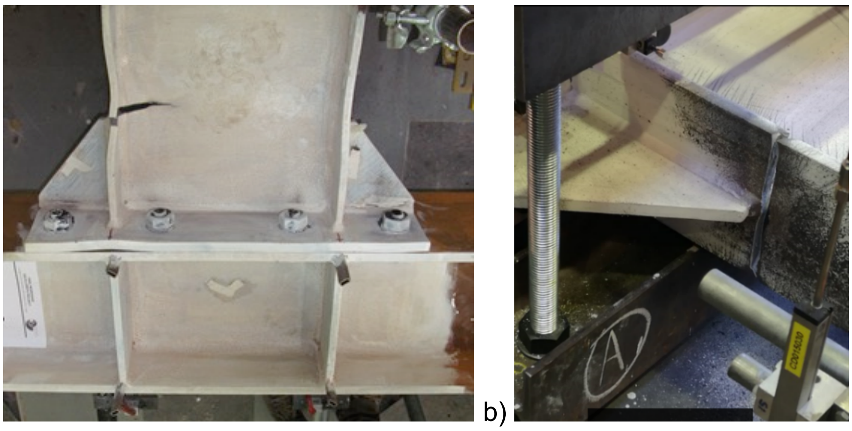

a) b)

Figure 6.26: Influence of beam depth on the failure mode of equal strength extended end-stiffenedjoints: ES2-TS-E-C2 (a) ES3-XS-E-C1 (b)

6.2.4 Influence of shot peening

The test results on equal strength extended stiffened joints fabricated using shot peeing (i.e. those identified with the subscript “sp”) for the welds of the connection clearly show that this treatment does not influence the response of the joints. To clarify this result, the comparison between the average envelope curves of the groups of ES1 and ES2 equal strength joints are depicted in Figure 6.27a and Figure 6.27b, respectively, while a comparison in terms of hysteretic loops is depicted in Figure 6.27c.

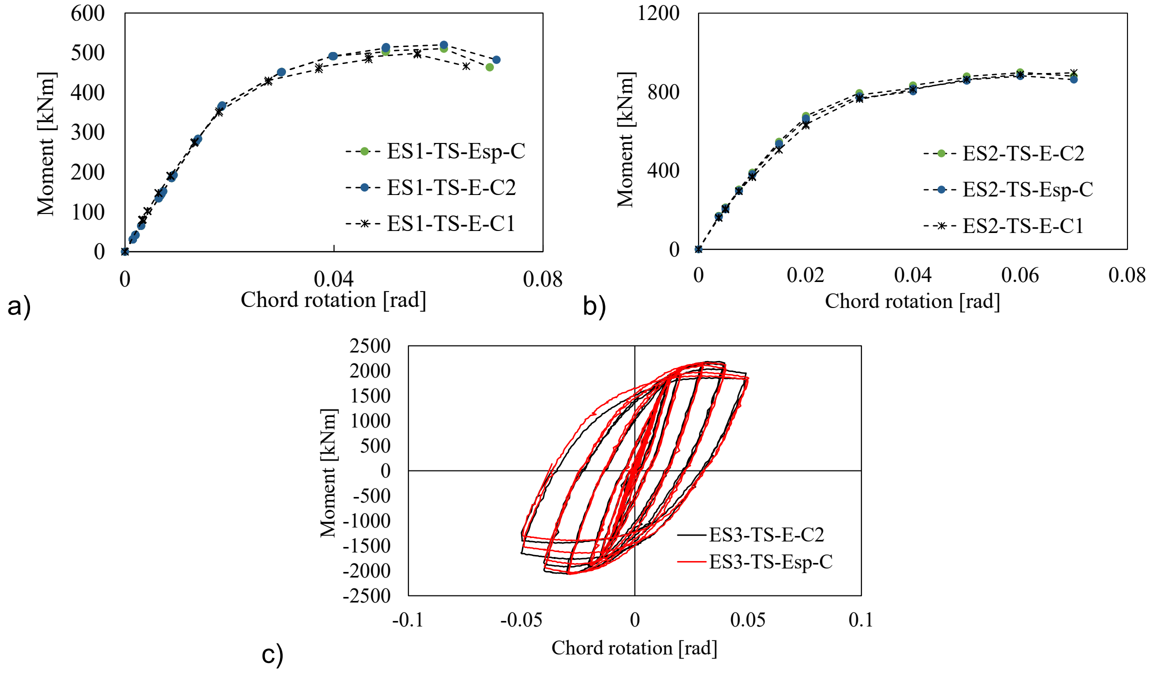

Figure 6.27: the influence of shot peening on equal strength extended stiffened joints: a) and b) average envelope curves, c) cyclic response curves

6.2.5 Influence of loading protocol

The influence of loading protocol on extended stiffened end-plate joints is very similar to that observed for haunched joints. Figure 6.28a, shows a comparison between the monotonic and cyclic response of the ES1-TS-F specimens. The influence of the type of cyclic loading protocol (ANSI/AISC 341-10 and EQUALJOINTS), see Figure 6.28b, is negligible due to the fact that the difference between the two concerns merely less elastic cycles in the case of the latter.

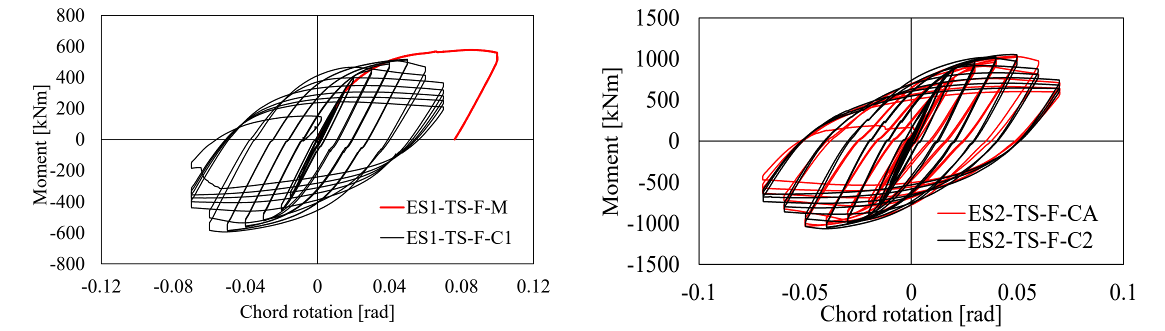

(a) (b)

Figure 6.28: Extended stiffened joints: a) Monotonic vs cyclic loading; b) hysteretic curves for two cyclic loading protocols

6.2.6 *Contribution of joint components to plastic rotation*

The contribution of joint components differs for full strength and equal strength joints. In the former case the most of plastic contribution is offered by the beam, with negligible contribution in elastic range provided by the other components, see Figure 6.29.

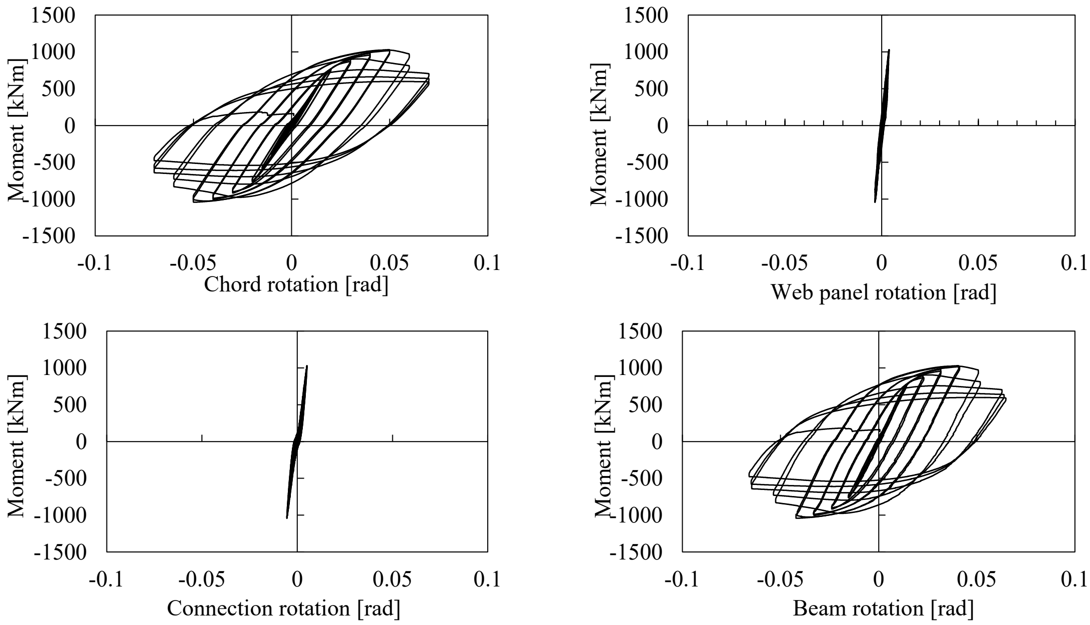

Figure 6.29: Contributions to plastic rotation of full strength ES2 joints: ES2-TS-F-C2

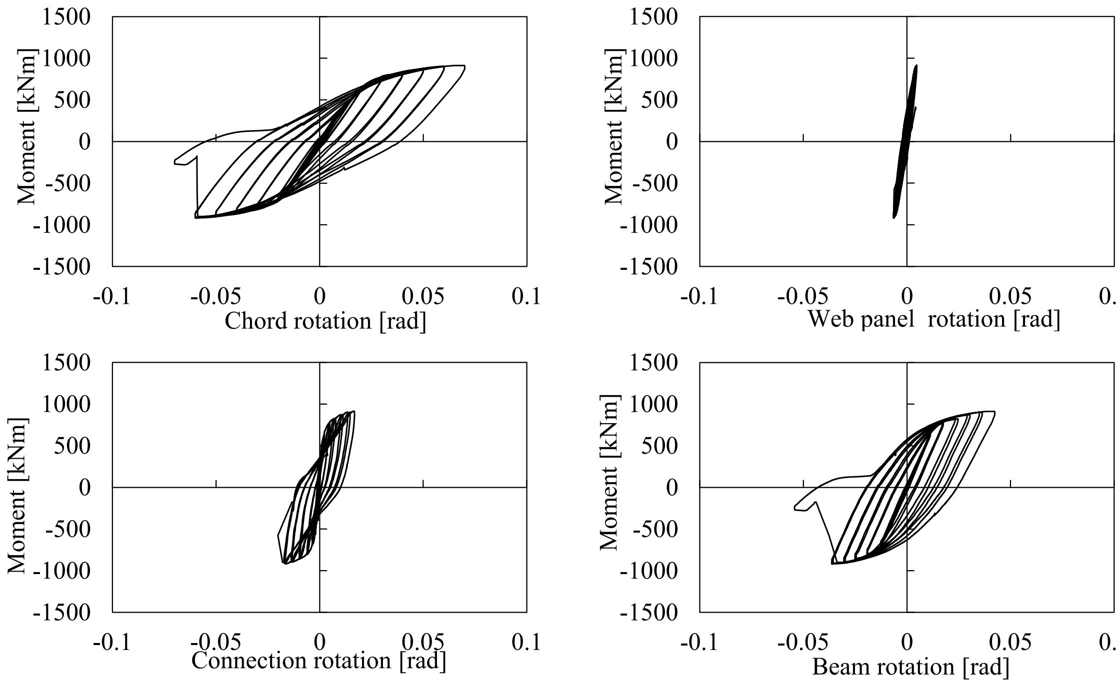

Figure 6.30: Contributions to plastic rotation of equal strength ES2 joints: ES2-TS-E-C1

The case of equal strength ES joints is different. Indeed, this type of joint exhibits plastic deformation mostly into the beam, with some plastic engagement of the connection while the column web panel is in elastic range. Therefore, it can be concluded that for ES equal strength joints the beam rotation ranges within 80-90% of the overall rotation, while the connection cover 10-20% of the total rotation.

6.2.7 Overall remarks on extended stiffened end-plate joints

On the basis of the experimental evidence the following remarks can be drawn:

- All full strength specimens exhibit a stable hysteretic response, with plastic deformation concentrated in the beam next to the rib stiffened. This failure mode is characterized by progressive strength degradation due local buckling of the beam. Column web panel behave in elastic range.
- The most of equal strength joints exhibit a stable hysteretic response without strength degradation, because the plastic deformation is balanced between the end-plate in bending and the beam.
- All joints except two double-sided ES3 assemblies satisfy both ANSI/ASIC 341 and EN1998-1. Therefore, it can be used for high ductility class structures.
- Further investigation is necessary to clarify the reasons of the brittle failure of two double-sided ES3 assemblies.
- The experimental tests confirm that the shift of center of compression into the connection is in line with the design assumption that were supported by pre-test advanced numerical simulation.
- The design over-strength for full strength connection (i.e. $\gamma_{ov}\times\gamma_{sh}$=1.25×1.2=1.5) is a satisfactory safety margin.

6.3 Extended unstiffened end-plate joints

The proposed modelling for unstiffened extended end-plate joints (type c) is presented in the schematics that follow. Three cases are presented: (c1) exterior joints, (c2) interior moment joints and (c3) interior braced joints. The height of the panel zone is assumed equal to h_b. The brace is connected to the top node of the joint element. The brace is connected to the pivot point of the scissors assembly.

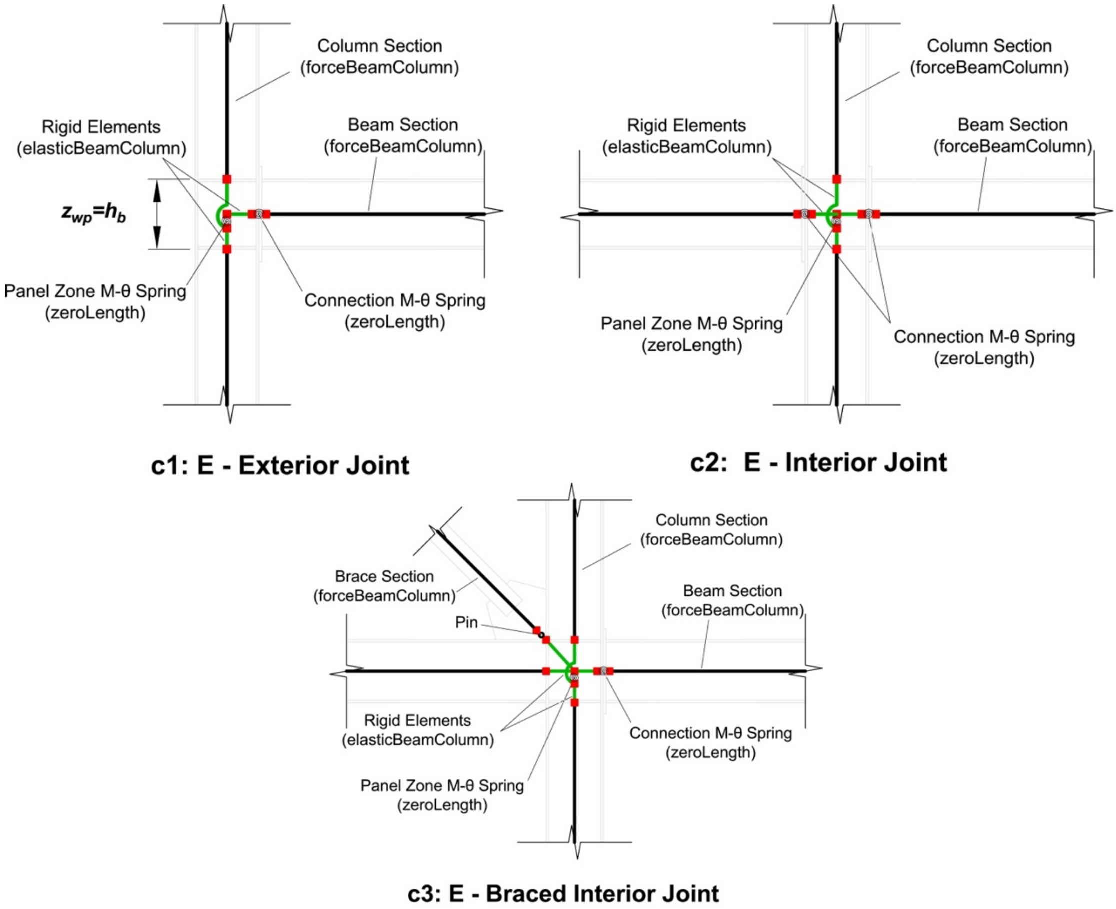

Figure 6.31: Modelling of joints with stiffened extended end-plate connections

A "good guess" estimation of strength-stiffness characteristics of the extended unstiffened joints is given hereinafter. The proposed values have been obtained on the basis of numerical simulations and experimental data on the pre-qualified joints for a set of building archetypes. The validity of these data is limited to the considered assumptions, namely building frames with span length within the range [6m – 8m] and interstorey height within [3.5m – 4m] and beam profiles varying from IPE360 to IPE600. However, once designed the actual geometry of the joint, the mechanical features should be reevaluated to achieve a more accurate prediction of the structural response.

The normalised strength values are consistent with the capacity design principles and the normalised stiffness values are averages for each joint design group.

Joint Type	Geometry	Strength		Stiffness	
		Connection:	Panel Zone:	Connection:	Panel Zone:
E-B-E: Equal strength with balanced panel zone	$z_{wp} = z_{eq}$	$\frac{M^n_{j.Rd}}{M^e_{pl,b,Rd}} = 1.0$	External nodes: $\frac{V^n_{wp.Rd} \cdot z_{wp}}{M^e_{pl,b,cf,Rd}} = 1.0$ Internal nodes: $\frac{V^n_{wp.Rd} \cdot z_{wp}}{2 \cdot M^e_{pl,b,cf,Rd}} = 1.0$	$\frac{s_{con,ini}}{s_b} = 28$	Ext. nodes: $\frac{s_{wp,ini}}{s_b} = 19$ Int. nodes: $\frac{s_{wp,ini}}{2 \cdot s_b} = 19$
E-B-P(0.6): Partial strength with balanced panel zone	$z_{wp} = z_{eq}$	$\frac{M^n_{j.Rd}}{M^e_{pl,b,Rd}} = 0.6$	External nodes: $\frac{V^n_{wp.Rd} \cdot z_{wp}}{M^e_{pl,b,cf,Rd}} = 0.6$ Internal nodes: $\frac{V^n_{wp.Rd} \cdot z_{wp}}{2 \cdot M^e_{pl,b,cf,Rd}} = 0.6$	$\frac{s_{con,ini}}{s_b} = 22$	Ext. nodes: $\frac{s_{wp,ini}}{s_b} = 19$ Int. nodes: $\frac{s_{wp,ini}}{2 \cdot s_b} = 19$
E-W-P(0.8): Partial strength with weak panel zone	$z_{wp} = z_{eq}$	$\frac{M^n_{j.Rd}}{M^e_{pl,b,Rd}} = 0.8$	External nodes: $\frac{V^n_{wp.Rd} \cdot z_{wp}}{M^e_{pl,b,cf,Rd}} = 0.6$ Internal nodes: $\frac{V^n_{wp.Rd} \cdot z_{wp}}{2 \cdot M^e_{pl,b,cf,Rd}} = 0.6$	$\frac{s_{con,ini}}{s_b} = 24$	Ext. nodes: $\frac{s_{wp,ini}}{s_b} = 14$ Int. nodes: $\frac{s_{wp,ini}}{2 \cdot s_b} = 14$

Notes:

i) Elasto-plastic behaviour is assumed for the connection springs, with 1% post-yield hardening. The assumed pre-capping plastic rotation capacity of the connection component is 18 mrad (ASCE 41-13, Table 9-6, yield of bolts). In OpenSEES the connection behaviour can be implemented e.g. by assigning a Bilin material (modified Ibarra-Medina-Krawinkler model) to the rotational DOF of the spring.

ii) The spring for the column web panel zone is modelled according to the established tri-linear model by Krawinkler (see Gupta and Krawinkler, 1999). The proposed strength value corresponds to the **first** yield point (plastic hinges at column flanges or continuity plates). A post-yield hardening of 1.5% is assumed. In OpenSEES the panel zone behaviour may be implemented by assigning Hysteretic or Steel02 material to the rotational DOF of the spring.

iii) When modelling the panel zone using (a) a parallelogram of rigid elements and pins or (b) the Joint2D macromodel, the kinematics are identical and the properties of the rotational spring are the same. In this case the elastic spring stiffness is: $s_{wp} = (V_{wp}/\gamma)z_{wp}$

iv) If the panel zone is modelled according to the "scissors" model, the strength and stiffness values of the rotational spring (calculated per Krawinkler's approach) have to be modified (see Charney and Downs, 2004).

v) $S_b = EI_b/L_b$ where I_b and L_b are respectively the moment of inertia and the length of the connected beam.

6.3.1 Performance parameters of tested joints

The performance parameters of unstiffened joints are obtained according to the procedure described in Figure 6.1b, being the beam almost in elastic range in all cases.

Table 6.4: **Performance parameters of tested extended unstiffened beam-to-column joints**

Specimen	$S_{j,ini}$, kNm/rad	$M_{b,Rk}$, kNm	$M_{b,Ru}$, kNm	γ_h	$\varphi_{j,u}$, rad	$\varphi_{j,pl}$, rad	$(M_{b,Rk}/M_{,b,pl})_{actual}$	$(M_{b,Rk}/M_{,b,pl})_{target}$
E1-TB-E-M	87486	290	422	1,46	0,067	0,064	0,75	1
E1-TB-E-C1	76596	310	461	1,49	0,040	0,038	0,80	1
E1-TB-E-C2	77419	301	455	1,51	0,041	0,036	0,77	1
E1-TB-P-C1	68068	300	412	1,37	0,035	0,027	0,77	0,6
E1-TB-P-C2	67069	300	402	1,34	0,046	0,037	0,77	0,6
E1-TB-PP-C	70707	301	395	1,31	0,036	0,030	0,77	0,6
E1-XW-P-C1	57480	298	358	1,20	0,082	0,074	0,77	0,8
E1-XW-P-C2	59310	301	385	1,28	0,079	0,072	0,77	0,8
E2-TB-E-M	148290	515	705	1,37	0,055	0,052	0,68	1
E2-TB-E-C1	130194	503	716	1,42	0,051	0,047	0,66	1
E2-TB-E-C2	119654	484	728	1,50	0,052	0,048	0,64	1
E2-TB-P-C1	131434	461	638	1,38	0,038	0,034	0,61	0,6
E2-TB-P-C2	176417	432	567	1,31	0,034	0,032	0,57	0,6
E2-TB-PP-C	134072	475	622	1,31	0,037	0,033	0,63	0,6
E2-XW-P-C1								0,8
E2-XW-P-C2	114523	500	657	1,31	0,069	0,065	0,66	0,8
E3-TB-E-C1	272822	1.063	1.394	1,31	0,035	0,031	0,63	1
E3-TB-E-C2	301250	1.060	1.360	1,28	0,034	0,030	0,63	1
E3-TB-E-CA	337234	995	1.406	1,41	0,037	0,034	0,60	1
E3-TB-P-C1	380625	923	1.280	1,39	0,046	0,044	0,55	0,6
E3-TB-P-C2	426875	1.037	1.354	1,31	0,046	0,044	0,62	0,6
E3-TB-PP-C	335253	991	1.324	1,34	0,049	0,046	0,59	0,6
E3-XW-P-C1	378552	950	1.129	1,19	0,085	0,082	0,57	0,8
E3-XW-P-C2	298606	874	1.101	1,26	0,073	0,070	0,52	0,8

The values obtained for the E joints are reported in Table 6.4. When small differences exist between the curves corresponding to hogging and sagging bending moments respectively, the minimum values are indicated (resistances and deformation capacity).

It can be observed that the strain hardening coefficient is relatively uniform for all specimens (except for few of them), averaging at about γ_h =1,35. The ultimate rotational deformations ($\varphi_{j,u}$) are generally higher than 0.04 rad (the minimum requirement specified in ANSI/AISC 341-10 for special steel moment frames) and the plastic rotations is generally larger than 0.035 rad (the minimum requirement specified in EN1998-1 for ductility class high). Therefore, both equal strength and partial strength unstiffened end-plate joints can be used in high ductile structures and can be considered qualified with the exception of the E3-TB-E-C2 and E2-TB-P-C2 specimens ($\varphi_{j,pl}$, rad = 0,030 rad).

From the two last columns of Table 6.4, it may be concluded that the targeted plastic resistance is rather well reached for partial-strength joints with balanced panel zone, much less for partial-strength joints with weak panel zone and not at all for equal strength joints. This confirms the conclusions of Section 5.4 in which the non-conservative analytical prediction of the column web was already highlighted.

6.3.2 Failure mechanisms

The failure modes of extended unstiffened joints are mostly characterized by plastic deformation of the connection (i.e. end-plate in bending) and column web panel. Hence, these types of joints substantially differ from both haunched and extended stiffened assemblies. The failure mostly occurs for the excessive concentration of plastic strain close to welds between the beam flange and the end-plate, which generally occurs on beam side for equal strength connections (see Figure 6.32) and into the end-plate for partial strength connections (see Figure 6.33). However, all tests show that the contribution of column web panel is significantly high with large plastic deformations.

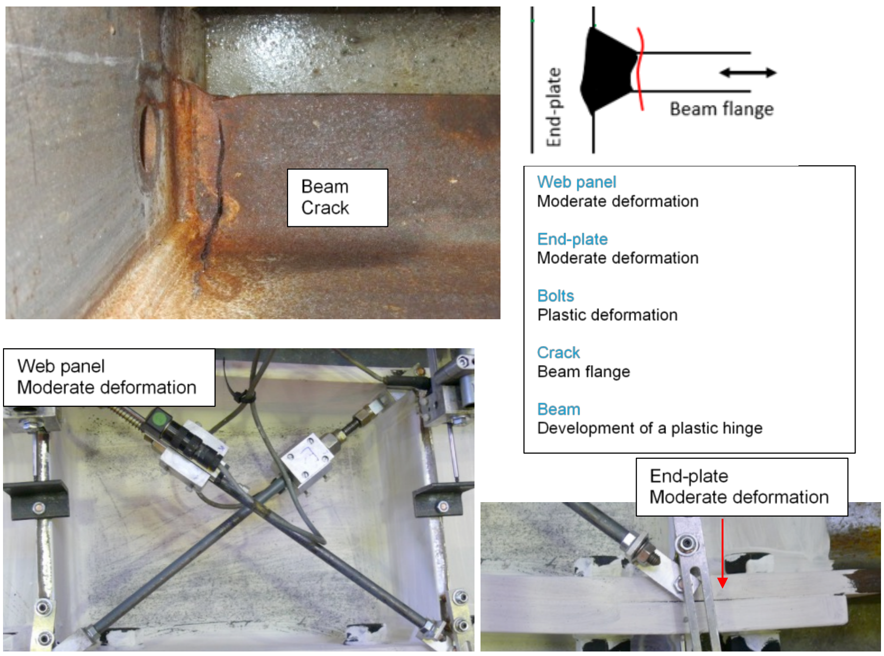

Figure 6.32: E2-TB-E-M joint failure mode

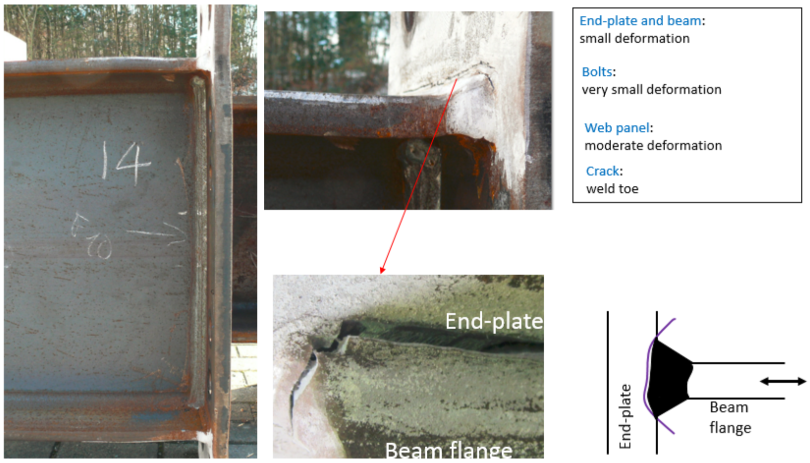

Figure 6.33: E3-TB-E joints: failure mode

6.3.3 *Influence of shot peening*

The test results on partial strength extended unstiffened joints fabricated using shot peening (i.e. those identified with the subscript “pp”) for the welds of the connection clearly show that this treatment does not positively influence the response of the joints as expected. To confirm this statement, the comparison between the results obtained for joint specimens without shot peening and with shot peening are depicted in Figure 6.34, Figure 6.35 and Figure 6.36. In terms of ultimate failure mode, no significant difference is obtained amongst the tested specimens; most of them failed with the apparition of cracks in the welds between the beam flanges and the end-plate.

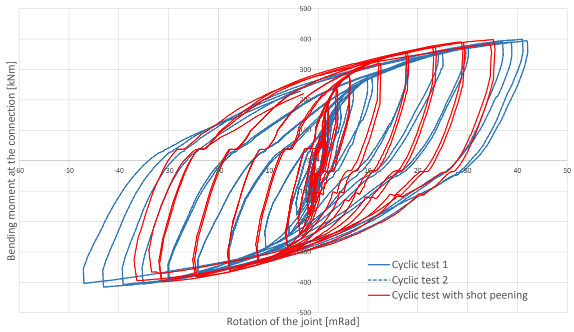

Figure 6.34: Influence of shot peening on E1-TB-P joints

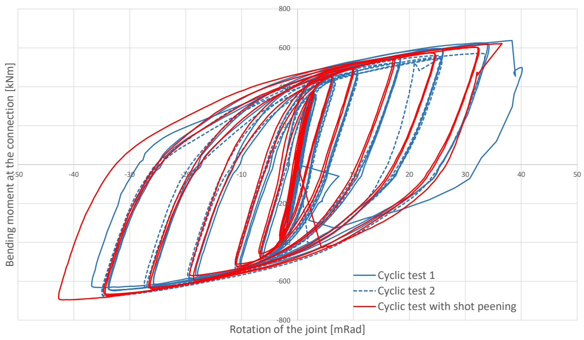

Figure 6.35: Influence of shot peening on E2-TB-P joints

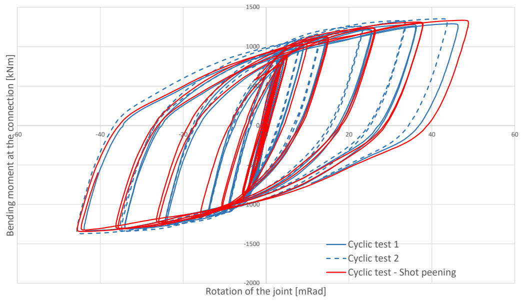

Figure 6.36: Influence of shot peening on E3-TB-P joints

6.3.4 Influence of loading protocol

For E1-TB-E tests reported in Figure 6.37, it can be observed that the maximum rotation obtained through the monotonic test is significantly bigger than the one observed through the cyclic tests while the ultimate failure load is the same. In Figure 6.38 providing a comparison between the monotonic and cyclic response of the E2-TB-E specimens, the situation is different. Indeed, it can be observed that the maximum bending moment reached through the monotonic test is equal or even slightly smaller than the ones observed through the cyclic tests while the maximum rotation is almost the same. All the tests were stopped due to the apparition of a crack close to the welds between the beam flanges and the end-plate. The influence of the type of cyclic loading protocol (ANSI/AISC 341-10 and EQUALJOINTS), see Figure 6.39, is negligible as already shown for the other joint configurations due to the fact that the difference between the two loading procedures mainly appears in the elastic cycles.

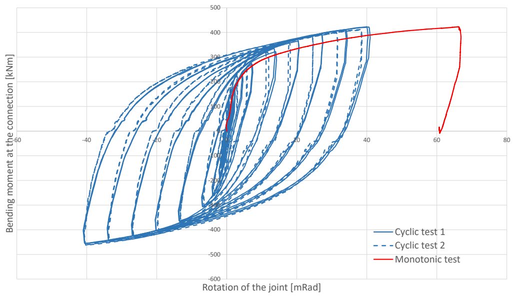

Figure 6.37: Comparison between the results obtained through monotonic and cyclic tests on E1-TB-E joints

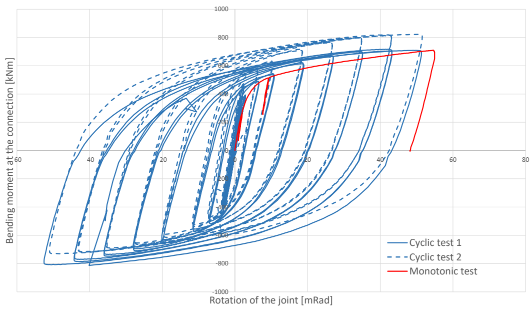

Figure 6.38: Comparison between the results obtained through monotonic and cyclic tests on E2-TB-E joints

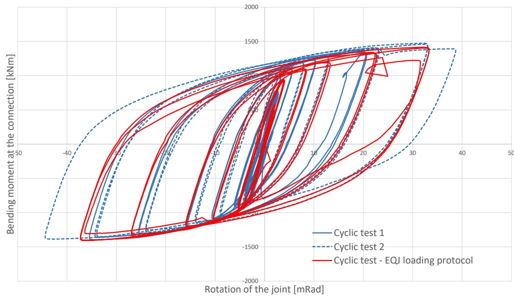

Figure 6.39: Influence of the cyclic loading protocol on the E3-TB-E specimen response

6.3.5 Contribution of joint components to plastic rotation

The contribution of the column web panels to the global deformation of the joints is seen to be significant for all joints tested, as seen in the various figures presented in Section 5.4. This is not really surprising as E joints are never “full strength ones”, but only, at the best, “equal joints”.

But unfortunately, it has also to be pointed out that the contribution of the panel is larger, and even sometimes significantly larger, than the one of the connection. This does not at all conform with Eurocode 8 specifications which specify that “the column web panel deformation should not contribute for more than 30% of the plastic rotation capacity (of the joints, in this case”). A reinforcement of the panel should therefore be possibly contemplated, in addition to the derivation of a more precise analytical prediction formula of the panel shear resistance.

6.3.6 Overall remarks on extended unstiffened end-plate joints

On the basis of the experimental evidence, the following conclusions may be drawn:

- All joints exhibit a stable hysteretic response.
- The ductility obtained conforms globally with the requirements of the norms, for ductile class.
- Unfortunately the contribution of the column web panel to the whole joint deformability is seen to be excessive, when compared to the EC8 requirement.
- The joint overstrength is rather constant and equals 1,35.
- A good correlation is obtained between calculated properties (Eurocode 3 Part 1-8) and experimentally reported ones.
- An effect of the beam size on the rotation capacity of the equal strength joints can be observed while this effect is less significant for the other specimens
- Shoot peening weld treatments do not influence the joint response.
- The influence of loading protocol on the joint response is seen to be rather negligible.

6.4 Dog-bone joints

As mentioned in previous sections, the dog-bone or RBS (reduced beam section) joints were considered as part of examining the use of European steel for large beam-column assemblies incorporating this type of dissipative connection. Accordingly, they represent a special case which is not directly related to the other connection configurations discussed above (i.e. haunched, extended stiffened and extended unstiffened). However, in order to provide information on the key parameters influencing the performance and main behavioural characteristics, representative results from three-dimensional continuum numerical simulations replicating the response obtained from tests, are also presented and discussed in this section. Focus is given to the effects of section selection, restraint conditions, panel zone design and RBS zone geometry. This is followed by a discussion on simplified modelling approaches that can be used within frame analysis and design oriented procedures.

6.4.1 Fabrication

The fabrication of the specimens (see Figure 6.40) is part of the American prequalification procedure. Indeed, these types of joints must be welded on-site. Therefore, attention is paid on this aspect. The fabrication of the members take place in Luxembourg, where the steel profiles are cut to length and connection elements are prepared: weld preparations, drills, stiffeners were welded, ready for welding on site. Beams and columns are subsequently shipped to the USA, and final welding between the main elements being connected is performed at the lab where the tests were performed.

Figure 6.40: Fabrication of specimens at the shop and welding at the lab

6.4.2 *Experimental Results on Specimen SP2*

Testing of Specimen 2 has been completed over the course of two days, with total testing time lasting nearly eight hours. During the 4% storey drift cycles, a maximum total force of 293 kips (1303.33 kN) was applied to the specimen. This figure also shows that the predicted elastic stiffness of the specimen, $K_{elastic}$ = 75 k/in (13.13 kN/mm), taken as an approximate value from finite element analysis performed previously on the specimen is very reasonable. The behaviour of SP2 is described in Figure 6.41.

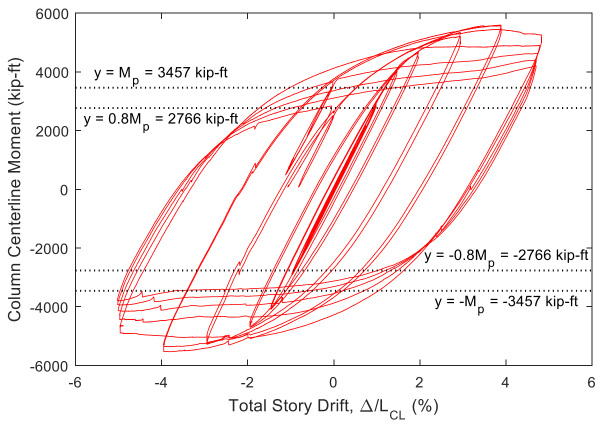

No	Storey Drift	Description of Event
1	1%	The specimen exhibits linear, elastic behaviour.
2	2%	Inelastic behaviour begins to occur.
3	3%	Local buckling of the web initiates.
4	4%	Visible flange local buckling initiates.
5	5%	Strength degradation of the connection. Significantly more local buckling in flanges and web.
6	5%	Test stopped for safety. Ductile tearing visible in flanges.

Figure 6.41: Experimental response of Dog-bone joints: SP2 specimen

Following the two cycles at 4% that completed the prequalification test, five complete cycles are performed at 5% story drift until failure occurred due to low-cycle fatigue. During this final cycle, the beam experienced fracture in both its top and bottom flanges at the location of the RBS, due to the concentration of severe local buckling, as shown in Figure 6.42a, b and c.

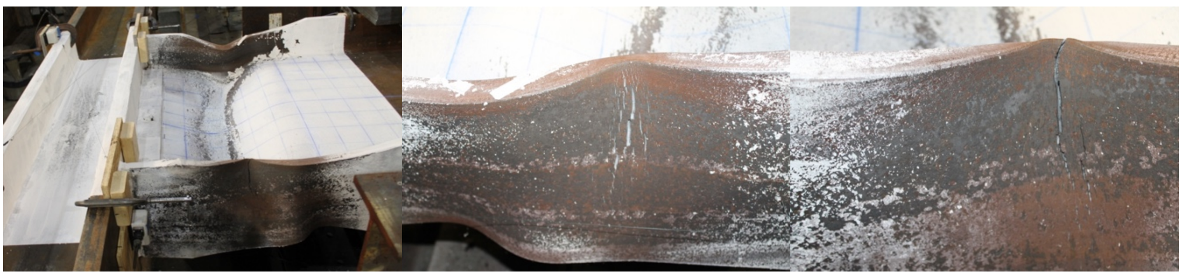

(a) (b) (c)

Figure 6.42: Experimental response of SP2 specimen: (a) Overall deformation of connection; (b) and (c) Fracture at flanges of beam

Figure 6.43a shows the moment vs. interstorey drift. At 4% storey drift cycles, the moment undergone by the specimen beam well exceeded 80% of the nominal plastic flexural strength, M_p The same holds true for story drifts of 5%. This satisfies the acceptance criteria for special moment frames as described in Section E3.6 of AISC 341-10. Figure 6.43b shows the inelastic contribution to the total story drift.

After early cycles in the testing, inelastic deformation contributes the majority to story drift. As the RBS begins to yield with subsequently larger deformations, a hinge forms, and most of the rotation seen by the connection comes from inelastic rotation occurring around this hinge.

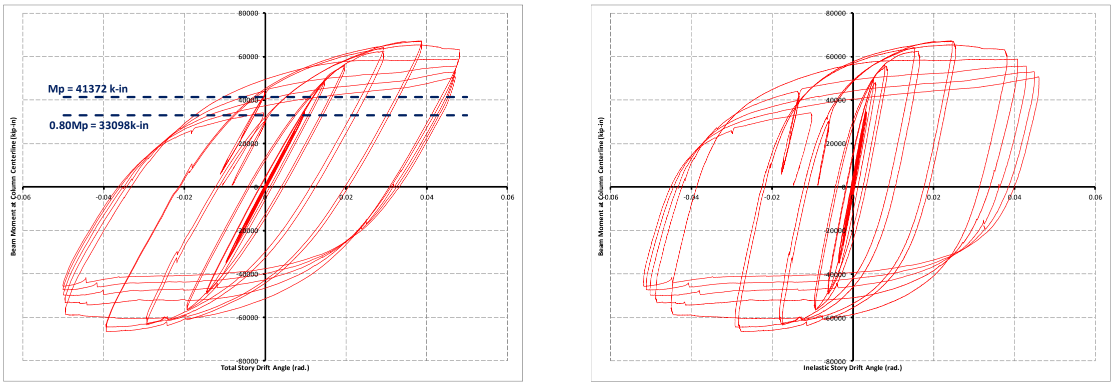

(a) (b)

Figure 6.43: Experimental response of SP2 specimen: Moment-Rotation Curve, (a) Total; (b) Inelastic

Though it is not a deformation that can be captured very well through images from testing, the panel zone shear deformation also plays an important role in the performance of the connection. Shear deformation of the panel zone is plotted in Figure 6.44a in terms of horizontal displacement of the column versus the moment at the column centerline. Again, peak readings are taken during the 4% cycles with drastic decreases occurring afterwards as the connection begins to yield and deform dramatically; in the final cycles, the moment decreases slightly while the horizontal deformation decreases greatly, as the RBS hinges and makes up for the bulk of deformation within the connection. The column panel zone is further investigated in Figure 6.44b, which plots the shear stress against the shear strain. Familiar patterns are again apparent, as both stress and strain peak during the 4% cycles. As the testing enters the 5% cycles, plastic deformations are extreme and the outputs become choppy, which can be seen in several of the last cycles illustrated in this figure.

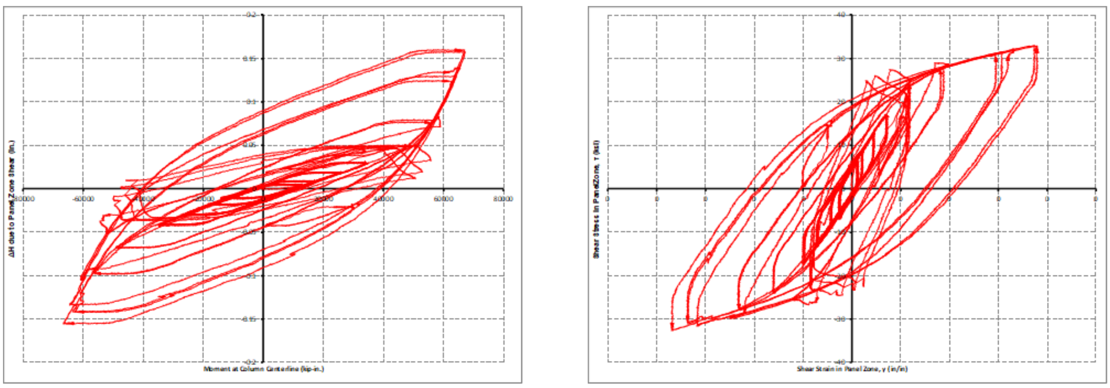

(a) (b)

Figure 6.44: Experimental response of SP2 specimen: (a) Panel Zone Shear Deformation; (b) Panel Zone Shear Stress vs Shear Strain

6.4.3 Experimental Results on Specimen SP4

Testing of Specimen SP4 has been completed over a 7-hour span on a single day. The loading protocol for SP4 is the same used for specimen SP2 (i.e. AISC341-10). However, due to complications, the test ends after the 4% story drift. At this point, the lateral bracing failed. Continuing the test would have endangered the staff and lab equipment.

Figure 6.45 illustrates the overall response curve and summarizes the main events during the test. The overall deformations of SP4 can be seen in Figure 6.46a. There is significant torsion acting on the deep column. Figure 6.46b shows the local buckling of the web with the grid lines.

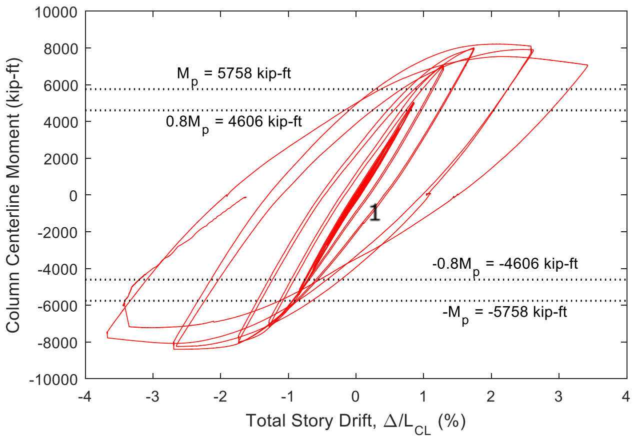

No	Storey Drift	Description of Event
1	1%	The specimen exhibits linear, elastic behaviour.
2	2%	The flanges began yielding on one side of the flange due to residual stresses from the test set up.
3	2%	The yielding in the web spread across the flanges after more cycles.
4	3%	The web began yielding. Local buckling of the web is occurring.
5	4%	Strength degradation of the connection occurs. There is significantly more web local buckling.
6	4%	Test was stopped. Lateral bracing failed.

Figure 6.45: Experimental response of Dog-bone joints: SP4 specimen

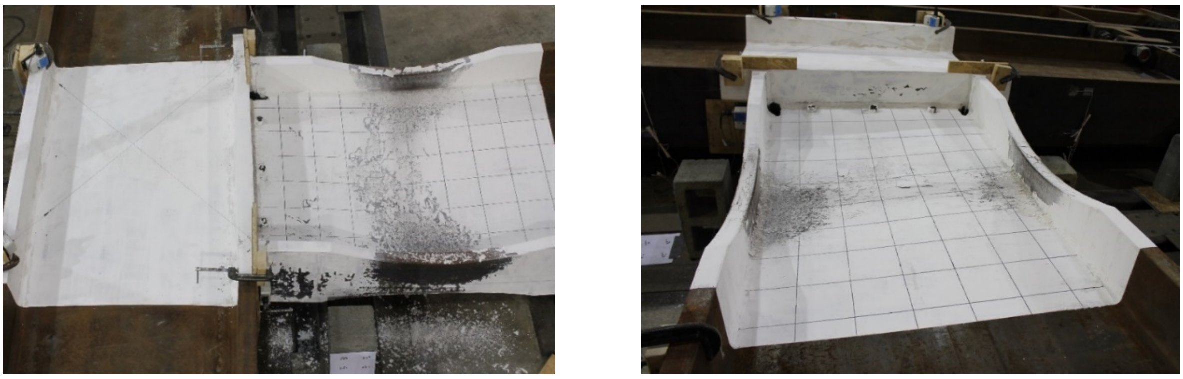

(a) (b)

Figure 6.46: Experimental response of SP4 specimen: (a) Overall deformation of connection; (b) Web local buckling and yielding

Figure 6.47a shows the applied moment on the connection versus the total story drift angle. Although strength degradation occurred, the strength of the connection is above 80% of the nominal plastic flexural capacity at the 4% story drift cycles. However, Figure 6.47a may be misleading about the magnitude that the experimental moment capacity exceeds the 80% nominal capacity. In this figure, the moment is calculated at the column centreline in accordance with AISC 341-10. This is partly due to the broad scope of connections covered in AISC 341-10.

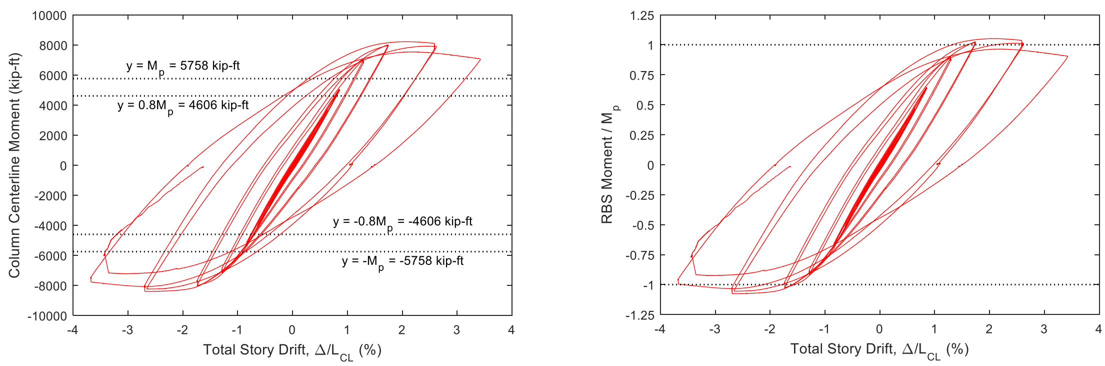

(a) (b)

Figure 6.47: Experimental response of SP4 specimen: (a)Moment-Rotation Curve, Total (SP4); (b) RBS Moment Ratio, Story Drift (SP4)

For RBS connections, the nominal plastic capacity is calculated for the RBS properties. Figure 6.47b illustrates the ratio between the applied moment at the RBS to the nominal moment capacity of the RBS. The experimental moment capacity is still greater than the 80% nominal plastic capacity.

6.4.4 Contribution of joint components

Characteristic results are presented for a connection with a size of W36x925 for the beam and W14x873 for the column. Moment at the column face is plotted against the beam chord rotation in absolute and normalised values in Figure 6.48(a) and Figure 6.49(b), respectively. The maximum developed moment is 22465 kNm, at a drift of 5%. The RBS offers a real moment reduction factor of 0.79, which is practically equal to the one assumed in the design. Four characteristic points are highlighted in the plot, explained hereafter. By observing the progression of yielding, the following response is shown: yielding initiates at the beam-column interface (drift 0.9%) and then progresses into the beam flanges of the RBS (drift 1.2%). The fully developed plastic mechanism (drift 2.6%) indicates that most of the plastic deformation is taken by the RBS, with limited panel zone shear distortion (see Figure 6.49). However, a concentration of plastic strains at the flange welds is present, indicating that the RBS does not totally reduce the strain demand. The plastic strain magnitude at the centre of the weld is reaching a value of 1.6% (at beam drift of 5%), compared to 6.3% experienced at the RBS.

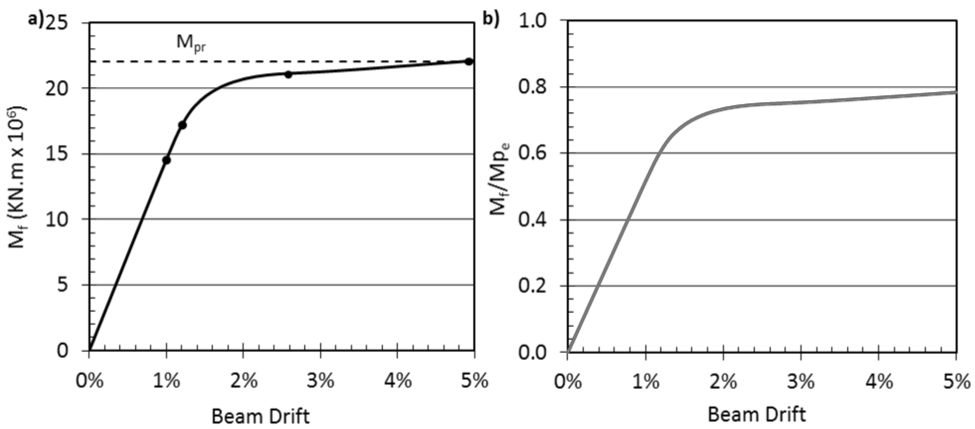

Figure 6.48: Moment at the column face versus the beam drift. a) absolute values, b) results normalised by the beam plastic moment of the full section M_{pe}

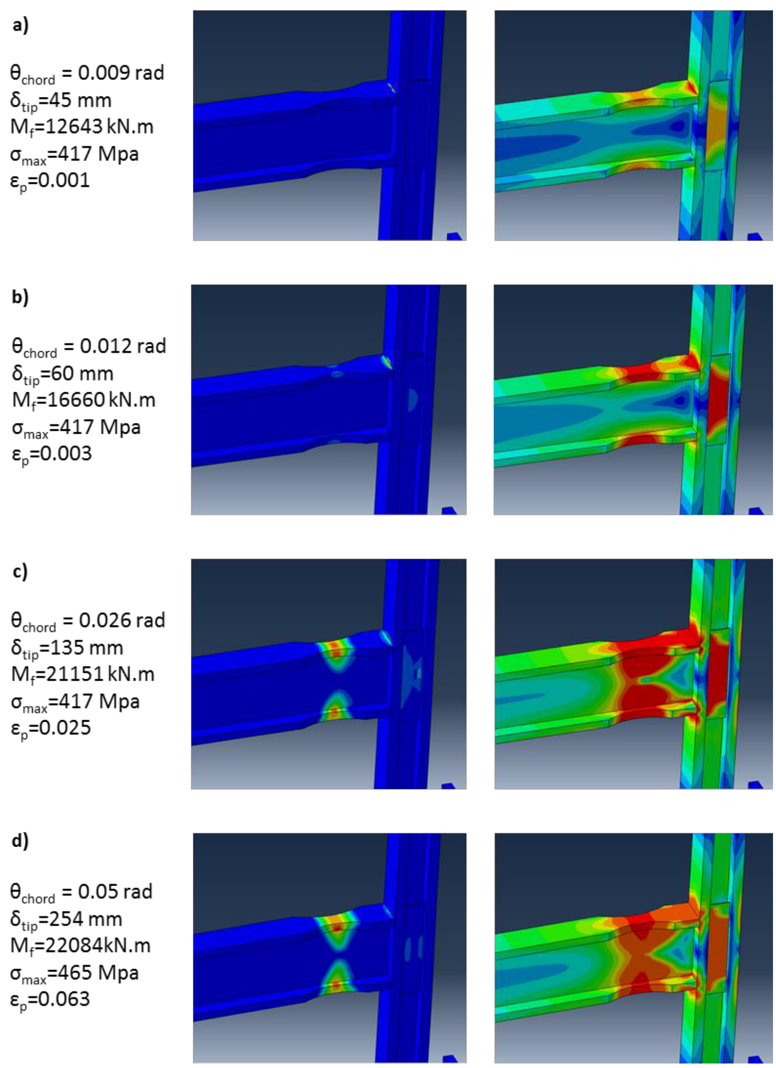

Figure 6.49: Plastic strain magnitude (left) and Mises stresses (right): a) initiation of yielding, b) progression of yielding into the beam flanges and PZ, c) initiation of strain hardening, d) fully developed mechanism

The contribution of each component in the total deformation can be observed by plotting the component rotations against the moment at the face of the column (see Figures 6.50 and 6.51). The contribution of the RBS to the total plastic rotation (at beam drift 5%) is about three times that of the panel zone (at beam drift 5%) which exhibits a practically elastic behaviour, despite the fact that yielding occurred. Rotation of each node of the beam centreline is plotted in Figure 6.51 against the distance x from the face of the column. The rotation of the plastic hinge at the middle of the RBS is about 0.037 rad, while the panel zone rotation is estimated as 0.009 rad.

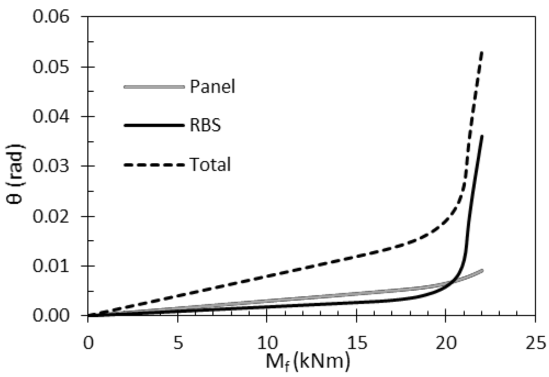

Figure 6.50: Total, RBS, and panel zone rotation versus the moment at the column face

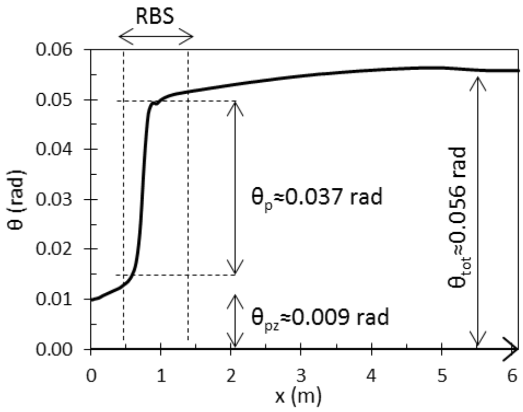

Figure 6.51: Rotation of centerline nodes of beam (θ) against distance from the face of the column (x)

After careful examination of the behaviour of four RBS connections which implement jumbo-sized members in a broad range of combinations, a number of key observations have been found to play an important role. To begin with, lateral instability was observed in the case of a connection represented by SP4 as described before, which implements the deepest column, along with a deep beam of the W40 shapes. The instability was characterized by a 51 mm lateral displacement of the bottom flange, along with twisting of the column. Furthermore, an increased plastic strain demand was observed at the beam flange-column flange welds of the connections which implemented heavier members. Moreover, the connections demonstrated a strong panel zone response, which means that ignoring the contribution of the column flanges in the nominal PZ strength, as given by AISC 358-10 (AISC, 2010b) may be on the conservative side. These findings signify that the size of the sections, the dimensions of the RBS, and the design of the PZ are important parameters that influence the response as discussed in the summarized discussions below.

6.4.5 Influence of member sizes

The analysis of Connection SP4 indicated the susceptibility of deep beams to lateral torsional buckling, which is expressed as an out-of-plane distortion of the bottom flange at the location of the RBS. Furthermore, the W40x593 column, which was the only one to exceed the depth prequalification limit, experienced a degree of twisting. In order to further investigate this behaviour, 4 additional analyses were carried out, varying the beam and column of the connection respectively. Connections SP5 and SP6 address the effect of column section, by keeping the W44x408 beam constant and varying the section of the column (SP5: W14x730; SP6: W36x487). On the other hand, connections SP7 and SP8 address the effect of beam section, by keeping the W40x593 column constant (SP7: W40x431; SP8: W36x387).

The effect of varying column characteristics is summarized in the plots below. The connections implement the same beam, with SP4 and SP5 exhibiting identical moment-drift behaviour. On the other hand, Connection SP6 exhibits a large drop in both post and pre-yielding stiffness (Figure 6.52), indicating significant LTB behaviour (Figure 6.53). The deformed state of the beams is illustrated in Figure 6.54 (for 5% drift). Finally, LTB amplitudes are plotted against the h/t^3_{cf} ratio for columns (Figure 6.55); it can be seen that this ratio can provide a good indicator of the column twist, and that LTB amplitudes for the same beam are closely related to the susceptibility of the respective column to twisting.

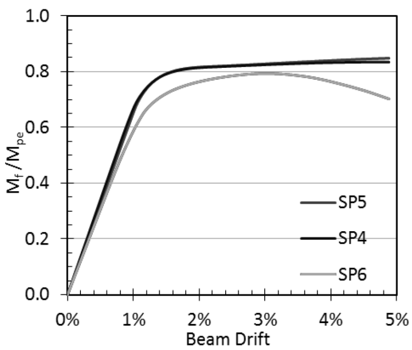

Figure 6.52: Moment at the column face of SP4, SP5, SP6 vs beam drift (normalised by M_{pe})

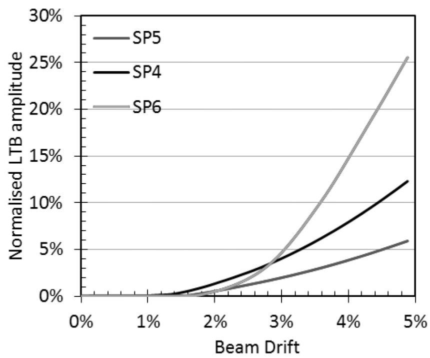

Figure 6.53: Lateral movement of bottom flange for SP4, SP5, SP6 (normalised by beam flange width)

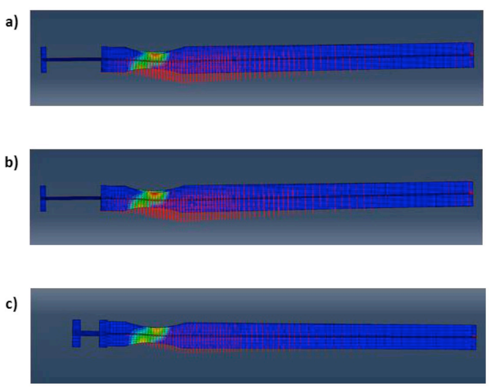

Figure 6.54: Lateral displacement vectors and plastic strain contours at 5% drift: (a) SP6, (b) SP5, (c) SP6

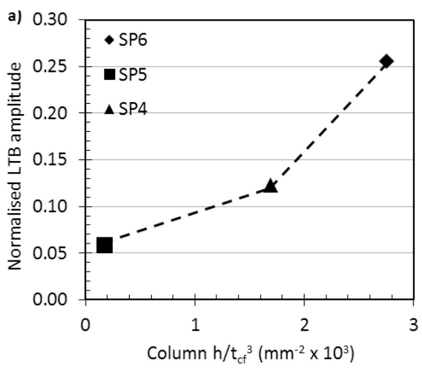

Figure 6.55: LTB amplitude at 5% drift (normalised by beam flange width) vs h/t^3_{cf} ratio

The effect of varying the beam section on the global moment-drift response, SP7 and SP8 exhibit similar behaviour to the reference case of SP4 (Figure 6.56). LTB behaviour is present in all connections as presented in Figure 6.57 and Figure 6.58. The slenderness of the beam web seems to be a good indicator of the LTB susceptibility and the resulting column twist. Column twist angles are plotted against the beam web slenderness for the connections examined in Figure 6.59.
It should be noted that in the context of the aforementioned study, lateral bracing of the bottom flanges of the beams has been provided only at the point of load application (controlled displacement). Addition of lateral bracing near the RBS zone would completely mitigate the LTB phenomenon.

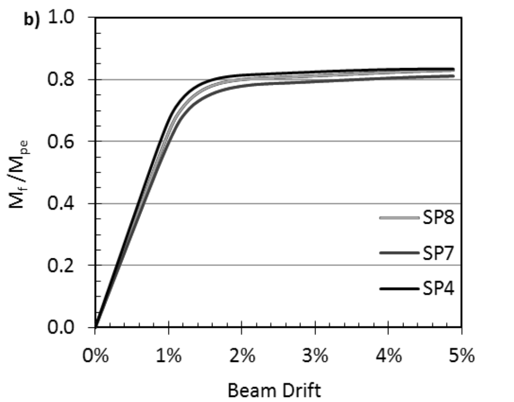

Figure 6.56: Moment at the column face of SP4, SP7, SP8, vs beam drift (normalised by *M_{pc}*)

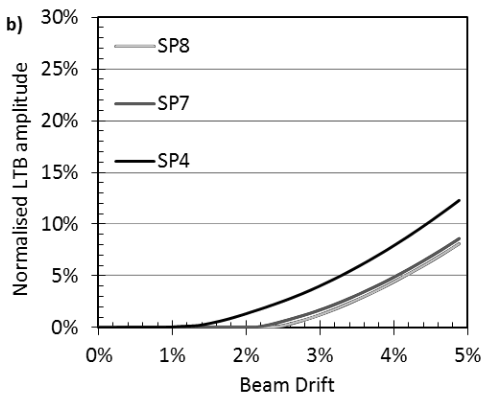

Figure 6.57: Lateral movement of bottom flange (SP4, SP7, SP8) (normalised by beam flange width)

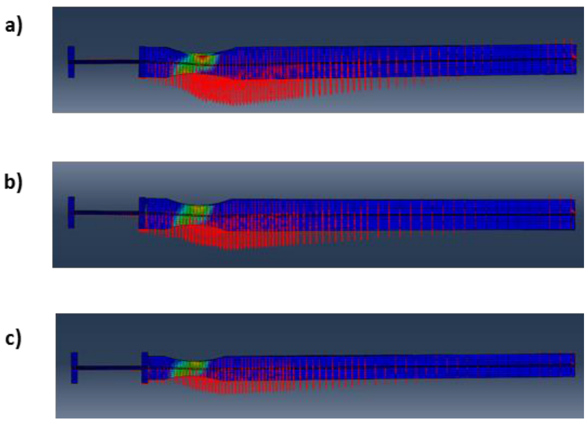

Figure 6.58: Lateral displacement vectors and plastic strain contours at 5% drift: (a) SP4, (b) SP7, (c) SP8

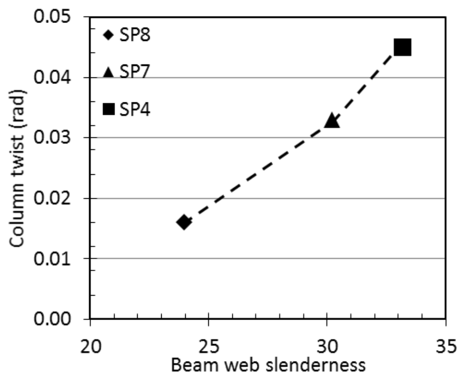

Figure 6.59: Column twist angle at 5% drift vs beam web slenderness.

6.4.6 *Influence of panel zone design*

Four different configurations of the designed connections with variation of the panel zone details have been considered. Representative results for SP3 are presented hereafter with 3 different configurations for panel zone thickness and a case of stronger material selection for the column. The resulting beam moment (at column face) vs chord rotation curves are presented in Figure 6.60. For the weak (100 mm thick) panel zone case, the moment capacity of the connection is significantly lower. Plastic rotation in the RBS zone and distortions of the panel zone are plotted against beam drift in Figure 6.61. In the case of the weak panel zone (no doubler plates), the RBS remains essentially elastic and all the plastic deformation is undertaken by the panel zone. By increasing the panel zone thickness to 136 mm via doubler plates, plastic rotation is divided almost equally between the panel zone and RBS. Further increase of the effective panel zone thickness to 156 mm or use of 65 ksi (455 MPa) material for the column leads to about 60% of the total deformation of the connection occurring in the RBS zone. The relative contribution of the RBS zone and the panel zone to the total (elastic & inelastic) deformation of the connection, for the panel zone designs considered is illustrated in Figure 6.62.

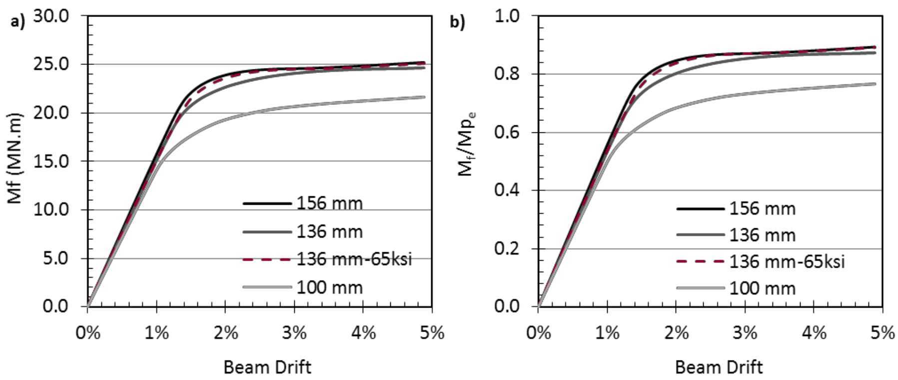

Figure 6.60: Moment at column face vs beam drift for various panel zone designs

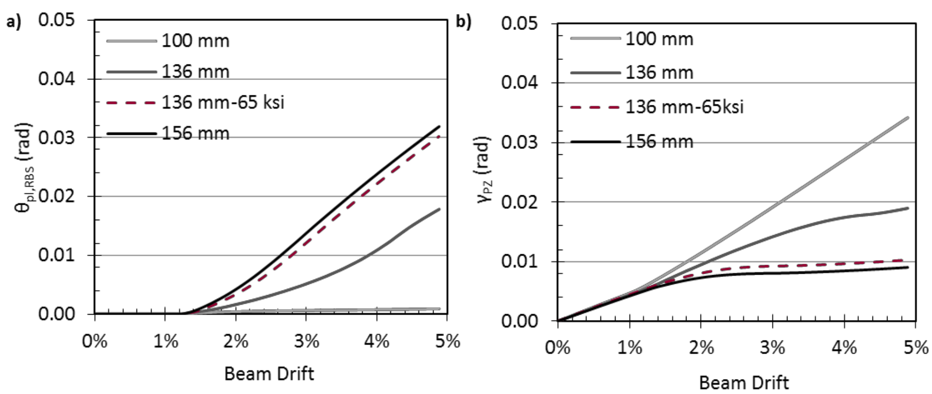

Figure 6.61: a) RBS plastic rotation, (b) panel distortion vs beam drift for various panel zone designs of SP3

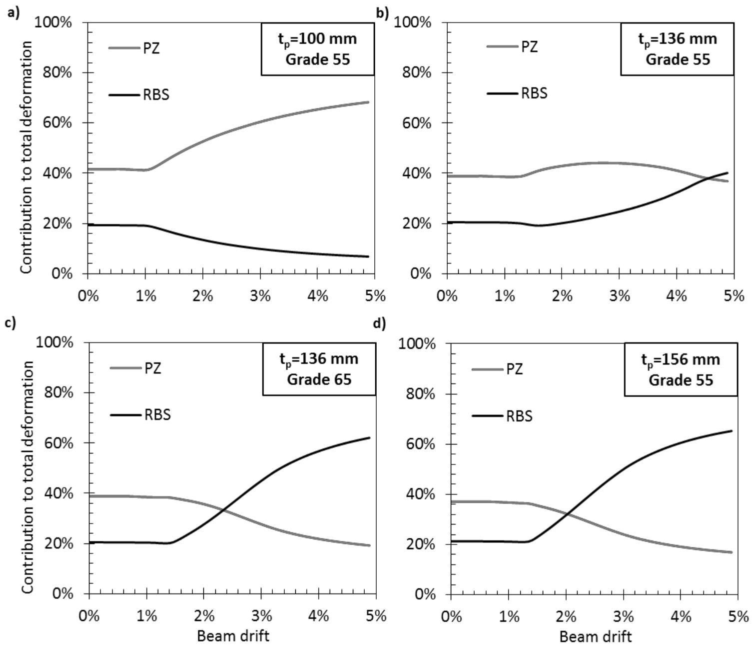

Figure 6.62: Contribution of RBS and panel zone to the total deformation of SP3

6.4.7 Influence of RBS design

Connection SP2 and SP3 have been analysed with various configurations for the geometry of the RBS cut zone, as defined by parameters A, B and C. In general, increasing the cut of the RBS leads to smaller moments developing at the face of the column. Parameter C which determines the depth of the cut is obviously governing the moment capacity of the connection and the shear demands imposed on the panel zone (i.e. deeper cuts imply lower moment capacity and also lower shear demands on panel zone). The effect of flange reduction (ranging from zero – no RBS – to the maximum value allowed by code) to the plastic strains (at 5% drift) can be observed in the contour plots in Figure 6.63.

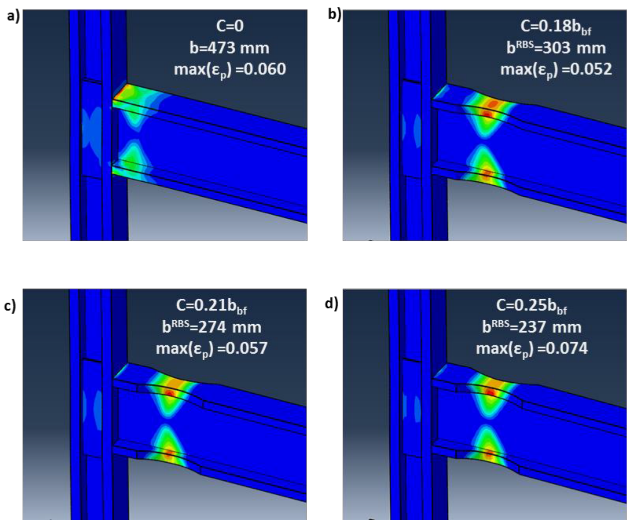

Figure 6.63: Plastic strain magnitude contours at 5% drift for SP3 for various cases of RBS cut depth

6.4.8 Simplified modelling procedures

The assessments presented above were carried out using three-dimensional continuum nonlinear modelling which, whilst presenting the most faithful representation of the response, is relatively time consuming and detailed background. For simplified simulation and design purposes, idealization of the components of the connection can be carried out. It should be noted however that RBS connections have a specific configuration that differs from other joints considered above. Nonetheless, several components can be represented in the same manner dealt with for other forms.

As for other connection forms, using the approaches of EN1993-1-8, the following components can be identified for RBS connections: column web in tension, column flange in bending, beam flange in compression, column web in compression, and column web in shear. It should be noted that the RBS cut zone is not part of the conventional component assembly of the connection, and should be modelled as part of the beam.

Figure 6.64 shows a schematic of a typical component assembly. The same procedures adopted for the same components within other types of connections can be used in this case to develop a bilinear monotonic and cyclic representation of the connection. The column web panel in shear or the column flange in bending can be critical components in this case, depending on the specific dimensions used.

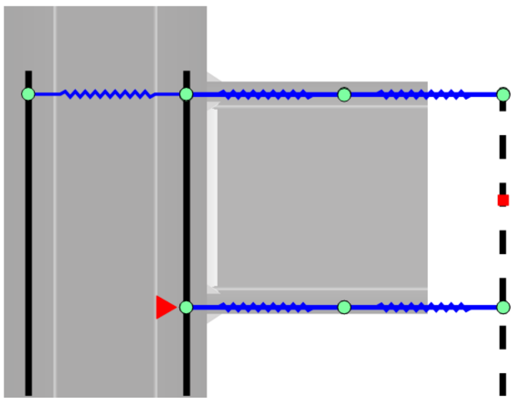

Figure 6.64: Schematic assembly for spring arrangement in SP connections

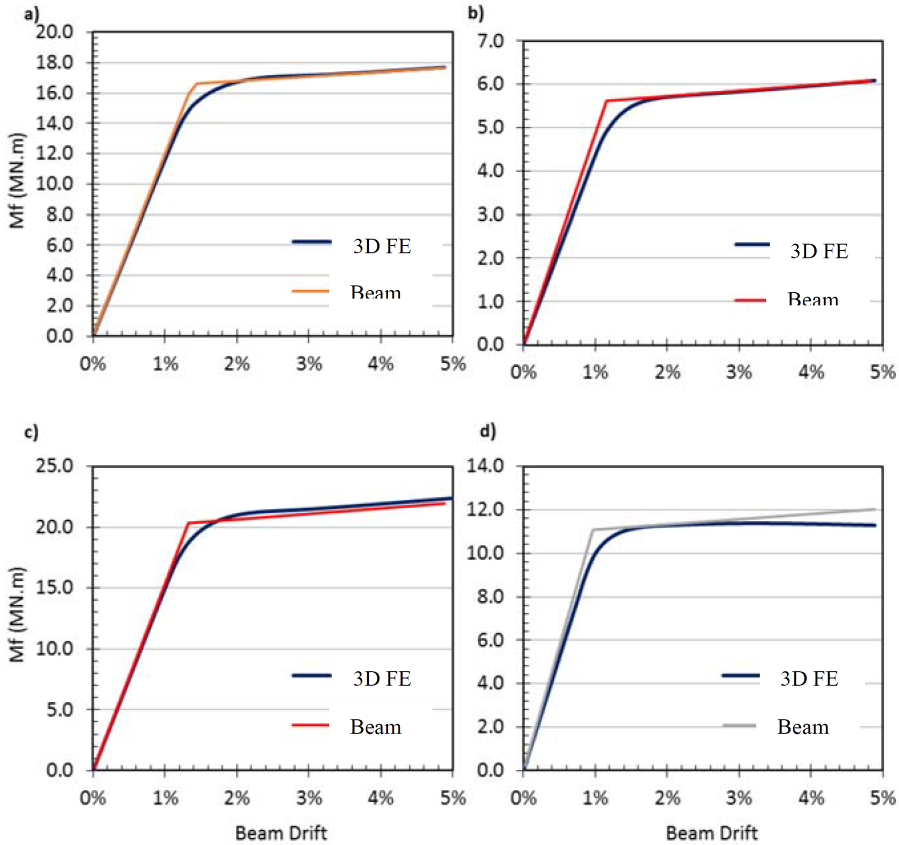

Figure 6.65: Comparison between 3D continuum FE and idealized beam models for SP1-SP4

As noted before, modelling RBS connections in frame analysis programs requires a representation of the connection components as discussed above, particularly the panel zone which can significantly influence the behaviour, as well as the reduction in section at the RBS cut zone. Using a simple approach (Grubbs, 1997), the elastic stiffness of two beam-column elements within the RBS zone can be modified to account for the loss in stiffness due to trimming of the flanges, while a zero-length zero-length rotational spring that connects the two nodes at the middle can be employed to account for inelastic response of the RBS.

A comparison between the overall moment-drift response, for SP1 to SP4, using three-dimensional continuum modelling as well as the simplified beam approach is illustrated in Figure 6.65. It can be observed that a satisfactory level of agreement is achieved between the two models, especially in terms of the plastic response of the RBS.

6.4.9 Overall remarks on dog-bone joints

On the basis of the experimental and numerical studies on radius cut RBS moment connections for steel structures with jumbo size members, the general behaviour of the RBS connections with increasing beam drift is characterized initially by yielding which occurs at the beam top flange-column flange interface, followed by initiation of yielding either at the RBS flanges or at the panel zone, depending on the relative strength of the two components. Accumulation of plastic strains is then exhibited at the component which is weaker.

Introducing a RBS can lead to a relief in terms of moment at the face of the column, of the order of 75%-95% compared to the plastic moment capacity of the untrimmed beam. The plastic strain demand developing at the beam-column intersection is also reduced, but does not disappear entirely.

The bottom flanges of deeper beams (that are in compression) have the tendency to move laterally with increasing beam drifts, exhibiting LTB behaviour. Increased lateral movement that can reach up to 25% of the beam flange width has been observed for beams with more slender webs. However, providing lateral bracing within a distance of $d_b/2$ from the end of the RBS, farthest from the face of the column, can substantially mitigate this effect.

Deep columns exhibit an increased susceptibility to twisting. A maximum angle of rotation of 0.12 rad has been observed for the column with the higher h/t_{cf} ratio, which is an indicator of low torsional resistance. A pronounced interaction exists between the susceptibility of columns to twisting and LTB of beams, with both effects magnifying each other. Providing lateral bracing according to the aforementioned requirement diminishes the twisting of columns, as the values of twist angles appear one order of magnitude smaller.

Slender beams can exhibit local buckling, which can manifest at the compression flange and the web. This effect can initiate at a beam drift of about 2.0% and can significantly reduce the plastic rotation capacity of the beam due to asymmetric plastic strain accumulation at the affected flange which can lead to premature ductile fracture. Providing lateral bracing near the plastic hinge does not help in this case.

The design of the panel zone (PZ) PZ is the main parameter that affects the inelastic rotation demands imposed on the RBS. Allowing for inelastic deformation to be undertaken by the PZ can relieve excessive plastic rotation demands on the RBS. In the case of slender beams, it was found that this relief can lead to a stabilising effect, as it can prevent the occurrence of premature LB. On the other hand, allowing for excessive rotational demands of the PZ increases the plastic strain and negative pressure imposed on the beam top flange-column flange interface, and thus increases the premature ductile fracture hazard of the weld.

The thickness of the beam flanges was found to play an important role on the ductile fracture potential of the beam-column interface top weld. Excessively thick flanges tend to impose a regime of high triaxiality, combined with increased plastic strain demands. This effect is significantly amplified when the PZ design is weaker or even balanced, leading to extremely large values of the rupture index. The percentage of flange reduction (RBS parameter *c*) was also found to be the governing parameter among the RBS dimensions. Larger values of *c* increase the plastic rotation capacity, provide higher relief in terms of moment at the column face, and reduce the shear force demand imposed on the PZ.

REFERENCES

Abidelah A, Bouchaïr A, Kerdal DE (2012). *Experimental and analytical behavior of bolted end-plate connections with or without stiffeners*. Journal of Constructional Steel Research, 76:13.

American Institute of Steel Construction (AISC) (2010). *Seismic Provisions for Structural Steel Buildings*, ANSI-AISC 341-10 Standard, American Institute of Steel Construction, Chicago, Illinois, USA, 2010.

American Institute of Steel Construction (AISC) (2010). *Specification for Structural Steel Buildings*, ANSI-AISC 360-10 Standard, American Institute of Steel Construction, Chicago, Illinois, USA, 2010.

American Society for Testing and Materials (ASTM) (2011). "*Standard Practices for Cycle-Counting in Fatigue Analysis."* ASTM Standard E1049-85, ASTM International, West Conshohocken, PA, USA.

American Society of Civil Engineers (ASCE) (2014). *Seismic Evaluation and Retrofit of Existing Buildings*. ASCE/SEI 41-13 Standard, Reston, Virginia.

ANSI/AISC 358-10 (2010). *Prequalified Connections for Special and Intermediate Steel Moment Frames for Seismic Applications.*

ANSI/AISC 358-16 (2016). *Prequalified Connections for Special and Intermediate Steel Moment Frames for Seismic Applications.*

ANSI/ASIC 341-16 (2016): *Seismic Provisions for Structural Steel Buildings*, American Institute of Steel Construction

Arce G. *Impact of higher strength steels on local buckling and overstrength of links in eccentrically braced frames*. MS thesis, Univ.of Texas at Austin, Austin, Tex. (advisor: M.D. Engelhardt).

ASTM E606 / E606M-12 (2012). *Standard Test Method for Strain-Controlled Fatigue Testing*, ASTM International, West Conshohocken, PA, www.astm.org

Bijlaard FSK, Nethercot DA, Stark JWB, Tschemmernegg F, and Zoetemeijer P (1989). *Structural properties of semi-rigid joints in steel frames*. IABSE Periodica, 2, 33.

Bjorhovde R, Colson A (1991). *Economy of semi-rigid frame design*, in Connections in Steel Structures II: Behaviour, Strength and Design, Bjorhovde R, Haaijer G, and Stark JWB (eds.), American Institute of Steel Construction, 418–430.

Brandonisio G, De Luca A, Mele E (2012). *Shear strength of panel zone in beam-to-column connections*. Journal of Constructional Steel Research, 71, 129–142.

CEN (2005). Eurocode 3: *Design of steel structures - Part 1-8: Design of Joints*. European Committee for Standardization (CEN), 2005.

CEN (2005). Eurocode 8: *Design of structures for earthquake resistance – Part 3: Assessment and retrofitting of buildings*. European Standard EN 1998-3:2005, Brussels.

Chang KL, and Uang CM (1997). *Designing after Northridge*. Modern Steel Constr., 37(3), 36-42.

Charney FA, and Downs WM (2004). *Modeling Procedures for Panel Zone Deformations in Moment Resisting Frames.* Proceedings, Connections in Steel Structures V, Amsterdam.

Chen SJ, Yeh CH, and Chu JM (1996). *Ductile steel beam-to-column connections for seismic resistance.* J. Struct. Engrg., ASCE, 122(11), 1292-1299.

Che S, Tu C (2004). *Experimental study of jumbo size reduced beam section connections using high-strength steel.* Journal of Structural Engineering. 130 (4), 582-587.

Chen S (1996). *A simple and effective retrofit method for steel beam-to-column connections.* Seventh US-Japan Workshop on the improvement of structural design and construction practices.

Chi B & Uang C (2002). *Cyclic response and design recommendations of reduced beam section moment connections with deep columns*. Journal of Structural Engineering. 128 (4), 464-473.

D'Aniello M, Landolfo R, Piluso V, Rizzano G (2012). *Ultimate Behaviour of Steel Beams under Non-Uniform Bending.* Journal of Constructional Steel Research, 78, 144–158.

D'Aniello M, Tartaglia R, Costanzo S, Landolfo R (2017). *Seismic design of extended stiffened end-plate joints in the framework of Eurocodes*. Journal of Constructional Steel Research, Vol 128, pp 512-527.

Dubina D, Ciutina A, Stratan A (2001). *Cyclic tests of double-sided beam-to-column joints* Journal of Structural Engineering 2001, 127:129-136.

Elnashai A, Elghazouli AY (1994). *Seismic behaviour of semi-rigid steel frames*. Journal of Constructional Steel Research, 29, 149–174.

Engelhardt MD, Winneberger T, Zekany AJ, Potyraj TJ (1998). *Experimental Investigations of Dogbone Moment Connections*. Engrg. J., 35(4), AISC, Fourth Quarter, 128-139.

Engelhardt MD, Winneberger T, Zekany AJ & Potyraj TJ (1996). *The dogbone connection: Part II*. Modern Steel Construction. 36 (8), 46-55.

Engelhardt MD, Fry G, Jones S, Venti M & Holliday S (2000). *Behavior and design of radius cut reduced beam section connections*. A Draft Report of SAC Task 7.

FEMA- 355D (2000). *State of the Art Report on Connection Performance.* Ch 3.

FEMA- 351 (2000). *Recommended Seismic Evaluation and Upgrade Criteria for Exixting Welded Moment-Frame Buildings*, Ch 6.

FEMA (2000a). FEMA 355D, *State of the art report on connection performance*. Report no.FEMA-355D.Washington (DC): Federal Emergency Management Agency (FEMA).

FEMA (2000b). FEMA-350, *Recommended seismic design criteria for new steel moment-frame buildings*. Federal Emergency Management Agency.

Gilton C, Chi B & Uang C (2000). *Cyclic response of RBS moment connections: weak-axis configuration and deep column effects*.Department of Structural Engineering, University of California, San Diego.

Güneyisi EM, D'Aniello M, Landolfo R, Mermerdaş K (2013). *A novel formulation of the flexural overstrength factor for steel beams*. Journal of Constructional Steel Research, 90, 60-71.

Güneyisi EM, D'Aniello M, Landolfo R, Mermerdaş K (2014). *Prediction of the flexural overstrength factor for steel beams using artificial neural network*. Steel and Composite Structures, An International Journal, 17(3), 215-236.

Guo B, Gu Q, Liu F (2006). *Experimental Behavior of Stiffened and Unstiffened End-Plate Connections under Cyclic Loading*. Journal of Structural Engineering, 132(9), 1352-1357.

Gupta A, and Krawinkler H (1999). *Seismic Demands for Performance Evaluation of Steel Moment Resisting Frame Structures.* Report No. 132 - John A. Blume Earthquake Engineering Center, Stanford University, California.

Gross JL, Engelhardt MD, Uang CM, Kasai K and Iwankiw, NR (1999). *Modification of Existing Welded Steel Moment Frame Connections for Seismic Resistance*, AISC Design Guide Series 12, American Institute of Steel Construction, Chicago, Illinois.

Grubbs KV (1997). *The effects of the dogbone connection on the elastic stittness of steel moment frames*. Master thesis, Dept. of Civ. Engrg., The University of Texas at Austin, Texas.

Jaspart JP (1997). *Contributions to recent advances in the field of steel joints. Column bases and further configurations for beam-to-column joints and column bases.* These aggregation, University of Liege, Belgium.

Jones SL, Fry GT & Engelhardt MD (2002). *Experimental evaluation of cyclically loaded reduced beam section moment connections*. Journal of Structural Engineering. 128 (4), 441-451.

Joints in Steel Construction: Moment-Resisting Joints to Eurocode 3 (P398). Edited by The Steel Construction Institute and The British Constructional Steelwork Association, 2013, ISBN 978-1-85-942209-0.

Kunnath SK, Malley JO (2002). *Advances in seismic design and evaluation of steel moment frames: recent findings from FEMA/SAC Phase II Project.* Journal of Structural Engineering. 128 (4), 415-419.

Lachal A, Aribert JM, Loho G (2006). *Analytical and experimental investigations of bolted haunched beam-to-column joints with a view of seismic design*. Advanced Steel Construction 2 (2006) 137-160.

Lee CH, Jung JH, Oh MH, Koo ES (2005). *Experimental Study of Cyclic Seismic Behavior of Steel Moment Connections Reinforced with Ribs*. Journal of Structural Engineering, ASCE, 131(1), 108-118.

Lee CH (2002). *Seismic Design of Rib-Reinforced Steel Moment Connections based on Equivalent Strut Model.* Journal of Structural Engineering, ASCE, 128(9), 1121-1129.

Lee CH and Uang CM (1997). *Analytical modeling of dual panel zone in haunch repaired, SAC, Technical report: Experimental investigations of beam-column subassemblies.*, Journal of Structural Engineering, ASCE, 1997, 123(1), pp.20-29.

Maquoi R, and Chabrolin B (1998). *Frame design including joint behaviour: final report*. EUR, Off. for Off. Publ. of the Europ. Communities, Luxembourg.

Maris C, Vulcu C, Stratan A and Dubina D (2015). *Validation through numerical simulations of the design procedure for bolted beam-to-column connections with haunches.* Pollack Periodica, 10(3), 95–107.

Mazzolani FM, Piluso V (1992). *Member behavioural classes of steel beams and beam-columns.* Proc. of First State of the ArtWorkshop, COSTI, Strasbourg, 517-29.

NIST (1998). *Modification of existing Welded Steel Moment Frame Connections for Seismic Resistance*, Draft Report, National Institute for Standards and Testing, Gaithersburg, MD.

Nussbaumer A, Borges L, Davaine L (2011). Fatigue design of steel and composite structures, ECCS Eurocode Design Manuals, ECCS Press/Ernst&Sohn.

Pachoumis D, Galoussis E, Kalfas C & Efthimiou I (2010). *Cyclic performance of steel moment-resisting connections with reduced beam sections—experimental analysis and finite element model simulation*. Engineering Structures. 32 (9), 2683-2692.

Popov E, Blondet M, Stepanov L. & Stojadinovic B. (1996) *Full-Scale Beam-to-Column Connection Tests*. University of California Department of Civil Engineering, Berkeley, CA.

Plumier A (1997). *The dogbone: back to the future. Engrg*. J. 34(2), 61-67.

Plumier A (1990). *New idea for safe structures in seismic zones.* IABSE Symposium. Mixed structures including new materials-Brussels. pp.431-436.

SCI/BCSA (2013). *Joints in steel construction: moment-resisting joints to Eurocode 3.* The Steel Construction Institute and The British Constructional Steelwork Association, London, UK. Publication Number: P398.

Shi G, Shi Y, Wang Y (2007). *Behaviour of end-plate moment connections under earthquake loading.* Engineering Structures 29, 703–716.

Shi Y, Shi G, Wang Y (2007). *Experimental and theoretical analysis of the moment–rotation behaviour of stiffened extended end-plate connections.* Journal of Constructional Steel Research, 63, 1279–1293.

Stratan A, Maris C, Dubina D and Neagu C (2017). *Experimental prequalification of bolted extended end plate beam to column connections with haunches.* ce/papers, 1(2–3), 414–423.

Stratan A, Maris C, Dubina D and Neagu C (2016). *Prequalification tests on bolted beam-to-column joints with haunches.* Proceedings of the 8th International Workshop "Connections in Steel Structures VIII," American Institute of Steel Construction, Boston, USA, 569–578.

Tartaglia R, D'Aniello M (2017). *Nonlinear performance of extended stiffened end-plate bolted beam-to-column joints subjected to column removal*. The Open Civil Engineering Journal Vol 11, Issue Suppl-1, Pages 369-383.

Tartaglia R, D'Aniello M, Rassati GA, Swanson JA, Landolfo R (2018). *Full strength extended stiffened end-plate joints: AISC vs recent European design criteria.* Engineering Structures, Volume 159, 15 March 2018, Pages 155–171.

Tremblay R, Tchebotarev N. & Filiatrault A (1997). *Seismic performance of RBS connections for steel moment resisting frames: Influence of loading rate and floor slab.* Proceedings, Stessa'97.

Uang C & Fan C (2001). *Cyclic stability criteria for steel moment connections with reduced beam section*. Journal of Structural Engineering. 127 (9), 1021-1027.

Uang C Yu Q, Noel S & Gross J (2000). *Cyclic testing of steel moment connections rehabilitated with RBS or welded haunch*. Journal of Structural Engineering. 126 (1), 57-68.

Uang CM, Bondad D, and Lee CH (1998). "Cyclic performance of haunch repaired steel moment connections: experimental testing and analytical modeling." Engineering Structures, Innovations in Stability Concepts and Methods for Seismic Design in Structural Steel, 20(4–6), 552–561.

Yu QS, Gilton C & Uang C (2000). Cyclic response of RBS moment connections: Loading sequence and lateral bracing effects. Department of Structural Engineering, University of California, San Diego.

Yu QS, Uang CM and Gross J (2000). "*Seismic rehabilitation design of steel moment connection with welded haunch"*, Journal of Structural Engineering, ASCE, 2000, 126(1), pp.69-78.

Zekioglu A, Mozaffarian H, Le Chang S, Uang C & Noel S (1997). *Designing after Northridge. Modern Steel Construction.*

Zhang X & Ricles JM (2006). *Experimental evaluation of reduced beam section connections to deep columns.* Journal of Structural Engineering. 132 (3), 346-357.

Zoetemeijer P (1981). *Bolted Connections with Flush End Plates and Haunched Beams. Tests and Limit State Design Methods*, Report 6-81-15, Delft University of Technology, Stevin Laboratory.